Chapter 2

Dynamics of rotor systems and vibration processes

2.1. System analysis of automatic balancing (self-balancing) machine rotors with liquid working bodies on the example of drum type washing machines

Ilona Drach[1], Vilen Royzman[2], Vitalii Tkachuk[3], Andrii Goroshko[4]
Khmelnitsky National University, Institutska 11, Khmelnytskyi, 280016, Ukraine
E-mail: [1]*cogitare410@gmail.com*, [2]*tkachukv.p@gmail.com*, [3]*royzman@ukr.net*, [4]*iftomm@ukr.net*

Abstract. The main objective of the research is a solution of problems, connected with increasing reliability, efficiency and safety of modern rotor machines.

The class of rotary machines with varying imbalance while operating is rather diverse. These are separators, centrifuges used in chemical, food manufacturing, sugar, mining, medical industries, as well as sandblasters, washing and wringing machines and many others.

On the example of washing machines within the framework of the linear theory of oscillations, the dynamics of rotor machines is investigated, and the main causes of their vibrations and noise are revealed by experimental methods.

The basic problem of these machines is decreasing of their vibroactivity. We will ground the effective method of balancing rotor machines without stop during exploitation conditions – passive automatic balancing with free movement of fluid.

The current work is dedicated to system research of the mentioned method, particularly for studies of fundamental natural phenomenon – self-balancing rotor with the help of passive auto-balancing units, which look like cavity chambers, partly filled with working media (fluid) being passive regulators of direct action that don't need energy supply and control system for movement of correction counterweights.

All theoretical materials are corroborated by results of experimental researches.

Keywords: rotor, vibration, automatic balancing (self-balancing), auto-balancing units (ABU), balancing effectiveness, vibroactivity, causes of vibration, washing-machine.

1. Introduction

Rotor mechanisms are used in a lot of areas of modern production, from mechanical engineering to computer and household appliances. Since these mechanisms have to operate under conditions of high velocities, strong vibrations, caused by shifting of rotor's center of gravity can become a serious problem and even lead to breakage of mechanism.

Problems of vibrations decreasing, stimulated by rotating rotors and having frequency of first rotor harmonic (also known as rotor vibration) are one of the most significant problems of construction, production and operation of almost all types of modern rotor machines [1]. Rotor vibration substantially defines reliability of these machines, for which high rotation frequencies, relatively small rigidity of construction are inherent, and critical operation modes are located within the limits of operation ranges of angular velocities [2].

Solution of tasks, concerning problems of decreasing rotor vibration is founded on the basis of linear theory of mechanical oscillations. The theory also indicates main directions of vibration control: vibroinsulation [3]; damping [4]; dynamic oscillation suppression [5]; perfecting methods of rotor balancing [6, 7], including those that take into consideration their flexibility [8].

Researches of rotor dynamics count more than 140 years, and the article of famous Scottish scientist W. Rankin [9] about rotational movement of rotor, written in 1869 is an evidence of this fact.

Practical value of this article is in the fact, that it for the first time adduced description of the effect of elastic and centrifugal forces on the rotation of flexible shaft. Other than this article showed how Poisson's theory about transverse vibrations of rods can be applied to dynamics of rotors.

Discoveries made in the research of rotors dynamics at the beginning of 20th century are described in details in A. Stodol's monograph [10]. Expect the rest it describes the dynamics of flexible shafts with disk, the dynamics of distributed rotors without reference regard gyroscopic moment, static balancing of critical velocities.

With increasing rating and rapidity of machines increases the range of reverse effect of working environment on machine's rotor. It leads to the fact that, on one hand, rotor experiences significant load-bearing disturbance and under these conditions performs forced oscillations, and on the other hand – becomes less resistant and, under certain circumstances, enters the mode, in which besides forced oscillations there are also self-oscillating components [11]. For the first time the problem about self-oscillations of rotors were brought up in M. Ya Kushul's research [12], where stationary almost periodical oscillations of imbalanced rotor were examined, in which the reason of the origin of self-oscillating component is internal friction in the material of rotor. Further this subject was developed by G. I. Anikeev in his work [13], where lubricating film in supports and existence of dry friction were considered as reasons of the origin of self-oscillations. In the research of K. M. Ragulskis [14] except theoretical and experimental research of rotors' vibrations, the objectives of evaluation of out-of-balance rotor systems by vibration parameters are examined, and also the use of static approach to research of vibrations is described. Questions of the steadiness of rotor frequencies research are described by V. I. Siminivskiy in work [15]. The influence on constructive and mode parameters is analyzed, methods of calculation of multimass rotors steadiness are proposed in this work.

Majority of authors, researching dynamics of rotor systems, posed a problem of selection optimal parameters of rotor in respect to decrease vibrations. Among works, in which these type of problems are solved, one can mention work of B. Ya Kalmens [16], in which providing vibration reliability of machines by treating constructions of elements on the design stage is described, and also creating criteria of vibration reliability that corresponds to safe exploitation conditions. Similar approach to decreasing amplitudes of vibration movement of rotor by selecting characteristics of supports or form of the rotor is described in work of A. S. Kelzone and Yu M. Malinin [17]. This work adduces solutions of optimization tasks both for transitional and stationary operating modes.

Drum washing machines have become more widespread due to the simplicity of automation, more gentle washing, saving of water and detergent compared to the activator ones; but they are more complex and less reliable. Automatic washing machines are mainly drum type.

A washing machine as a object of research of the dynamics and vibration and noise decreasing is a particular interest. The reason is permanent presence of accidental imbalance because of bedclothes and small parts of machines and equipment in the drum and also as a result of low requirements for manufacturing and assembly accuracy of its parts and units in order to steer clear of possible increasing in value of manufacture.

Let's consider a rotary system using the example of a washing machine with a horizontal axis of rotation and implement theoretical studies using the theory of linear oscillations.

We will analyze the results and consider passive liquid auto-balancing as a means of reducing the vibration of rotary machines with variable imbalance.

The class of rotary machines with varying disbalance while operating is rather divers. These are separators, centrifuges used in chemical, food manufacturing, sugar, mining, medical industries, as well as sandblasters, washing and wringing machines and many others. For these machines traditional methods of reducing vibrations are of low efficiency, and the most effectual way is autobalancing by means of hollow chamber partly filled with working bodies.

To eliminate the imbalance of the rotating body, liquid auto-balancing devices (ABD) are used in the form of a hollow chamber with liquid working bodies. They are a standard feature in most household washing machines [18-21], but are also used in heavy industrial rotary machines. As an example, for washing machines, liquid stabilizers are used, which consist of a hollow ring similar to a rubber hoop but usually with a rectangular section containing a small amount of liquid.

The ring, as a rule, attaches to the drum. The fluid moves freely and seeks to combine the main central axis of inertia of the rotor with its axis of rotation.

The main idea appeared already in 1912, and the US patent was granted in 1916 (Leblanc, 1916 [22]), where the working principle of the liquid balancer was outlined. Namely, when the machine rotates at a high angular velocity Ω, the liquid forms a thin layer on the inner surface of the outer wall, depicted in Fig. 1.

A situation is considered when there is an unbalanced mass m, for example, due to the uneven distribution of clothes in the washing machine. The rotor has a critical angular velocity Ω_{cr}, where the centrifugal forces are balanced by the forces due to regenerative springs. Below this velocity ($\Omega < \Omega_{cr}$) ,the center of mass of the fluid will be located "on the same side" as the unbalanced mass, as shown on the left side of Fig. 1 (here M denotes the mass of the empty rotor, and M is the mass of the fluid contained in camera) At a certain supercritical angular velocity $\Omega > \Omega_{cr}$ (say, during the drying process), the center of mass of the fluid moves to the "opposite side" relative to the unbalanced mass, as shown in the right side of Fig. 1, resulting in a "mass imbalance" and, thus, decreasing Thus, the centrifugal forces will decrease and the amplitude of the rotor fluctuations will decrease.

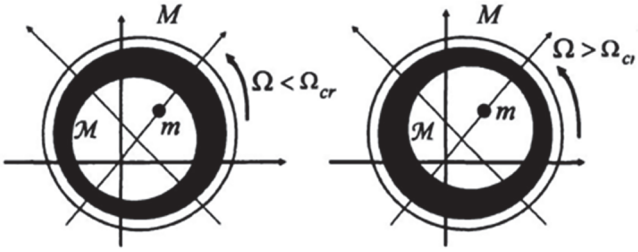

Fig. 1. Principle of operation of the liquid stabilizer for Leblanc

The original model consisted of one or more very narrow concentric channels (narrow in the radial direction, but wide in the axial direction, that is perpendicular to the plane in Fig. 1) partially filled with "liquid or very small steel balls or metal shreds" [22]. Thearle (1932) [23] considered and criticized the fluid balancer of Leblanc; and later Dan Hartog (1985) [24] supported Thearle's views. Here it is said that the Leblanc's balancer cannot work with the liquid, but only with the steel balls, and thus the invention was not recognized. This is probably due to very narrow channels, which mainly prevent the formation of surface waves.

Nevertheless, an automatic washing machine, equipped with a liquid balance, was introduced in 1940 and patented in 1945 (Dyer, 1945) [25]. The model of the liquid balancer was very similar to modern models, with a wide concentric camera, wide enough to allow the formation of a surface wave with large amplitudes.

The idea, therefore, is not new; but recently there has been a renewed interest in it both in industry and in scientific fields.

Experimental studies of liquid dampers were carried out by Kashara and others [26] and Nakamura [27]. As for mathematical models, simple models with lumped masses were considered by Bai in [28], Jun in [6], Maiewskyi in [29], Chen in [3], Urbiola-Soto and Lopez-Parra in [30]. The first and last two of these articles also include experimental studies. Jung's article [6] contains several numerical simulation results based on the computational fluid dynamics.

It should be emphasized that for the first time E. L. Thearle made an attempt to substantiate theoretically the principle of the action of Leblanc's ABD, ring, swing, and ball ABDs in the cycles of his articles [23]. He proposed a flat model of the rotor and the ABD. Within its framework, there is a single critical speed in the rotor, the excess of which the rotor begins to rotate light side outward and begins to manifest self-centered rotor phenomenon, which was laid by Thearle in the basis of the principle of the operation of all passive ABDs. In fact, here the phenomenon of self-centeredness appears as a phenomenon of self-balancing. The approaches and

results of the work of E. L. Thearle formed the basis of subsequent studies in the field of balancing the rotors of machines with passive ABDs. And the result obtained without taking into account the specific properties of the relatives, the forces of resistance, and thus the theoretically unreasonable and experimentally unconfirmed conclusion about the limitations of the range of performance of such auto-balancing devices by the supercritical (or retrograde) rotor rotation area is unexplored to this day. Therefore, a more detailed explanation of this phenomenon remains necessary.

Consequently, a more detailed explanation of the fluid balance dynamics remains necessary.

The approaches and the results of E. L. Thearle's work formed the basis of the following studies: J. Larry, O. Gusarov [31], V. P. Nesterenko [32], H. S. Hoon, L. J. Young, S. Suzuki, Ye M. Pashkov [33], Chung-Hyo Jung [6], M. A. Langthjem, T. Nakamura [34], Cunico M. W. M. [35] and other researchers in the field of balancing rotors of machines with passive liquid SBD. And the result obtained without taking into account the specific properties of correcting the masses, the forces of resistance, and thus, the theoretically unreasonable and experimentally unconfirmed conclusion about the limited range of performance of such automobile balancing devices with the supercritical (after resonance) rotor rotation zone is unexplored even nowadays.

According to the results of the review of Internet sources by the main manufacturers and industrial users of passive SBDs (in particular ball and liquid devices), there are such well-known companies as LG Electronics Inc. [18], Whirlpool Corporation [19], SKF AutoBalancer Systems [20], Samsung Electronics Co. Ltd [21]. However, information on the practical implementation of the above devices for automatic balancing of rotors of machines was not found. Such developments exist only as ideas in patents. Known companies use the idea of passive auto-balancing in advertising their products, which indicates the relevance of such SBDs, but their widespread use on serial machines is hampered by the unresolved many problems in the theory and practice of balancing rotors passive SBD, the presence of a number of phenomena and contradictions that have not yet found the proper theoretical justification.

Traditional methods are ineffective for machines with variable rotor imbalance and for balancing machine rotors without a halt in maintenance conditions. Automatic balancing by means of devices with free correcting masses movement is the most reliable, perspective and often the only possible method for reduction of vibration in such machines.

The current work is devoted to system research of the method mentioned, particularly to studying the fundamental natural phenomenon – rotor self-balancing with the help of passive auto-balancing units (ABD) which look like cavity chambers, partly filled with working media (liquid, granular materials) being passive regulators of direct action which don't need supply of energy and control system for correcting masses movement.

2. Mathematical model of washing machines and the results of its investigation

Matrix form was used to acquire mathematical equations that represent the oscillation of multiply connected tank-drum system fastened to the elastic suspensions for main types of machines and ring type centrifuges with the horizontal and vertical rotational axes. The problems have been solved in linear approach by using II type Lagrange equations.

The research is based on the theoretical analyzing concepts of rotor systems described in [36, 37].

Let us examine osciliations of elastic – suspended tank, containing console – fastened rotating imbalanced drum. Such sketch is typical for machines with the horizontally – stated tank for linen, for instance as in "Viatka", "LG F1222ND" and etc.

Assumptions used for schematization of the object of research are such that real typical construction was replaced by the design diagram (dynamic model), in which the absolutely solid body (tank with mass m_1) is elastically attached to the block by random number of bearings and is it capable of shifting in the space, having 6 degrees of freedom (Fig. 2). There is a cavity inside

this body, in which the rotor rotates with the angular velocity ω, having mass m_2, leaning on the absolutely rigid bearings, contained in the same body.

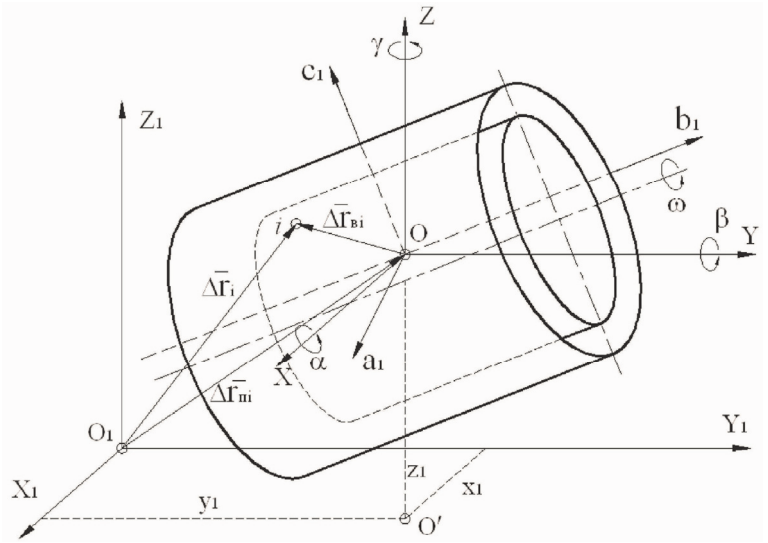

Fig. 2. Design diagram

As generalized coordinates, presetting system's location in space, three Cartesian rectangular coordinates of the machine drum inertia centre (axes a_1, b_1, c_1, serving as principal central axes) and three angles α, β, γ, specifying rotations of these axes of coordinates regarding to the immovable, connected with the frame, coordinate axes X_1, Y_1, Z_1, or parallel to them axes X, Y, Z, coinciding in the drum's centre of mass O, generally not laying on the drum's rotation axis, are assumed.

In such coordinate system oscillations can be presented as a superposition of six helicoidal motions with the propellers' immovable axes X_1, Y_1, Z_1, and generally the system of tank-drum carries out six-unit oscillations.

In order to constitute differential equations of the system's motion we will use second type Lagrange.

m_1 – mass of the tank; $J_{a_1}^{(1)}, J_{b_1}^{(1)}, J_{c_1}^{(1)}$ – tank inertia moments with respect to the main central axes a_1, b_1, c_1 accordingly; m_2 – mass of the drum.

Tank-drum system's kinetic energy can be calculated as a sum:

$$T = T_1 + T_2, \tag{1}$$

where, $T_1 + T_2$ – kinetic energies of the tank and drum, correspondingly.

According to Konig's theorem kinetic energy of the tank [36] can be written as:

$$T_1 = \frac{1}{2}\left[m_1(\dot{x}_1^2 + \dot{y}_1^2 + \dot{z}_1^2) + J_{a1}^{(1)}\dot{\psi}_{a1}^2 + J_{b1}^{(1)}\dot{\psi}_{b1}^2 + J_{c1}^{(1)}\dot{\psi}_{c1}^2\right], \tag{2}$$

where $\dot{\psi}_{a1}^2$, $\dot{\psi}_{b1}^2$, $\dot{\psi}_{c1}^2$ – vector projections of angular velocity $\bar{\psi} = \bar{\alpha} + \bar{\beta} + \bar{\gamma}$ to the axes a_1, b_1, c_1.

In order to constitute expression of the drum kinetic energy we need to study its movement in general case (Fig. 3), when the centre of the drum mass in point S does not agree with the centre of the tank masses at the point O. Let's designate drum eccentricity by a letter e.

Let us introduce extra coordinates of the system into examination: performing the

reciprocating movement X_2, Y_2, Z_2 with start at the point S and X_3, Y_3, Z_3 with start at the point D, firmly connected with the drum.

The coordinate axes a_2, b_2, c_2 are considered as main central axes of drum inertia.

The start point for data recording D we receive as a result of drum's rotation axis intersection with a plane, passing at the point S through the centre of masses perpendicularly to the drum rotation axis. In the reference state and in the case of eccentricity absence ($e = 0$) the point S is congruent with the point D.

It is presumed that in the initial state the axes Y, Y_1, Y_2, Y_3 and b_1, b_2, b_3 is parallel to the axis of drum rotation.

In the examined coordinate system the movement of the drum generally can be represented as a complex motion: reciprocating movement at the point S with the centre of masses and rotation around this centre with the angular velocity of $\overline{\Omega} = \overline{\dot{\psi}} + \overline{\omega}$.

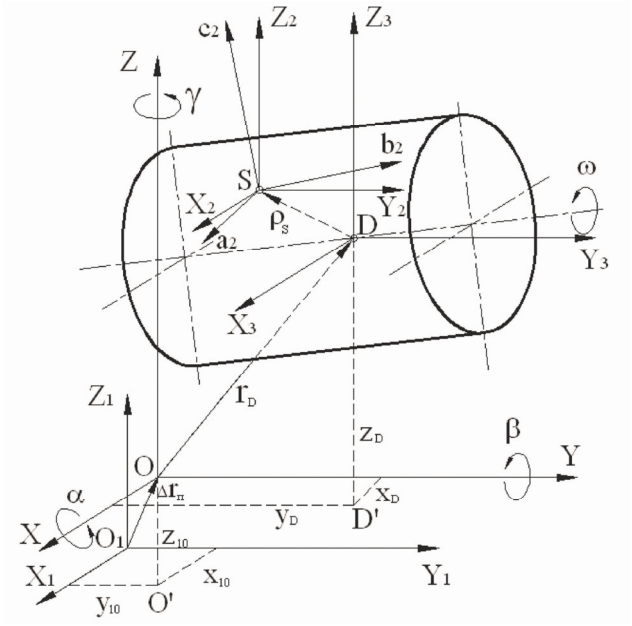

Fig. 3. Movement of the drum in general case

Using the Konig's theorem we can write the expression for the kinetic energy of the drum:

$$T_2 = \frac{1}{2}\left[m_2\left(V_{Sx1}^2 + V_{Sy1}^2 + V_{Sz1}^2\right) + I_{a2}^{(2)}\left(\Omega_{a2}^2 + \Omega_{c2}^2\right) + I_{b2}^{(2)}\Omega_{b2}^2\right]. \tag{3}$$

Expression for the kinetic energy of the tank-drum system will be following:

$$\begin{aligned} T = {} & \frac{1}{2}\left[m_1\left(\dot{x}_1^2 + \dot{y}_1^2 + \dot{z}_1^2\right) + I_{a1}\dot{\alpha}^2 + I_{b1}\dot{\beta}^2 + I_{c1}\dot{\gamma}_{c1}^2\right] \\ & + m_2\dot{x}_1\left(\dot{\beta}z_D - \dot{\gamma}y_D + \omega e\cos\omega t\right) - m_2\dot{\gamma}y_D\left(\dot{\beta}z_D + \omega e\cos\omega t\right) \\ & + m_2\dot{\beta}\omega e\left(z_D\cos\omega t + x_D\sin\omega t\right) + m_2\omega^2 e^2\cos\omega t \\ & + m_2\dot{y}_1\left(\dot{\gamma}x_D - \dot{\alpha}z_D\right) - m_2\dot{\gamma}\dot{\alpha}x_D z_D + m_2\dot{z}_1\left(\dot{\alpha}y_D - \dot{\beta}x_D - \omega e\sin\omega t\right) \\ & - m_2\dot{\alpha}y_D\left(\dot{\beta}x_D + \omega e\sin\omega t\right) + \frac{1}{2}I_{b2}^{(2)}\omega\left(\omega + 2\left(\dot{\beta} + \alpha\dot{\gamma} - \dot{\alpha}\gamma\right)\right). \end{aligned} \tag{4}$$

Let us find the expressions for the potential energy and the energy dissipation within dampers

of the tank-drum system.

Oscillating tank-drum system potential energy is determined by supports elastic deformations.

It is presumed that the tank-drum system is joined with the body of washing-machine through n elastic elements and m dampers.

In order to simplify dependencies, we will presume that the principal rigidity axes and constants of viscous friction of all elastic elements or dampers are parallel to the main central inertia axes of the tank-drum system.

Then projections of the rigidity vector of i-th elastic element to the coordinate axes X_1, Y_1, Z_1, which represent their main rigidities, will be C_{xi}, C_{yi}, C_{zi}, and for every i-th damper as projections of vector of constants of viscous friction are h_{xi}, h_{yi} and h_{zi}, moreover the latter also represent main constants of viscous friction. Such simplification is practically compatible with the structural composition of the elastic elements in existing washing-machines, and their other compositions do not promise any additional advantages.

Under these conditions following expression will represent the equation of potential energy of the tank-drum system:

$$\Pi = \frac{1}{2}\sum_{1}^{n}(C_{x_i}\Delta r_{x_{1i}}^2 + C_{y_i}\Delta r_{y_{1i}}^2 + C_{z_i}\Delta r_{z_{1i}}^2), \tag{5}$$

where $\Delta r_{x_{1i}}$, $\Delta r_{y_{1i}}$, $\Delta r_{z_{1i}}$ – fastening points movements along the axes X_1, Y_1, Z_1 relatively to the movable system of elastic elements; n – number of elastic elements of the tank-drum system.

Dissipation energy in the dampers owing to action of viscous friction, which depends on the velocity of motion of the points, will be following:

$$D = \frac{1}{2}\sum_{1}^{m}(h_{x_i}\Delta \dot{r}_{x_{1i}}^2 + h_{y_i}\Delta \dot{r}_{y_{1i}}^2 + h_{z_i}\Delta \dot{r}_{z_{1i}}^2), \tag{6}$$

where $\Delta \dot{r}_{x_{1i}}$, $\Delta \dot{r}_{y_{1i}}$, $\Delta \dot{r}_{z_{1i}}$ – velocities along the axes X_1, Y_1, Z_1 of connection points of the dampers to the tank-drum system; m – number of dampers in the tank-drum system.

Differential equations of the tank-drum system oscillation will be received by applying II type Langrage equations and taking into account the energy dissipation by assuming Rayleigh type damping [37]:

$$\frac{d}{dt}\left(\frac{\partial T}{\partial \dot{q}_j}\right) - \frac{\partial T}{\partial q_j} + \frac{\partial \Pi}{\partial q_j} + \frac{\partial D}{\partial \dot{q}_j} = 0, \tag{7}$$

where j – number of generalized coordinates, which in this case is equal to 6.

By carrying out prescribed by the equations of Lagrange Eq. (7) according to six generalized coordinates, i.e. X_1, Y_1, Z_1, α, β, γ, mathematical operations, which assume that $\omega = \text{const}$ and by omitting indexes at X_1, Y_1, Z_1, we receive a system of six differential equations:

$$m\ddot{x} + m_2\ddot{\beta}z_D - m_2\ddot{\gamma}y_D + x\sum_{1}^{n}c_{x_i} + \beta\sum_{1}^{n}c_{x_i}z_i - \gamma\sum_{1}^{n}c_{x_i}y_i$$
$$+\dot{x}\sum_{1}^{m}h_{x_i} + \dot{\beta}\sum_{1}^{m}h_{x_i}z_i - \dot{\gamma}\sum_{1}^{m}h_{x_i}y_i = m_2\omega^2 e\sin\omega t,$$

$$m\ddot{y} - m_2\ddot{\alpha}z_D + m_2\ddot{\gamma}x_D + y\sum_1^n c_{y_i} - \alpha\sum_1^n c_{y_i}z_i + \gamma\sum_1^n c_{y_i}x_i + \dot{y}\sum_1^m h_{y_i} - \dot{\alpha}\sum_1^m h_{y_i}z_i + \dot{\gamma}\sum_1^m h_{y_i}x_i = 0,$$

$$m\ddot{z} + m_2\ddot{\alpha}y_D - m_2\ddot{\beta}x_D + z\sum_1^n c_{z_i} + \alpha\sum_1^n c_{z_i}y_i - \beta\sum_1^n c_{z_i}x_i + \dot{z}\sum_1^m h_{z_i} + \dot{\alpha}\sum_1^m h_{z_i}y_i - \dot{\beta}\sum_1^m h_{z_i}x_i = m_2\omega^2 e\cos\omega t,$$

$$J_{a_1}\ddot{\alpha} - m_2\ddot{y}z_D + m_2\ddot{z}y_D - m_2\ddot{\beta}y_Dx_D - m_2\ddot{\gamma}x_Dz_D - 2J_{b_2}^{(2)}\omega\dot{\gamma} - y\sum_1^n c_{y_i}z_i + z\sum_1^n c_{z_i}y_i + \alpha\left(\sum_1^n c_{z_i}{y_i}^2 + \sum_1^n c_{y_i}{z_i}^2\right) - \beta\sum_1^n c_{z_i}x_iy_i - \gamma\sum_1^n c_{y_i}x_iy_i - \dot{y}\sum_1^m h_{y_i}z_i + \dot{z}\sum_1^m h_{z_i}y_i + \dot{\alpha}\left(\sum_1^m h_{z_i}{y_i}^2 + \sum_1^m h_{y_i}{z_i}^2\right) - \dot{\beta}\sum_1^m h_{z_i}x_iy_i - \dot{\gamma}\sum_1^m h_{y_i}x_iy_i = m_2y_D\omega^2e\cos\omega t,$$

$$J_{b_1}\ddot{\beta} + m_2\ddot{x}z_D - m_2\ddot{z}x_D - m_2\ddot{\alpha}y_Dx_D - m_2\ddot{\gamma}y_Dz_D + x\sum_1^n c_{x_i}z_i - z\sum_1^n c_{z_i}x_i - \alpha\sum_1^n c_{z_i}y_i\,x_i + \beta\left(\sum_1^n c_{x_i}{z_i}^2 + \sum_1^n c_{z_i}{x_i}^2\right) - \gamma\sum_1^n c_{x_i}y_iz_i + \dot{x}\sum_1^m h_{x_i}z_i - \dot{z}\sum_1^m h_{z_i}y_i - \dot{\alpha}\sum_1^m h_{z_i}y_ix_i + \dot{\beta}\left(\sum_1^m h_{x_i}{z_i}^2 + \sum_1^m h_{z_i}{x_i}^2\right) - \dot{\gamma}\sum_1^m h_{x_i}y_iz_i = -m_2\omega^2e(x_D\cos\omega t - z_D\sin\omega t),$$

$$J_{c_1}\ddot{\gamma} - m_2\ddot{x}y_D + m_2\ddot{y}x_D - m_2\ddot{\alpha}x_Dz_D - m_2\ddot{\beta}y_Dz_D + 2J_{b_2}^{(2)}\omega\dot{\alpha} - x\sum_1^n c_{x_i}y_i + y\sum_1^n c_{y_i}x_i - \alpha\sum_1^n c_{y_i}z_i\,x_i - \beta\sum_1^n c_{x_i}z_iy_i + \dot{\gamma}\left(\sum_1^n c_{y_i}{x_i}^2 + \sum_1^n c_{x_i}{y_i}^2\right) - \dot{x}\sum_1^m h_{x_i}y_i + \dot{\gamma}\sum_1^m h_{y_i}x_i - \dot{\alpha}\sum_1^m h_{y_i}z_ix_i - \dot{\beta}\sum_1^m h_{x_i}z_ix_i + \dot{\gamma}\left(\sum_1^m h_{y_i}{x_i}^2 + \sum_1^m h_{x_i}{y_i}^2\right) = -m_2\omega^2ey_D\sin\omega t.$$

Differential equations in matrix form are:

$$[M]\ddot{q} + ([G] + [D])\dot{q} + [A]q = [Q], \tag{8}$$

where $[M] = \left\|P_{ij}\right\|_1^6$ – matrix of inertia coefficients; $[G] = \left\|q_{ij}\right\|_1^6$ – matrix of gyroscopic coefficients; $[D] = \left\|\alpha_{ij}\right\|_1^6$ – matrix of coefficients of damping; $[A] = \left\|\alpha_{ij}\right\|_1^6$ – matrix of coefficients of rigidity; $q = \{x, y, z, \alpha, \beta, \gamma\}^T$ – matrix-column of generalized coordinates; $Q = \{Q_x, Q_y, Q_z, Q_\alpha, Q_\beta, Q_\gamma\}^T$ – matrix-column of generalized factors of forces.

Also, the coefficients, for example, of the matrix A have the following expressions:

$$a_{11} = \sum_{i=1}^{n} c_{x_i}, \quad a_{15} = a_{51} = \sum_{i=1}^{n} c_{x_i} z_i, \quad a_{16} = a_{61} = -\sum_{i=1}^{n} c_{x_i} y_i,$$

$$a_{22} = \sum_{i=1}^{n} c_{y_i}, \quad a_{25} = a_{52} = -\sum_{i=1}^{n} c_{y_i} z_i, \quad a_{26} = a_{62} = \sum_{i=1}^{n} c_{y_i} x_i,$$

$$a_{33} = \sum_{i=1}^{n} c_{z_i}, \quad a_{34} = a_{43} = \sum_{i=1}^{n} c_{z_i} y_i, \quad a_{35} = a_{53} = -\sum_{i=1}^{n} c_{z_i} x_i,$$

$$a_{44} = \sum_{i=1}^{n} c_{z_i} y_i^2 + \sum_{i=1}^{n} c_{y_i} z_i^2, \quad a_{45} = a_{54} = -\sum_{i=1}^{n} c_{z_i} x_i y_i, \quad a_{46} = a_{64} = -\sum_{i=1}^{n} c_{y_i} x_i z_i,$$

$$a_{55} = \sum_{i=1}^{n} c_{x_i} z_i^2 + \sum_{i=1}^{n} c_{z_i} x_i^2, \quad a_{56} = a_{65} = -\sum_{i=1}^{n} c_{x_i} y_i z_i,$$

$$a_{66} = \sum_{i=1}^{n} c_{y_i} x_i^2 + \sum_{i=1}^{n} c_{x_i} y_i^2, \quad a_{12} = a_{13} = a_{23} = a_{24} = a_{36} = 0,$$

where c_{x_i}, c_{y_i}, c_{z_i} – projections of the stiffness vector of the i-th elastic element to the coordinate axes X_1, Y_1, Z_1.

According to their structure elements a_{ij} of the matrix A can be divided into four groups and named analogously to the components of the inertia tensor. The first group comprises from elements a_{ij}, those which have $i, j \leq 3$ and $I = j$. They represent summarized rigidity, which values are essentially positive.

The second group includes elements a_{ij}, having $i, j > 3$ and $i = j$. They represent torsional rigidity of the tank-drum system suspension. According to signs they are similar to the inertia moments with respect to the coordinate axes, in other words they are always positive.

The third group includes elements a_{ij}, having $i, j \leq 3$ and $i \neq j$. They represent static moments of rigidity with respect to system's coordinate planes. According to signs they are similar to the static moments of masses with respect to coordinate planes, in other words they can be positive, negative and zero.

And, finally, the forth group includes elements $i, j > 3$, having $i \neq j$. They represent centrifugal moments of rigidity with respect to pairs of coordinate planes. According to signs they are similar to the centrifugal moments of inertia, in other words they can be positive, negative and zero.

Such analogy provides a possibility for developing simple rules, at which the non-diagonal elements of the rigidity matrix – static and centrifugal moments of rigidity will become zero, and it is necessary for separation of the system's oscillations. Particularly, static and centrifugal moments of rigidity will become zero, if coordinate planes with respect to which they have been determined, will be planes of symmetry of the tank-drum system suspension. Analogous assumptions remain valid about the elements structure of the damping matrix D.

For complete separation of free oscillations (when the drum is not rotating), in addition to the rigidity matrix A, it is necessary that the matrix of inertia coefficients M would have a diagonal form, and it is possible when center of mass of the tank coincidence with the centre of mass of the balanced drum.

However in practice because of linen random distribution inside the drum it is impossible to receive complete coincidence between center of mass of the balanced drum and tank. However, for reducing vibroactivity of the washing-machine it is essential to seek that the centre of mass of the tank would be on the rotation axis of the drum and that they would be as much as possible closer to its centre of mass at uniform positioning of linen.

Realized analysis of differential equations of motion allowed to formularize requirements

concerning the washing-machine structure, which should be followed during the design stage: the centre of the tank mass must be on the rotation axis of the drum; rotation axis of the drum must be the main central axis of drum inertia; there must be a coincidence between centre of mass of the tank and drum; there must be a coincidence between the rigidity centre of the system of elastic supports with the gravity centre of the tank and between main rigidity axes and main central axes of tank's inertia. The main axes of viscous friction constants must coincide with the main central axes of tank's inertia.

The system of Eq. (8) considered above has both solutions qualitative and quantitative. Carried out calculation referring machines "Viatka" and "Volga" is about determining resonances and providing their adjustment, on the first stage by separating oscillations by means of repositioning of masses and rigidity of the whole machine, and then – shifting every single resonance be variation of masses and rigidities, influencing only on the value of this resonance, have corroborated validity of formularizes requirements to the design of machines with low vibroactivity.

Nevertheless, calculations are not always successful. And the matter here is not related with the incomplete design diagrams and equations of oscillations, but it is connected with the fact that looking only on the drafts of the machine it is difficult to precisely determine exact values of rigidity coefficients, damping, inertia and masses, that are included into the equations, which are adduced for chosen design diagram. A lot of elements of the machine should be considered at the same time as mass, and rigidity, and also as vibration exciter (resonator) and vibration suppressor (damper). Under conditions of high amplitudes of oscillations some of components, that are considered as being rigid under conditions of lower amplitudes by right, deform, involve adjacent elements into oscillation, fastening to themselves a certain part of their mass and rigidity, in other words they change the initial conditions of the problem and, therefore, values of designed shapes and oscillation frequencies.

All of this requires the development of equipment and experimental methods of machine dynamics research in order to accelerate their adjustment, examination and specifying calculations, identifying parameters of masses, rigidity and damping, that are included in equations of effective search for the reasons of occurring defects and efficiency checking of measures taken for their elimination.

3. Relationship between the rotor balance and operability of rolling bearings

Problems of balancing rotors and dynamics of machines are closely connected with the work of bearings and ensuring their efficiency.

On the one hand, the design of the bearing unit, the stiffness of the coupling with the parts clamps, the mounting gaps, the organization of lubrication, its viscosity and temperature affect the overall dynamic state of the machine and the movement of the rotor, and on the other hand, the imbalance determines the value of loads on the bearing and specifies, depending on listed above factors the nature of the movement of the pin in the bearing, the mode of its operation, causes one or another type of its destruction.

The practice of washing machines of various designs has shown that the rolling bearings are often out of order in the drum mounting unit to the body.

In most cases, the breakdowns are the malfunctioning of treadmills, balls and (or) breakage of the separator of bearings. The purpose of experimental research of bearings is to search for possible reasons for their unsatisfactory work.

Most bearing defects are due to their overload, unsatisfactory organization and the composition of lubrication.

In a much lesser extent, the robotability of bearings at low loads is studied and in this section attention is drawn to this fact, since it is related and was discovered during the study of balancing rotors.

In the study of the dynamics of washing machines, there was a discrepancy between the

working capacity of roller bearings, the balance of the drum and the load on the bearing.

It is known that the normal mode of the ball bearing operation corresponds to a mode in which the balls roll without slipping [1, 2]. In the presence of slipping the balls in the bearing, the rolling friction is replaced by sliding friction, which leads to an increase in the wear of both running tracks and the balls themselves, and in the final result - to jamming of the balls, breakage of the separator, etc. It is precisely this case that occurs in carefully balanced machines in the mode of washing and other modes with small vibrations.

In this connection, the research of the working capacity of roller bearings was reduced to determining the value of the slipping of balls at different values of the drum imbalance.

4. Presentation of research materials

The evaluation of the ball bearings was performed on the basis of measurements of the speed of the separator and shaft and the comparison of the measured values with the theoretical ones. In a perfectly selected bearing, the number of revolutions of the separator and the shaft of the rotor on which the inner races of bearing are located, expressed by the ratio:

$$n_c = \frac{n_s}{2} \cdot \frac{d_0 - d_b \cos\beta}{d_0}, \tag{9}$$

where n_s – number of rotations of the shaft of the engine rotor; d_0 – diameter of placement of centers of rolling bodies; d_b – diameter of the rolling body (balls or roller); β – the contact angle of the body of rolling with the track of the inner races.

For a ball bearing in the absence of an axial force, the contact angle $\beta = 0$, then Eq. (9) will take the form:

$$n_c = \frac{n_s}{2}. \tag{10}$$

Eq. (10) is valid in the case if the balls in the bearing roll without slip [3].

Measurement of the number of revolutions of the separator of bearings was performed at an imbalance of the rotor 22000 g·cm, equal to the maximum possible imbalance in the nominal drum load (4 kg of dry linen), without an imbalance and when acting on the drum only the axial force. To get dependence $n_c = f(n_s)$ of separator rotation frequency (n_c) on the rotational speed of the shaft (n_s) the record was performed on the passage from 0 to maximum engine speed. Depending on the received values, dependency charts were constructed $n_c = f(n_s)$. The same graphs were applied theoretical dependence Eq. (10).

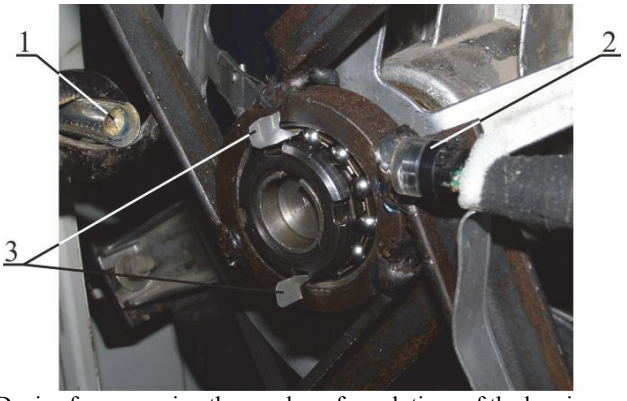

Fig. 4. Device for measuring the number of revolutions of the bearing separator:
1 – incandescent lamp; 2 – photodiode FD-10K; 3 – blinds

Taking into account that at the point of attachment of the drum, ball bearings are located in hard-to-reach places with limited space, a special device for measuring the rotation of the separator has been developed.

The device is an optoelectronic pair consisting of a miniature incandescent lamp 1 (Fig. 4) and a photodiode FD-10K 2 with a small size of photosensitive area. To modulate the light coming from the lamp on the photodiode on the separator of the investigated bearing, special curtains are installed 3. The lamp and the photodiode were installed in such a way that the beam of light during the rotation of the separator was covered with blinds.

The photodiode was connected through a matching device to the "Amphiton" amplifier, signals from which were fixed to the photocell of the oscilloscope H071.4M (Fig. 5).

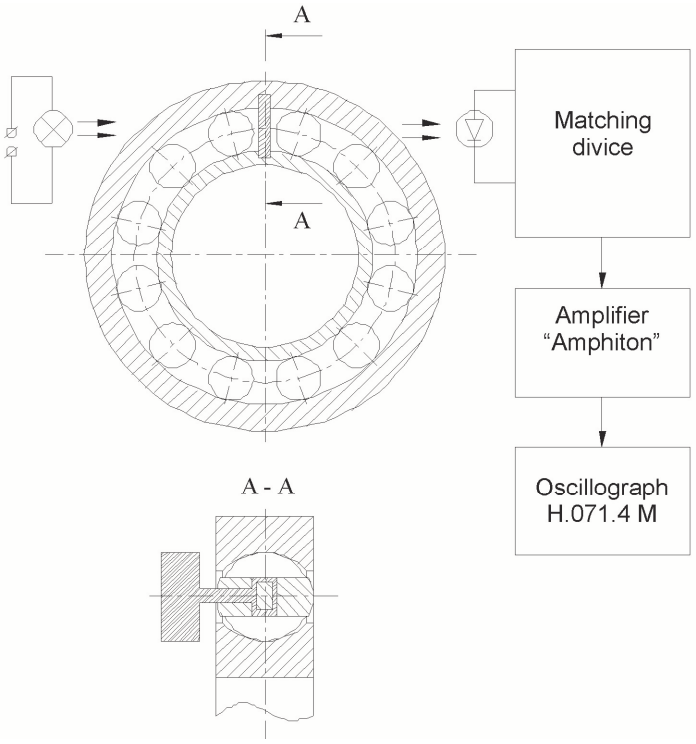

Fig. 5. Block diagram of measuring the rotational speed of the ball bearing separator

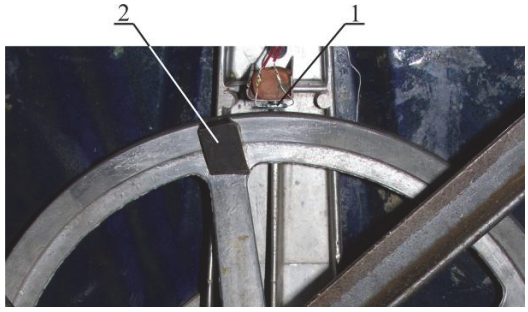

Fig. 6. Rotary shaft sensor: 1 – reed switch; 2 – magnet

Simultaneously, on the oscilloscope's film, the speed of the drum shaft was recorded with the help of a speed sensor. The sensor was made on the basis of the reed switch, which has the ability to lock the electric circuit when passing through a magnetic field. Practically this was done as

follows. On the plate, which was rigidly connected with the installation case, a reed switch 1 (Fig. 6) was stuck with soldered to the ends of its conductors, and the magnet 2 was stuck on the pulp of the unit.

Since the pulley is rigidly connected to the rotor shaft, the speed of their rotation was the same. Thus, with every revolution of the shaft, the magnet, fixed on the pulley, and the magnetic field formed by it, approached the reed switch and locked its contacts. In a closed reed switch on the electric circle, the current, which was the signal of the speed indicator, began to flow.

Experiments were carried out on the washing machine “Aisha” with new and worn bearings.

In order to reduce the random error of measurements, each experiment was conducted several times.

After decoding the received records of the rotational numbers of the bearing separator and the drum shaft, dependences were constructed $n_c = f(n_s)$ shown in Figs. 7 and 8.

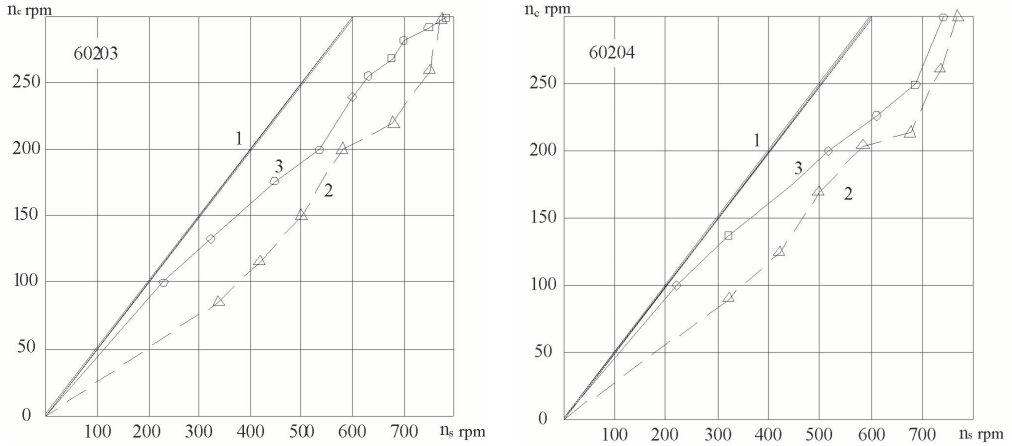

Fig. 7. Dependence of the rotor speed of the bearing separator on the rotational speed of the shaft (non-worn bearings): 1 – theoretical dependence; 2 – without drum loading; 3 – with imbalance 22000 g·cm

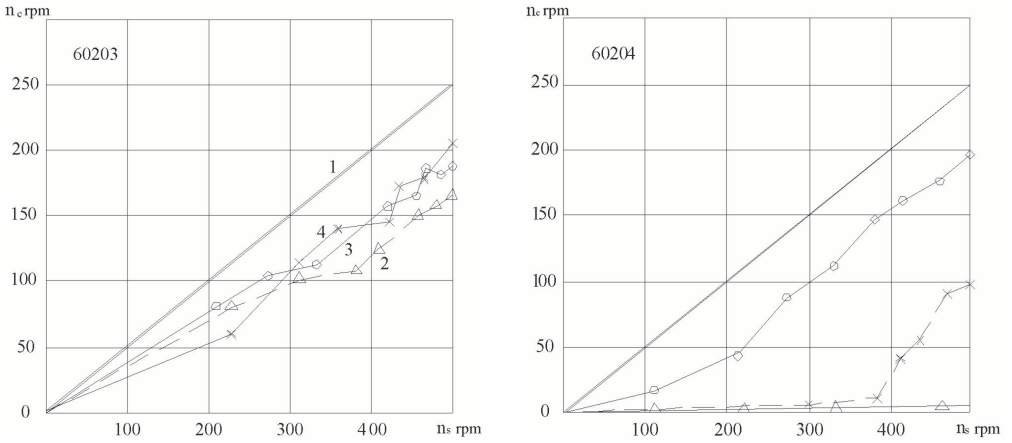

Fig. 8. Dependence of the rotor speed of the bearing separator on the rotational speed of the shaft (worn bearings): 1 – theoretical dependence; 2 – without drum loading; 3 – with an imbalance of 22000 g·cm; 4 – with an axial load of 4 kg

As can be seen from the received graphs, for new and worn bearings, there is a considerable lag behind the number of revolutions of the separator from its theoretical value. When slipping the balls in the bearing, the friction of the roller is replaced by sliding friction, which can lead to

an increase in wear, both in treadmills and in the balls itself. Significant interest is also the fact that when the load on the bearings slipping decreases. On the basis of the obtained results it can be concluded that in order to reduce the size of the slider of balls in bearings, bearings with some initial load, for example, creating some preliminary axial load, should be used.

In the course of this study it was found that roller bearings create noise and high-frequency perturbations, in which certain elements of the machine resonate.

These disadvantages are forcing to find ways to reduce the number of roller bearings in the design of the machine or complete relief from them.

On the basis of the obtained results it can be concluded that for reducing the size of the balls slip, it is necessary to use bearings with some initial load, for example, creating some preliminary axial load or switching to the ball bearings of a lighter series.

In addition, studies have shown that decreasing the drum imbalance, for example, with the help of the ABD, leads to an increase in the degree of slipping of the balls. Therefore, it seems advisable, together with the installation in the drum of the machine ABD or the implementation of other measures that reduce the imbalance of the drum to move on the bearings of a lighter series or bearings of slip.

In this study, in lieu of four ball bearings No. 60203 1 Fig. 9, the knot of the tank of the washing machine to the housing, were made and tested bearings of sliding 2, 3 in the form of 2 cylindrical bushes, the working drawing is depicted in Fig. 7 from self-lubricating material “Hraphiton-K”. The technical characteristics of which are given in Table 1.

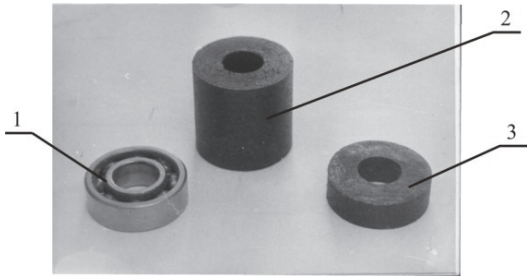

Fig. 9. Bearings of the tank mounting unit for the washing machine to the housing:
1 – ball bearing No. 60203; 2 – cylindrical bush is made of “Hraphiton” (performance 2);
3 – cylindrical bush is made of “Hraphiton” (performance 1)

Table 1. Basic statistical characteristics of the antifriction properties of the material “Hraphiton-K”

The name of the characteristic	Value
Density, kg/m^3	1080
Strength, MPa when stretching	46
Strength, MPa with compression	81
Thermal conductivity at 50-125 °C W/m·K	0,88-1,02
Heat capacity at 50-125 °C KJ·kg·K	1,88-2,35
Friction coefficient without lubrication	0,22-0,35
Friction coefficient with limited lubrication 10 %	0,08
Friction coefficient with limited lubrication 50 %	0,07
Intensity of wear ($\times 10^{-7}$) mm^3/N·m without lubrication	100
Intensity of wear ($\times 10^{-7}$) mm^3/N·m with limited lubrication 10 %	5,1
Intensity of wear ($\times 10^{-7}$) mm^3/N·m with limited lubrication 50 %	4,0

Detailed researches of the first variant (replacement of all rolling bearings with sliding bearings) showed the presence of wear in the form of an enlarged radius of 1-1.5 mm rounding the transition from the end part to the creature’s inner surface from the side of the end closest to the pulley. The reason for such wear was a one-sided, almost static load transmitted by the pulley from the tension of the pass.

When working with similar bearings in a machine, when there is a flexible coupling between the pulley and the shaft of the drum and the effort on the side of the pulley is absent, the observed defect was not observed. However, the aforesaid wear was not reflected in the performance of the machine and may be permissible.

In this case, if the customer acknowledges the specified wear as inadmissible, we have conducted a third-version study, when one ball bearing closer to the pulp, stayed in place, and instead of the other three, the bushes of the material Hraphiton were delivered.

Long-lasting, at least 300-hour machine research in the course of experimental studies has shown the possibility of using this version as well, since none of the roller bearing or slip bearings were defective.

At the same time, in the zone of high sound frequencies (above 200 Hz), the sound power level decreased by a total of 20 %, which also confirms the expediency of the transition to these bearings.

All of the foregoing suggests the replacement of at least three rolling bearings 1 Fig. 9 of the Aisha washing machine reel bearings in the form of bushes 2 or 3 of Fig. 9 made of Hraphiton material in accordance with the drawing (Fig. 10), such material or ready-made bushings may be made by Khmelnytskyi National University.

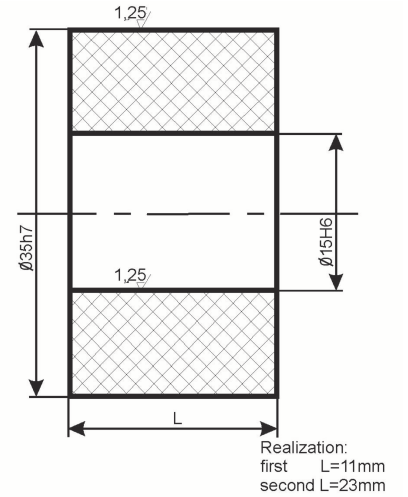

Fig. 10. Working drawing of the bush

Conclusions that we can draw include the following:

1. A device and method for contactless measurement of the value of slipping balls in roller bearings were developed by measuring the frequency of rotation of the separator by a photoelectric sensor.

2. The connection between the magnitude of the imbalance in the drum and the working capacity of rolling bearings is investigated.

3. It is shown that the decrease of the unbalance value leads to an increase in the value of the slipping of balls in the bearing.

4. It was found that when increasing the radial load on the bearing or in the presence of an axial load, the slip of the balls decreases.

5. On the basis of the conducted research it was established that simultaneously with the decrease in the value of disturbing forces, for example, due to the establishment of the ABD, it is advisable to switch to bearings of slip or ball bearings of a lighter series.

Let's consider in more detail one of modern methods of elimination of negative influence of vibration of rotary machines (in particular washing machines of a drum type) – passive automatic balancing by liquid working bodies.

5. Theoretical part

Developing mathematical model describing behavior of liquid in ABU uses the properties of liquid listed below:

– whatever volume of liquid can have any change of its shape being forced by whatever small load;

– viscosity forces are considered only for fast motion when shears in liquid change fast; those forces are not considered for solving problems of liquid balance.

Equation describing condition of stationary motion of solid body with liquid in its hollow [38] in accordance to the principle of least action in the form of Hamilton-Ostrogradski is:

$$\delta W = -\frac{1}{2}\frac{k_0^2}{I_0^2}\delta I + \delta P = 0, \tag{11}$$

where $W = \frac{1}{2}\frac{k_0^2}{I} + P$ – varied potential energy of the system; P – potential energy of forces acting on the system: gravity and centripetal forces, k_0 – value of the constant k in case of uniform rotation of the whole system as one solid body around some immobile line with angular speed ω, I_0 – value of I (moment of inertia of system) for stabilized motion.

Thus, in case of stationary motion of system equation W has extreme value.

Let's assume a solid body being in uniform field of gravity and centripetal forces and having one fixed point O, cylindrical hollow with radius R and height h, and being partially filled with liquid. Axis x_3'' of the immobile system with coordinate origin in fixed point of the body is directed vertically. Mobile axes fixed with body will be drawn so that the axis x_3 would go through gravity center of the system. Gravity center of the system is shifted at the value e relative to geometric axis of the body.

To consider mechanical system without surface tension of liquid potential energy of system and inertia moment of system relative to axis x_3'' are defined by the formulas:

$$\begin{aligned} P &= Mg(x_{c1}\gamma_1 + x_{c2}\gamma_2 + x_{c3}\gamma_3), \\ I &= A\gamma_{12} + B\gamma_{22} + C\gamma_{32} - 2D\gamma_2\gamma_3 - 2E\gamma_1\gamma_3 - 2F\gamma_1\gamma_2, \end{aligned} \tag{12}$$

where A, B, C – axial inertia moments, D, E, F – centripetal inertia moments of system; M – system mass; x_{c1}, x_{c2}, x_{c3} – coordinates of gravity center of system; γ_i – projections of ort i_3'' of immobile axis x_3'' to mobile axis are connected by equation:

$$\gamma_{12} + \gamma_{22} + \gamma_{32} = 1.$$

Condition Eq. (11) considering $\omega I = k$ gives equations in generalized coordinates of solid body in stationary motion:

$$\begin{aligned} \frac{\partial W}{\partial \gamma_1} &= -\omega^2[(A-C)\gamma_1 + D\gamma_1\gamma_2\gamma_3^{-1} - E(\gamma_3 - \gamma_1^2\gamma_3^{-1}) - F\gamma_2] + Mg(x_{c1} - x_{c3}\gamma_1\gamma_3^{-1}) = 0, \\ \frac{\partial W}{\partial \gamma_2} &= -\omega^2[(B-C)\gamma_2 - E(\gamma_3 - \gamma_2^2\gamma_3^{-1}) + E\gamma_1\gamma_2\gamma_3^{-1} - F\gamma_1] + Mg(x_{c2} - x_{c3}\gamma_2\gamma_3^{-1}) = 0. \end{aligned} \tag{13}$$

Eq. (13) lets solution:

$$\gamma_1 = \gamma_2 = 0, \quad \gamma_3 = 1, \tag{14}$$

which will be true at any value of ω, if gravity center of system is located on the axis x_3, which is in turn the general symmetry axis, in condition that:

$$x_{c1} = x_{c2} = 0, \quad D = E = 0. \tag{15}$$

Solving Eq. (14) corresponds to uniform rotation of the whole system around axis x_3' aligned with axis x_3'', with angular speed ω, and axis x_3' being general inertial axis of system, what is condition of auto-balancing. In this condition free surface of liquid will have the shape of revolving paraboloid:

$$\frac{1}{2}\frac{\gamma\omega^2}{g}({x_1}^2 + (x_2 + e)^2) - \gamma\, x_3 - p_0 = C^*, \tag{16}$$

where $\gamma = g\rho$ – volume weight of liquid.

Let the point O′ be the coordinate origin, axis x_3' be directed as revolution axis, and axis x_2' go through points O and O′. Although another coordinate system $Ox_1x_2x_3$ will be considered, in which axis x_3 is geometric axis, axis x_2 coincides with axis x_2'.

Free surface has the shape of revolution paraboloid with parameter $1/\beta = 2g/\gamma\omega^2$, what depends on angular rotation speed; growing angular rotation speed makes parameter decrease and paraboloid be similar to surface of circular cylinder: $r^2 = {x_1}^2 + (x_2 + e)^2 = b^2$ and in limit when $2g/\gamma\omega^2 \to 0$ it becomes a circular cylinder. Correspondently, in horizontal section with axis $x_3 = 0$ that coincides with lower base of the hollow, free surface of liquid has circle shape with center O and radius R_1. Let's find relation between radius R_1 and quantity of liquid in the cylindrical hollow V. Therefore, we'll find constant C^* in Eq. (16) in condition that volume of liquid retains in rest (when $\omega = 0$) and in revolution.

There are three cases of liquid position in the hollow which depend on relation between liquid and imbalance:

1) quantity of liquid is greater than it's needed to balance imbalance (Fig. 11);

2) quantity of liquid is that liquid can balance imbalance in considered frequencies (Fig. 12);

3) quantity of liquid is not enough to balance imbalance (Fig. 13).

Thus, the free surface of heavy liquid revolving around vertical eccentrical axis will be described by equation:

$$x_3 = \frac{\omega^2}{2g}({x_1}^2 + (x_2 + e)^2) - \left(\frac{\omega^2}{2g}R^2 - \frac{\omega^2 V}{2\pi g h} - \frac{h}{2}\right). \tag{17}$$

Considering horizontal section (Fig. 11), it's possible to make conclusion that liquid displaces towards to rotor axis, opposite to imbalance. Its motion stops when total imbalance of liquid and rotor becomes equal zero, that's the balance where principal inertia axis of rotor system coincides with revolution axis. It's automatic balancing when liquid has such shape.

If equation of free surface of liquid Eq. (16) is known one can define equation for liquid optimal volume what is necessary for accurate balancing imbalance in considered frequencies of rotation of system with given physical and geometrical parameters:

$$\left(R^2 h - \frac{h + \beta(e-R)^2}{4}\left(\sqrt{\frac{h}{\beta} + (e-R)^2} - e + R\right)^2 + \frac{3\beta}{32}\left(\sqrt{\frac{h}{\beta} + (e-R)^2} - e + R\right)^4 + \frac{(R-e)^4\beta}{2}\right)\pi = V. \tag{18}$$

In this case radius α of free liquid surface in horizontal section made by the plain $x_3 = 0$ equals:

$$R_1 = R - e. \tag{19}$$

It explains that thickness of the layer in horizontal section made by plain $x_3 = 0$ opposite to imbalance shouldn't exceed $2e$. Thus, only thin layer of liquid takes part in changing imbalanced state of rotating system.

In the third case (Fig. 13) constant C^* will be found from Eq. (20).

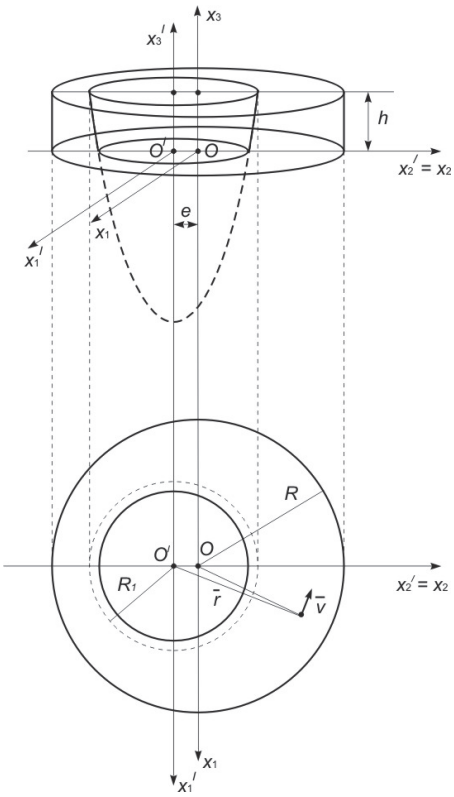

Fig. 11. Position of liquid in the hollow (case 1)

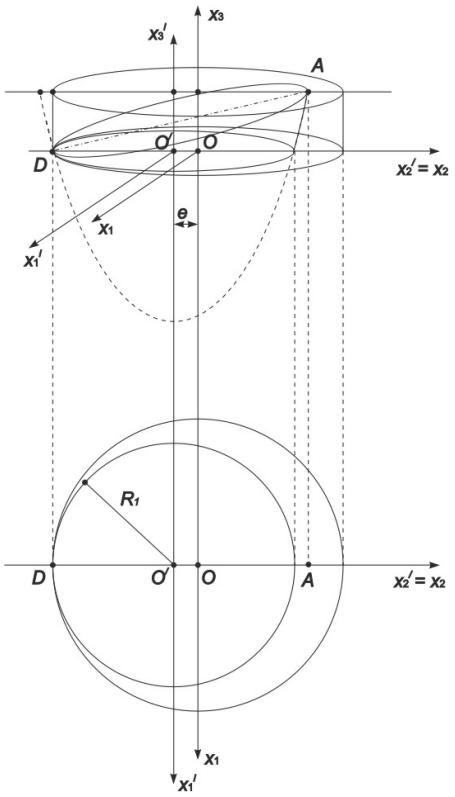

Fig. 12. Position of liquid in the hollow (case 2)

In Fig. 13 thickness of the layer in horizontal section having area $x_3 = 0$ opposite to imbalance is much less than $2e$. Thus, volume of the liquid is not enough to reduce deviation of longitudinal axis of the rotor from revolution axis. Research of liquid's free surface helps make conclusion that not the whole volume of liquid is involved into balancing of imbalance. Optimal volume of liquid to balance imbalance in the given revolution frequencies is estimated by Eq. (18):

$$\pi R^2 h - \left[\frac{R^2 h}{2} \cdot \arccos\left(\frac{C - \beta\,(R^2 + e^2)}{2eR\beta}\right) - \frac{h(-C^2 + 2C\beta(R^2 + e^2) - \beta^2(R^2 - e^2)^2)}{4e\beta^2} + \frac{h(h + 2C)}{2\beta} \cdot \left(\pi - \mathrm{tg}\left(\frac{-C^2 + 2C\beta\,(R^2 + e^2) - \beta^2(R^2 - e^2)^2}{2e\beta\,\left(C - \beta\,\,(R^2 + e^2)\right)}\right)\right)\right] = V. \tag{20}$$

This value may be treated as maximal volume of liquid necessary for accurate balancing at the given geometric dimensions of cylindrical surface. Eq. (19) delivers that thickness of the layer in horizontal section having area $x_3 = 0$ opposite to imbalance shouldn't exceed $2e$. Thus, only thin layer of liquid takes part in changing imbalance of revolving system. Finding this fact confirms experimental conclusion about highest effectiveness of using multichamber ABU.

Hence if to set liquid ABU on the rotor, then at any angular speed ω of stationary motion of system liquid, which moves around absolute rotation axis under action of centripetal forces, flows towards to the side opposite to imbalance and tends to bring the common gravity center to rotation axis.

Value of the constant C^* in the right part of the Eq. (16) is estimated by volume of liquid in the hollow of solid body (ABU).

Motion stability of heavy body with hollow partially filled with liquid demands minimum W [38].

Condition of minimum W in our case is narrowed to inequality:

$$(C_0 - A_0)\omega^2 - Mgx_{c3}^0 - a > 0, \tag{21}$$

where $A_0 = B_0$ (because hollow is cylindrical), A_0, B_0, C_0 – general inertia moments of body having unperturbed motion:

$$a = \rho g \int_0^{2\pi} \int_{R_1 - e\cos\varphi}^{R} \left[\frac{\omega^2}{g^2}\left(\frac{\omega^2}{2}r^2 - C\right) + 1\right]^2 r^3 dr. \tag{22}$$

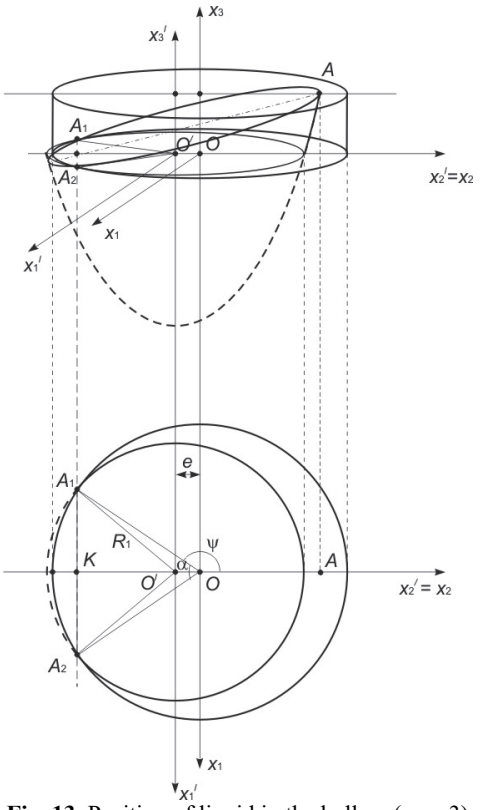

Fig. 13. Position of liquid in the hollow (case 3)

Matching condition Eq. (11) with condition $(C_0 - A_0)\omega^2 - Mgx_{c3}^9 > 0$ of stability of uniform vertical rotation of solid body with liquid in case when its hollow is completely filled up with liquid shows that having free surface of the liquid destabilizes stationary rotation of the system.

Stability condition Eq. (21) can still be tolerated at high-speed rotation if hollow with liquid is oblate enough ($A_0 < C_0$) when the height of cylindrical hollow h is much greater its radius R.

Condition Eq. (21) is valid if liquid that fills the hollow has ultimate viscosity. In case considered here when liquid rotates together with body as one, liquid's viscosity has no effect on its motion.

In case of nonstationnary motion of hollow, which is partially filled with liquid, results look different: one should consider oscillation of free surface of liquid. Some simplifying assumptions [38] show that there's always risk of losing stability when natural frequency of any form of natural oscillation of liquid is close to nutation frequency of the body carrying liquid. Infinite range of forms of natural oscillation of liquid corresponds to infinite range of instability regions, however practice testifies that only a few first regions can be practicable. One may assume that internal friction damping natural oscillations of liquid neutralizes regions of instability of higher orders. Natural frequencies and hence regions of instability depend on how much the hollow is filled up.

Research of this space model describing steady motion of rotor with cylindrical hollow which is partly filled with liquid indicates that liquid auto-balancing is possible on steady motion of the system with any angular velocity.

However, offered model doesn't explain how exactly and under action of what forces liquid moves inside the ABU chamber.

Therefore, next step of the research was creating mathematical model for liquid motion in ABU chamber being under force of change of total system imbalance and bend.

6. Physical content of fluid balancing

In the absence of an ABD, the value of the system imbalance remains unchanged in magnitude and direction, and since there is a relationship between the deflection of the shaft, the magnitude of the imbalance and the angular velocity of rotation:

$$f = e_0 \frac{(\omega/\omega_{kr})^2}{1-(\omega/\omega_{kr})^2},$$

then, obviously, with the increase of the angular velocity ω, the deflection f is continuously increases by subcritical rotation of the shaft.

In the case of an ABD, the imbalance of the system $\overline{e_C}$ consists of a stationary imbalance created by the unbalance $\overline{e_0}$ of the shaft, and an imbalance created by the liquid $\overline{e}$. At $\omega = 0$, the liquid imbalance is zero (Fig. 14(a)).

At the initial moment of rotation, the unbalance of the shaft results in a deflection f, which coincides in the direction with the rotor imbalance (Fig. 14(b)). The centrifugal forces reject fluid to the walls of the ABD and its bulk is concentrated in the deflection, as shown by the established law of pressure distribution in the liquid. With an increase in the speed of rotation of the rotor, the direction of the deflection begins to lag behind the direction of the imbalance at the angle δ (in the presence of fluid in the ABD chamber, the angle δ should be deducted from the total imbalance of the rotor) (Fig. 14(c)). The liquid tends to occupy the position at the furthest point from the axis of rotation, namely in the trough, and moves along with it from the imbalance. This in turn leads to a change in the total imbalance of the system in terms of direction and magnitude (increases as the value of the total imbalance is defined as the geometric sum of the vectors $\overline{e_0}$ and $\overline{e}$ and depends on the angle between these vectors α). This change leads to an increase in deflection, and an increase in the speed of rotation results in an increase in the angle δ. The fluid following the deflection changes the total imbalance by increasing the angle α and decreasing the total imbalance (Fig. 14(d)). That in turn leads to a decrease in the value of the deflection. Consequently, with an increase in the speed of rotation due to the decrease e_C, we have a decrease in the deflection by magnitude even in the subcritical rotor rotation mode.

Because:

$$\mathrm{tg}\delta = \frac{2n\omega}{\omega_{res}^2 - \omega^2},$$

then when the speed of rotation approaches the critical δ, it increases and goes to 90°.

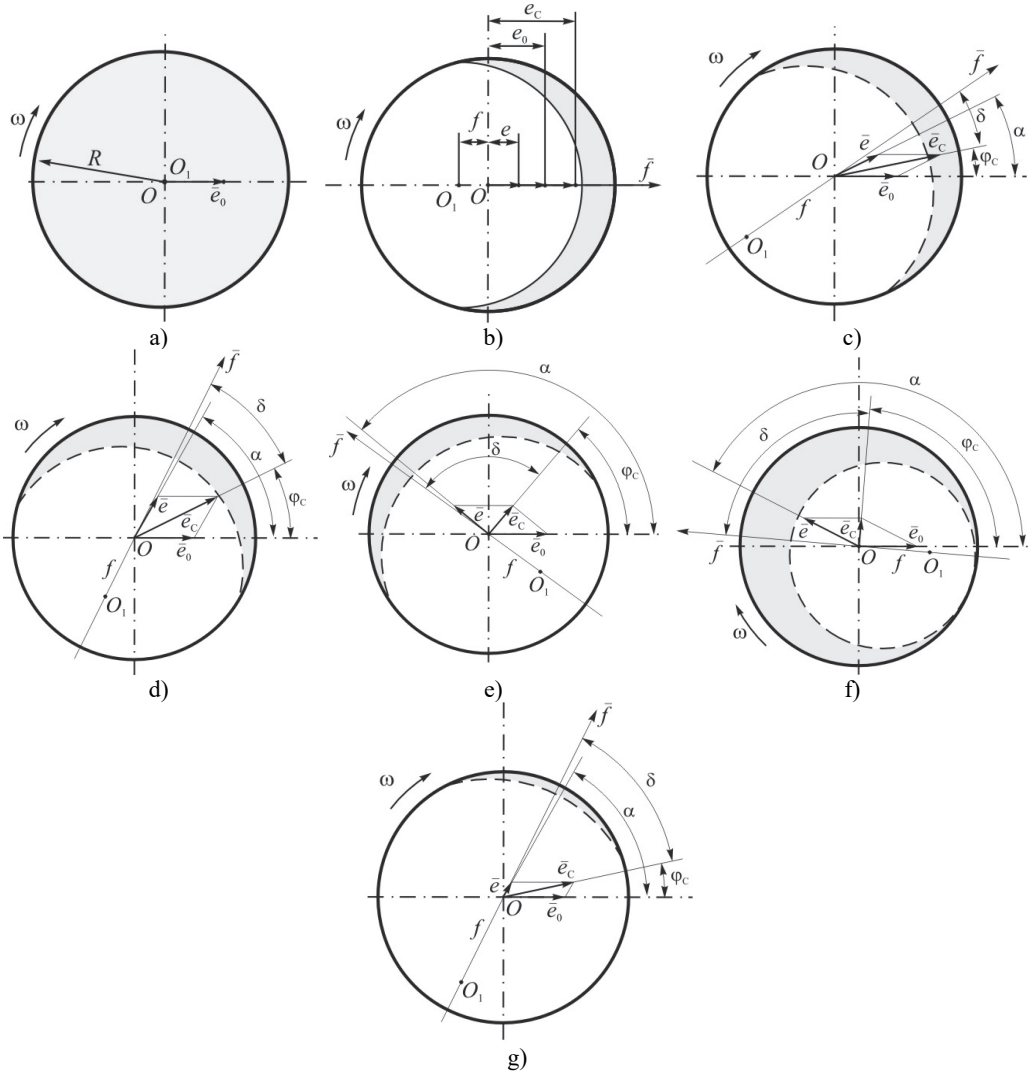

Fig. 14. Vector model of process of auto-balance liquid

Because δ is the angle between the deflection and the total imbalance, and φC is the angle between the stationary and total imbalances, the angle between the deflection and the stationary imbalance when rotating the rotor with the angular velocity is equal to 90° $+\varphi C$ (Fig. 5).

In the case where the stationary imbalance and the imbalance created by the liquid are equal to the magnitude of $e_0 = e$, then φC will be approximately equal to δ (Fig. 6). And so, the angle between the deflection and the stationary imbalance will be directed to 180°. Consequently, when passing the resonance speed of rotor rotation, the fluid along with the deflection of the shaft will be shifted to an angle of 180° relative to the stationary imbalance. After this, there will be an automatic balancing of the shaft imbalance with the fluid, which will lead to a significant reduction in the rotor's vibrations.

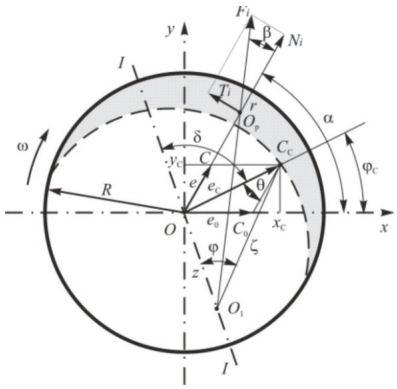

Fig. 15. Forces acting in the SBD in the presence of resistance

With a further increase in angular velocity, a balanced system is rotated without changing the relative position of the liquid and stationary imbalance.

With a small imbalance created by the liquid $e \ll e_0$, the total imbalance of the system will mainly be determined by the magnitude and direction of the stationary imbalance and will not change significantly with the increase of the angle δ (Fig. 7). Consequently, the size of the deflection of the shaft, due to the total imbalance of the rotor, will not be significantly reduced.

Therefore, the amount of liquid that creates a small imbalance in comparison with the stationary imbalance will not be sufficient to balance the system. To increase the imbalance generated by the liquid, it is possible by increasing its mass or the radius of the chamber ABD.

With constant parameters of ABD increasing the mass of fluid can achieve the equilibrium of liquid and shaft, in which we will have the maximum balance of the system.

A further increase in the mass of the liquid will not affect the imbalance created by it, and, consequently, on the balance of the system, because the liquid will be located concentrically around the axis of rotation, which in this case is already the main axis of inertia of the system.

The mass of fluid in the ABD can significantly affect the stability of its placement in relation to stationary imbalances. Since, due to the hydraulic properties of the liquid medium, which can arbitrarily change its shape under the influence of any small forces, the emergence of random minor external perturbations can significantly affect the location of its center of mass, and, consequently, change the state of equilibrium of the system. Moreover, the larger the mass of the liquid, the larger the direction and direction will be the change of the vector of its imbalance.

The basic idea is that at rotation velocity of the system $\omega < \omega_{rot}$ external resistance (friction forces in bearings, friction forces of cylinder against the air etc.) conditions bend plane (I-I) delay against total imbalance plane (OCc) for the phase angle δ (Fig. 15) and appearing in this condition tangential force T of centrifugal inertial force F, and specific properties of liquid (fluidity, ability of any liquid volume to freely change its shape being forced by irrespectively low force, viscosity forces are considered only for quite fast motion when liquid displacements change quite fast) enable drawing liquid in ABU chamber to position that reduces the total imbalance of the system even at pre-critical rotation velocity. Analysis of geometric model (Fig. 15) shows that when external resistance is sufficient liquid that is in stable balance can balance rotor at pre-critical angular velocity.

It will be shown analytically.

Total rotor eccentricity with liquid is defined as:

$$e_c = \sqrt{x_c^2 + y_c^2} = e\sqrt{1 + 2k\cos\alpha + k^2},$$

where $k = D_0/D$ – relation of rotor and liquid imbalance.

Analysis of geometric model (Fig. 15) shows that balance condition that doesn't take into

account tension forces is missing tangential force: either $\mathrm{tg}\beta = 0$, or:

$$f[\mathrm{tg}\alpha\cos(\delta + \varphi_c) - \sin(\delta + \varphi_c)] = 0. \quad)$$

The last equation is decomposed into two conditions (zero index corresponds to angles for liquid balance ($\beta = 0$)):

$$f = 0, \quad (23a)$$

$$\mathrm{tg}\alpha_0\cos\left(\delta + \varphi_{0_c}\right) - \sin\left(\delta + \varphi_{0_c}\right) = 0. \quad (23b)$$

Condition Eq. (23a) corresponds to no deflection condition that contradicts condition of the problem of elastically strained rotor. If liquid is in balance:

$$\mathrm{tg}\alpha_0 = \mathrm{tg}\left(\delta + \varphi_{0_c}\right),$$

what comes from condition Eq. (23b).

Taking into account values of e, e/e_0, ec and $\theta = \alpha - \varphi c$ [4]:

$$\sin\alpha_0 = \frac{1}{k}\sin\delta\sqrt{1 + 2k\cos\alpha_0 + k^2}. \quad (24)$$

It appears from Eq. (24) that if external resistance is missing in the system ($\delta = 0$, $k \neq 0$) liquid balance coincides by the angle with rotor imbalance ($\alpha = 0$), what is approved by the conclusion that liquid increases imbalance in system without external damping.

The expression for angle α_0 corresponding liquid balance ($\beta = 0$) is obtained through algebraic transformations of Eq. (24) when $\delta \neq 0$, $k \neq 0$:

$$\alpha_0 = \pi - \arccos\left(\sin^2\delta + \sqrt{(\sin^2\delta - 1)\cdot(\sin^2\delta - k^2)}\right). \quad (25)$$

Analyzing Eq. (25) gives positive arccosine argument and that's why even in pre-critical frequency of the rotor when $\delta \in (0, \pi/2)$ angle $\alpha_0 \in (\pi/2\,, \pi)$.

Effectiveness of balancing is characterized by relation of misalignment with rotational axis of mass center of the system with liquid and without it λ_0:

$$\lambda_0 = \frac{\sqrt{1 + 2k\cos\alpha_0 + k^2}}{k}, \quad (26)$$

if $1 + 2k\cos\alpha_0 + k_2 = 0$ balance will be complete, therefrom the only solution will be $k = 1$ if $\cos\alpha_0 = -1$, and if $\alpha_0 = \pi$. Hence, the greatest balancing effect will be reached when imbalance of liquid that is involved into balancing is close to initial imbalance of the rotor ($k \approx 1$). Liquid which takes part in balancing makes concentric circles what has no influence on total imbalance of the system.

Eqs. (24) and (26) contain relations of angular velocity to critical one, external resistance factor, relation of initial imbalance to liquid imbalance and relative dimensions of ABU. Obtained analytical relationships between these parameters allow solving applied problems to select optimal parameters of liquid ABU for particular rotor system, find effect of varying parameters of the system rotor – ABU – liquid on effectiveness of balancing.

Internal friction between layers of real liquid hinders its motion and creates delay effect of viscous fluid engaging auto-balancing. Tangential component of centripetal force T is decreasing by decreasing angle β and in some moment can't overcome friction force. That's why viscosity makes balancing incomplete.

Results of theoretical researches for vertical rotor arrangement are also applied for the case of horizontally arranged rotor under the mode of liquid capture (when sum of centrifugal force and friction force are bigger then gravity).

Theoretical results were proved by experimental researches.

7. Experimental part

7.1. Case of vertically arranged rotor

Equipment, apparatus and methods of research of working bodies conduct in SBD.

Research installation is the system rotor-SBD with the vertical axis of rotation.

1. Breadboard model of automatic balancing device. For the investigation of working bodies conduct in the automatic balancing device in under-resonance and over-resonance zones of the rotor rotation a breadboard model of automatic balancing device was elaborated and made of optically-transparent material, which enables to keep up with the work of the SBD in all modes of operation visually or by the help of modern means of video recording.

The breadboard model of SBD is the ring with external diameter of Ø400 mm, two concentric partitions with diameters of Ø300 and Ø200 mm which form three concentric chambers for arrangement of working bodies. General appearance of the elaborated breadboard model of SBD is shown in Fig. 16.

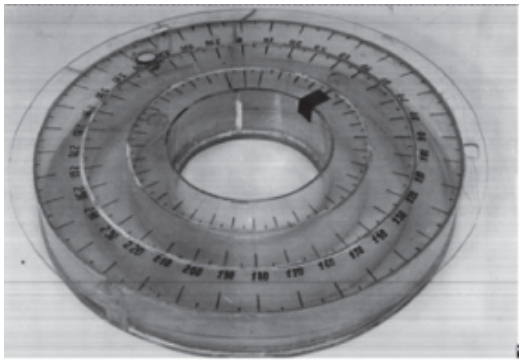

Fig. 16. General appearance of the SBD breadboard model

All three chambers are isolated from each other which allow using simultaneously both fluid and rigid working bodies in the SBD. Colored water in different colors as fluid working body was used for each chamber of the SBD. Metal and plastic balls with diameters of 6, 8, 12 and 16 mm were used as rigid working bodies. Metal and plastic balls with diameters of 1; 1, 5; 2; 4 mm were used as dry substances. The scale with scale factor of 5 grades was marked on the surface of the ring edge to determine the places of arrangement of working bodies in the SBD during the experiment. The position of misbalanced mass (misbalance) is fixed on this scale with the help of a thin color strip, of size 10×20 mm with adhesive layer on one of its surfaces. The bottom of the SBD is mat to increase the contrast of visual observation of the working bodies' position. Fixing rods are made on the external side surface of the SBD at angle 120° to fix the breadboard model on the rotor.

2. The construction of the research installation. The research installation is a rigid cantilever vertical rotor, resiliently hung to the frame.

In order to provide sufficient rigidity of both the rotor and the SBD, fixed on it, the first one is made in the form of a hollow cylinder of stainless steel plate with the bottom on one side which is rigidly fixed on the axis of rotation.

Rotor axis through swinging bearings is connected with a rigid platform which is joined to the frame of the installation by means of four resiliently damper brackets (typical meaning of the

proper vibration frequency of all the system on the brackets is equal to 2-2,5 Hz). The SBD breadboard model is set on the free end of the hollow cylinder (further – a drum). It is put into the drum and is fixed to it on its external diameter. Due to this, necessary rigidity of fixing of the SBD on the rotor and conformity of axes are ensured. The SBD breadboard model has an inner aperture, enough for free access to the inner cavity of the drum which enables to change the rotor misbalance without demounting the SBD both on the place of arrangement and on the size by means of fixing to the inner side the given load which is additionally held by forces during experiments.

Such construction of rotor provides necessary level of security of personnel against occasional tear of the load-misbalance or weakening of the SBD fastening.

Rotor drive is operated by a synchronous electric motor with power on the shaft equal to 180 W through the lowering V-belt transmission. The motor is fed with the alternative current which power can be changed in a wide range with the help of automatic transformer with the operation system. Due to it the installation enables to rotate the rotor at various frequencies in scope of 0, 5-30 Hz (30-1800 rpm), to set different angular accelerations at rotor dispersal, to stop at under-resonance, resonance and over-resonance zones of the rotor rotation for a given period of time with the aim of detailed investigation of the SBD operation.

For a high-velocity video recording the inner surface of the drum was lightened by incandescent lamp of 200 W, arranged with the help of bracket in the inner cavity of the rotor. To obtain steady light the inner surface of the drum was covered by mat color.

3. Measuring, registering equipment and preparation of installation Demonstrating auto balancing process as a whole, high-speed video shooting of working bodies' behavior is suggested to be used. For this aim, we have elaborated a testing stand to analyze auto balancing process with applied video and computer techniques. Block scheme of the stand is found at Fig. 17.

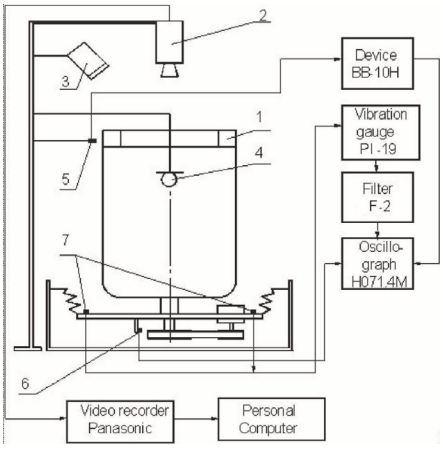

Fig. 17. Bloc-scheme of the equipment connecting: 1 – the SBD breadboard model, 2 – video camera, 3 – stroboscope, 4 – incandescent lamp, 5 – induction data unit, 6 – revolutions data unit, 7 – accelerometers

The velocity of the rotor rotation was measured by means of the noncontact marker of revolutions elaborated on the basis of Hall's data unit.

Accelerometers were installed on the rotor platform. Signal from the accelerometers was carried to vibration gauges PI-19 where it was integrated twice after intensification in order to obtain amplitudes of the shifting of the system platform-rotor.

Amplitudes of rotor vibrations proper were measured by means of the elaborated optical electronic device.

Video camera was placed vertically over the SBD on the axis of rotation of the rotor. Video recording of balancing was carried out synchronically with the recording of vibrations level of the rotor.

The most interesting and representative slides were recorded in the computer in BMP format and were processed further with the help of graphic packages ACAD and Photopaint.

4. Methods of high-velocity video recording of the SBD operation.

The methods of high-velocity video recording of the SBD operation on the vertical rotor consist of three stages: preparatory, investigation of transition modes, investigation of stationary and quasi-stationary modes.

4.1. Preparatory stage includes:

– Balancing of rotor with the SBD breadboard model in the absence of working bodies in it;

– Selection of dimension and place of arrangement of the rotor artificial disbalance;

– Determination of optimum volume or quantity of working bodies in the SBD;

– Determination of optimum light of the SBD;

– Determination of necessary movement velocity of magnetic videotape;

– Determination of optimum position of video cameras (choice of sight angle and distance to the SBD;

– Test starting of all system for coordination of interaction of its separate sections.

Balancing of the rotor with the SBD breadboard model in the absence of working bodies in it was carried out using the method of rounds of test load at the working frequency of the rotor rotation.

Meaning of the rotor artificial misbalance was determined at its working frequencies of rotation in the following way. The mass of artificial misbalance was increased gradually with step of 5 g from starting to start and the rotor vibration level was measured.

Critical maximum meaning of misbalance mass was considered to be that one at which vibrations amplitude reached 35 mm (higher meanings in the given construction of the installation cause impacts of moveable elements with the frame) or when the electric motor is not able to increase revolutions during transition through system resonance and rotor "is suspended" at the critical rotation frequency.

The meaning of misbalance mass obtained according to these criteria, reduced for 5 g (the size of one step) and which is equal to 30 g was considered as the initial maximum meaning for further investigation.

Criterion of optimum volume of working fluid or of quantity of working bodies in the SBD was considered to be visibility of the process of automatic balancing on all revolutions of the rotor, i.e., when the position of working bodies or fluid in relation to the place of arrangement of artificial misbalance was clearly visual in the light of stroboscope and on the videotape. Determination of such meanings of volume or quantity was carried out by means of experiments.

As a result of such investigation volumes fluid (colored water) were obtained which constituted 0.45, 0.3 and 0.25 l for external, medium and internal chambers of the SBD correspondently.

Maximum quantity of working bodies separately for each of diameters of balls was obtained in the same way.

4.2. Video recording of movement of working bodies in the SBD in stationary modes of the rotor rotation.

Resonance angular velocity of the rotor rotation is equal to $\omega_{res} = 12^{-16}$ s^{-1}. For the investigation of working bodies conduct in the SBD at under-resonance, resonance and over-resonance frequencies of the rotor rotation, the latter was given angular velocity of $0.5\omega_{res}$ and $0.75\,\omega_{res}$ (under-resonance zone), ω_{res} (resonance zone), $0.5\,\omega_r$ and ω_r (over-resonance zone), where ω_r is equal 90 s^{-1} – nominal frequency of the rotor rotation.

Video camera and equipment were switched on in the period of time equal $\Delta t = 10^{-15}$ s of the rotor delay at the determined frequency of rotation when position of working bodies relatively to marks on the SBD frame stabilized.

Video recording at each of the above mentioned frequencies had been carried out for 20-30 s – time sufficient for recording not less than 10-20 full revolutions of the rotor.

Experimental research of the SBD operation and its results.

Fig. 4 shows the most typical and representative computer slides of the video recording of the fluid position in the SBD at under-resonance (Fig. 18(a), $\omega = 8$ s^{-1}), resonance (Fig. 18(b), $\omega = 12.5$ s^{-1}) and over-resonance (Fig. 18(c), $\omega = 90$ s^{-1}) frequencies of the rotation of the rotor with the SBD.

Analysis of these and other slides shows that fluid compensates rotor misbalance at under-resonance, resonance and over-resonance frequencies of its rotation. Theoretical explanation of the fluid's position in relation to misbalance, witnessed by video-recording, can be given if one takes into consideration of hydromechanical properties of the fluid and damping of the rotor system.

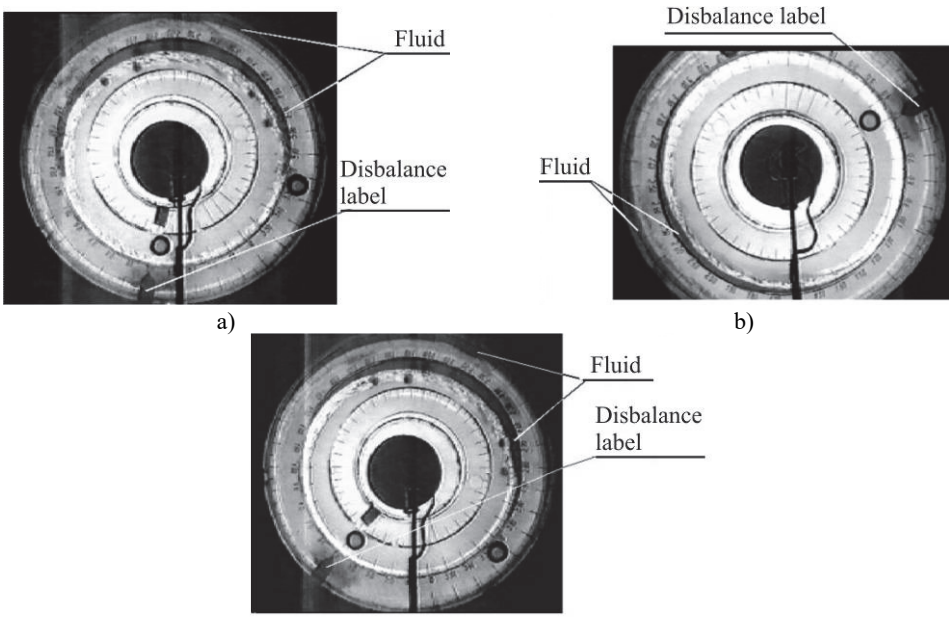

Fig. 18. Video shots: a) before resonance, b) at resonance, c) beyond resonance

7.2. Case of horizontal rotor

For simplification of understanding of results presented in the article we will remind on which physical phenomena existing theories of self-balancing by passive fluid SBD are based. For this we will examine weightless horizontal bank with self-balancing disk with mass M set up on it (Fig. 19). Rotation axis (bearing axis) is marked as O_1O_1 (Fig. 19), self-balancing disk center of mass – C, geometric center of disk – O. In composure state geometrical center O lies on bearing axis O_1 and center of mass C, if there is unbalanced state, is shifted on e distance. In this case rotor's imbalance equals $\overline{D} = \bar{e}M$. Rotor passing through resonance has next theoretical explanation. After the beginning of the movement as a consequence of centrifugal force action $F_i = Me\omega_2$, occurs bending deflection of rotor y, which depends on hardness of rotor c and it is increased when angle speed is increasing according to the formula $y = Me\omega^2/(c - M\omega^2)$. When angle speed is approaching to resonance the value of bending deflection considerably increases and tends to $+\infty$ (Fig. 20(a)) [36].

After passing critical speed (resonance) self-centering of rotor, decreasing of bending deflection from $-\infty$ to $-e$ happens. It is worth noting that if the speed is critical changing of bending deflection from $+\infty$ to $-\infty$ happens, and also relative position of rotor's points mentioned above is changed. (Fig. 19(c)). So far as fluid in self-balancing device will be trying to locate in

most distant from the rotation axis place, that is it will coincide with direction with bending deflection, summary center of mass of Cc disk-fluid system will be shifted to side of eccentricity increasing (imbalance). That is self-balancing by passive fluid SBD is effective on above resonance rotation frequencies [36].

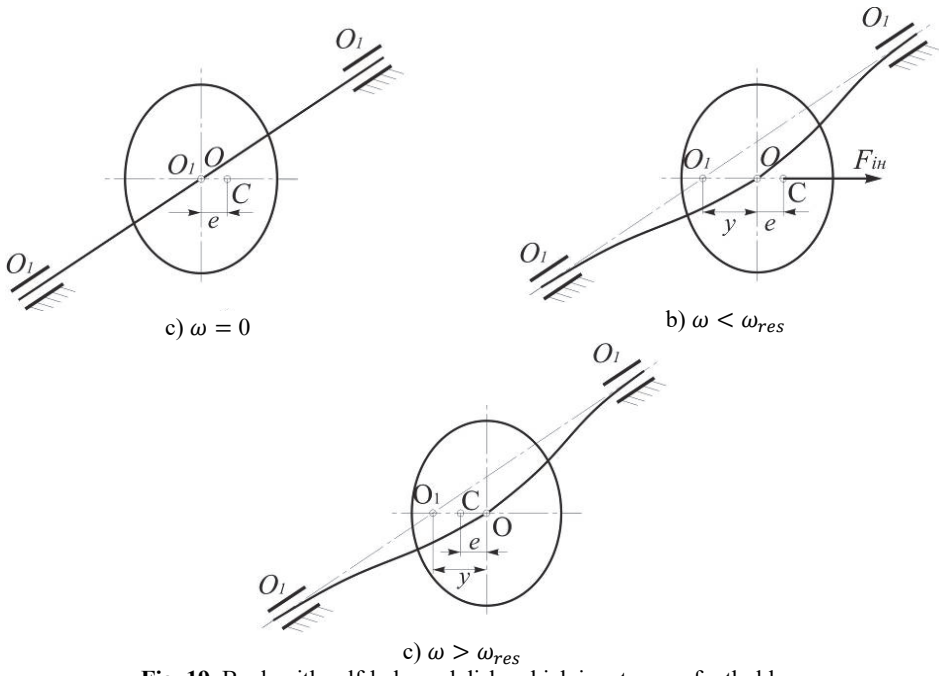

c) $\omega = 0$ b) $\omega < \omega_{res}$ c) $\omega > \omega_{res}$

Fig. 19. Bank with self-balanced disk, which is set up on footholds

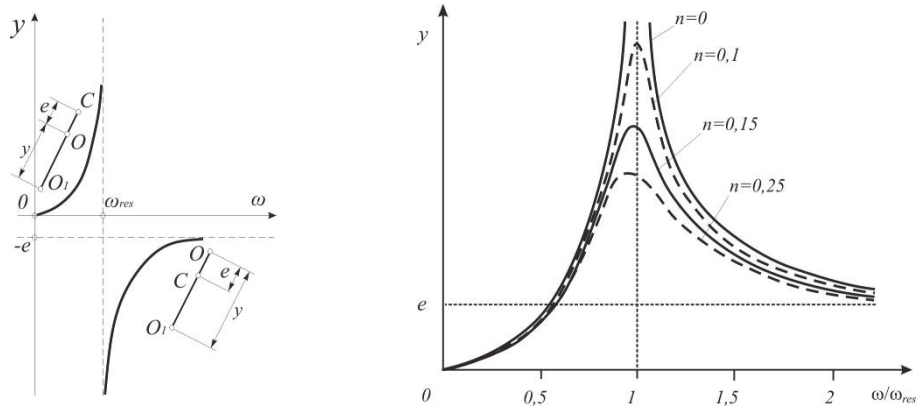

a) b)

Fig. 20. a) Graph of rotor's bending deflection dependence on angle rotation speed; b) AFC of rotor when damping coefficients are different

When studying already existing theoretical points of rotor self-balancing authors had wish to examine what is happening with rotor in resonance zone, as bending deflection cannot be endless and also instant change of rotor's bending deflection from $+\infty$ to $-\infty$ is impossible. While studying works about researches of rotor vibration when passing through resonance it was determined that real AFC of rotor systems on which forces of viscous (Fig. 20(a)).

Vibration amplitudes are equal not to infinity but friction influence (Fig. 20(b)), are different from theoretical specific values which are indicated by damping coefficient. With damping

increasing not only vibration decreasing will happen but also shifting of maximum in the zone of lower frequencies of rotor rotation.

In addition, authors pay attention to the fact that change of bending defection direction relatively to rotation axis occurs on resonance. Relative position of eccentricity and bending deflection are also changed (Fig. 19(c)). That is if the distance from rotation axis O_1 to center of mass C was indicated as sum $y + e$ in below resonance zone, then this distance (O_1C) is indicated as disparity $y - e$ in above resonance zone.

Authors made an assumption that change of relative position of bending deflection and eccentricity happens not instantly at the resonant speed, but progressively and begins at below resonance frequencies of rotation and it happens like that. When approaching the resonance in consequence of damping action (external and internal friction forces) the lag of bending deflection plane from centrifugal force is happening, because rotor is not able to overcome large distance in limited time. Eccentricity direction begins to pass ahead plane of bending deflection on phase angle δ (Fig. 21), which increases with speed increasing. After resonance angle between eccentricity and bending deflection direction becomes 180°. When rotor is passing resonance, it is rotated both around bearing axis $O_1(\omega)$ and geometric center $O(\omega_1)$, that is bank twisting is happening. It means that redistribution of tensions, mutual change of squeezing and extension tensions happen in fibers of rotor.

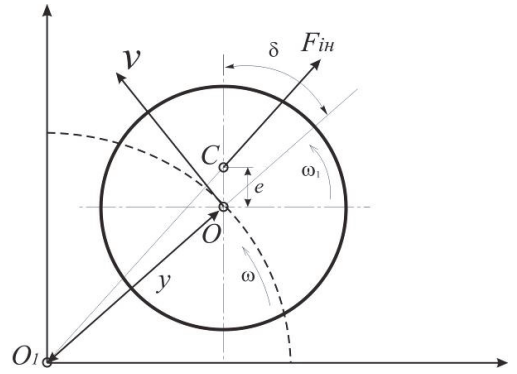

Fig. 21. Rotor movement when passing resonant speed

If fluid exists in self-balancing disk under influence of centrifugal force it tries to take up a position in most distant place from rotation axis, which is saved in direction of bending deflection. It leads to changing of summary system imbalance, which consist of rotor imbalance and fluid imbalance in size and in direction. So far as for certain constant angle speed lag of bending deflection from summary imbalance δ is constant, with changing summary imbalance direction the position of bending deflection relatively to initial eccentricity (that is angle of lag relatively to initial imbalance is increased). Fluid follows the bending deflection, and changes again summary imbalance, which leads to further increasing of lag angle δ. Process can continue until angle will not acquire 180°, and it will lead to decreasing of bending deflection value and changing of its position relatively to e.

For verification of these assumptions authors made a decision to conduct experimental studies on improved laboratory plant for demonstration of critical speeds of bank. When working in educational laboratories of the university self-balanced device (SBD) was made and set up on bearing. Bank of the equipment if located horizontally and bounded with bank of electric motor through flexible connector. Bank has two supports on frictionless bearings.

Created SBD presents a disk with external diameter 150 mm made of steel, with two circular isolated one from another camera with diameters 100 and 130 mm, for placing in them working mediums, and set up imbalance. For possibility of observation of working mediums behavior front wall (cover) of self-balancing device is made of optically transparent material – Plexiglas. This

SBD was fastened by collet clamp, provided in construction of SBD. General look of SBD is given on Fig. 22.

Rotor's drive is made by electric motor of alternating current with power 180 watt though muff coupling. Due to autotransformer and control system the plant has possibility to define rotor rotation with different frequencies, which are in range from 0 to 5000 rpm. Also, it gives possibilities to make acceleration with different age accelerations of the rotor and allows it to rotate with constant angle speed in below critical, critical and above critical zones.

Unbalancing the rotor was made with the help of load (imbalance) fastened with the help of threaded connection on back butt of SBD. SBD has two geometrically isolated cameras, which helps to use fluid as working medium in each of them simultaneously and separately. Colored water was used as a working medium.

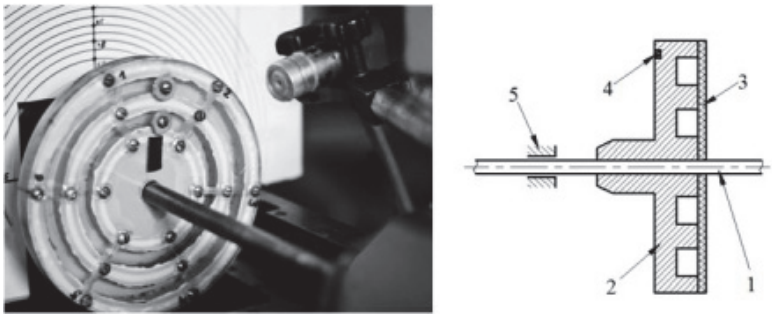

Fig. 22. Scheme of mounting SBD: 1 – bank, 2 – SBD, 3 – cover, 4 – imbalance, 5 – bearings

Position of unbalanced mass (eccentricity) was marked on front butt of SBD with the help of thin black stripe with dimensions (10×20) mm and sticky layer on one of its surfaces.

Created plant allowed to make experimental researches of self-balancing of the rotor with horizontal rotation axis and to observe fluid behavior in SBD.

Research of self-balancing process and fluid behavior in SBD were made on described plant with using next special devices:

– Video camera Panasonic AG-DVX100BE;
– Lamps with halogen lamps (power – 1000 watt each);
– Inductive sensor, marker of turns;
– ADC (analog-to-digital converter);
– Notebook computer.

When video filming is fast it is necessary to have high illumination. That is why two lamps with halogen lamps of power 1000 watt each were used for illumination of the object. Lamps were directly set up close to object of the filming. Video camera was placed horizontally, frontally and in the direction of rotor rotation axis.

Methodology of conducting researches of the SBD work on horizontal rotor with the help of speed filming consisted of:

– Rotor balancing with SBD model without fluid in it;
– Matching value and place of artificial imbalance of the rotor;
– Determination of optimal fluid volume in SBD;
– Synchronous recording of the fluid position in SBD and signal of vibration detector.

Rotor balancing with SBD model without fluid in it was made by using cargo workaround method [36] on working frequency of rotor rotation. Then plant was turned on and vibration recording on computer were made in conditions of smooth rotor acceleration from 0 to 2000 rpm. After rotor of the plant was unbalanced by mounting cargo with mass 10 g. on the butt of SBD with the help of threaded connection. Cargo on SBD was marked with the help of color stripe, then the plant was turned on and vibration recording on computer were made in conditions of smooth rotor acceleration from 0 to 2000 rpm.

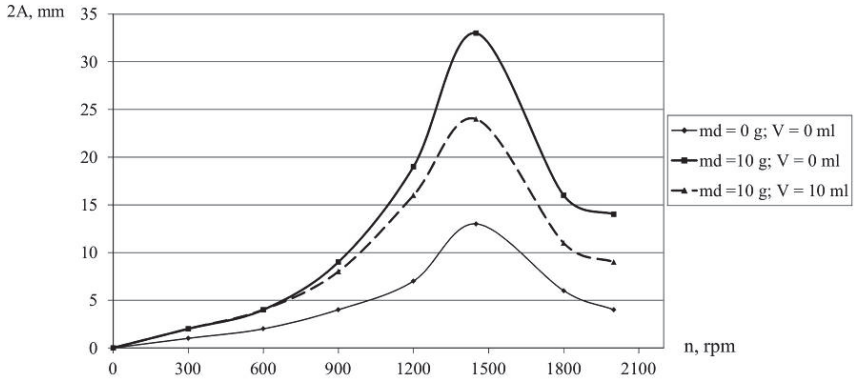

Fig. 23. Amplitude-frequent characteristics

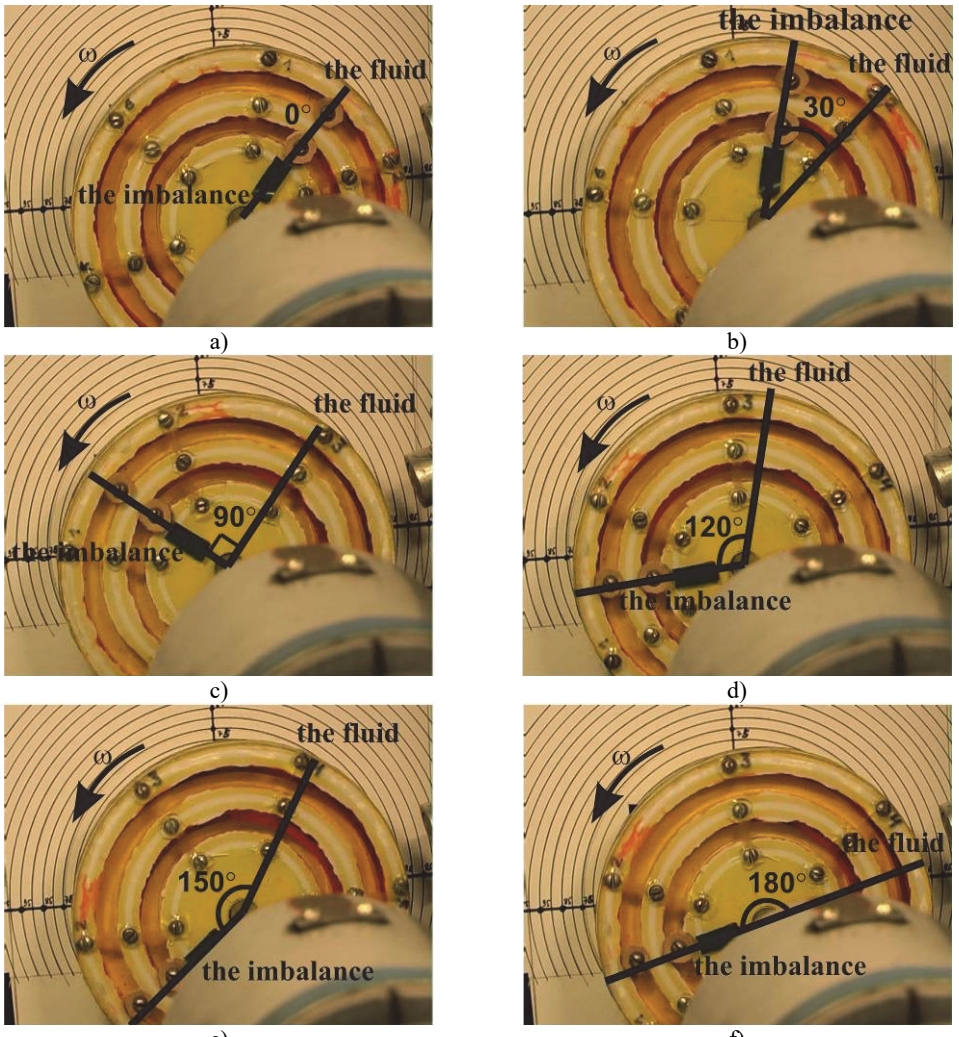

Fig. 24. Shots of video recording of fluid position in SBD when passing through resonance:
a) $\delta = 0°$ ($n = 600$ rpm); b) $\delta = 30°$ ($n = 900$ rpm); c) $\delta = 90°$ ($n = 1000$ rpm);
d) $\delta = 120°$ ($n = 1100$ rpm); e) $\delta = 150°$ ($n = 1200$ rpm); f) $\delta = 180°$ ($n = 1300$ rpm)

By filling in each camera of SBD with 10 ml of water, without changing position or mass of imbalance, the plant was turned on again. Rotor vibrations were recorded on computer in text file in conditions of smooth rotor acceleration from 0 to 2000 rpm. Simultaneously were made video record of fluid behavior in SBD.

Amplitude-frequent characteristics of rotor when passing through resonance are illustrated on Fig. 23. Shots of created video film with angles of fluid progressive shift aside opposite to imbalance are shown on the Fig. 24.

8. Conclusions

In Article theoretically obtained and experimentally verified main requirements for the structure of washing-machines. On the basis of investigations of mathematical model vibration of washing machines a number of recommendations for the design of washing machines were provided:

- Center of mass of the tank needs to be the drum's rotation axis;
- Rotation axis of the drum needs to be the main axis of tank's inertia;
- There needs to be a coincidence between drum's and tank's center of mass;
- Rigidity center of elastic supports system needs to coincide with tank's center of gravity, and main rigidity axes – with main central axes of tank's inertia;
- Main axes of constants of viscous friction need to coincide with main central axes of tank's inertia.

It was also investigated that bearings are the most widespread and most vulnerable elements of any rotary mechanism. Bearings shall spatial fixing rotors and accept most of the static and dynamic forces arising in the mechanism. Therefore, the technical condition of bearings is the major component determining working capacity of the whole mechanism. In article researches, a stock of working capacity of the of rolling and plain bearings by means of the experimental stand are described.

The current work is devoted to system research of the fundamental natural phenomenon – rotor self-balancing with the help of passive auto-balancing units (ABD) which look like cavity chambers, partly filled with working media (liquid) being passive regulators of direct action which don't need supply of energy and control system for correcting masses movement.

The results of experimental and theoretical research of fluid behavior in passive self-balancing devices, which are installed in rotors with vertical and horizontal rotation axes when passing the resonance, are given in this article. Received relations showed that automatic balancing by fluid is effective for elastically deformed rotors or (and) rotor on elastic supports, where exists the difference in phases between the direction of centrifugal force and flexure (or movement) of the rotor. As experimental results showed, this difference in phases occurs when rotor reaches resonance speed and increases up to 180° when passing the resonance. In this case the tangential force occurs, under the influence of which the fluid moves to the side of flexure, opposite to imbalance, and further equilibration of the rotor already at resonance rotation frequency. The influence of gravity under conditions of horizontal arrangement of SBD rotation axis, is in decreasing of tangential component, which moves fluid in position opposite to imbalance and leads to decreasing of balancing accuracy in comparison with vertical rotation axis.

References

[1] **Racic Z., Racic M.** Practical approach for solving vibrations of large turbine and generator rotors – reconciling the discord between theory and practice. Proceedings of the 10th International Conference on Vibrations in Rotating Machinery, Graz, Austria, 2017.

[2] **L'vov M., Uryev E.** Use of modal weight sets for residual modal unbalance assessment of high speed balance quality of flexible rotors. Proceedings of the 10th International Conference on Vibrations in Rotating Machinery, London, 2012.

[3] **Chen Hai-Wei, Ji Wei-Xi, Fan Sheng-Yao** A method for vibration isolation of a vertical axis automatic washing machine with a hydraulic balancer. Journal of Mechanical Science and Technology, Vol. 26, Issue 2, 2012, p. 335-343.

[4] **Chen Hai-Wei, Zhang Qiu-Ju** Stability analyses of a vertical axis automatic washing machine with a hydraulic balancer. Mechanism and Machine Theory, Vol. 46, Issue 7, 2011, p. 910-926.

[5] **Chen Hai-Wei, Zhang Qiu-Ju** Dynamic analysis and design of a balancer for a three-column centrifuge. Shock and Vibration, Vol. 2016, 2016, p. 7957821.

[6] **Jung C. H., Kim C. S., Choi Y. H.** A dynamic model and numerical study on the liquid balancer used in an automatic washing machine. Journal of Mechanical Science and Technology, Vol. 22, Issue 9, 2008, p. 1843-1852.

[7] **Alyokhin S., Petrosov S., Zheltushkin L., Alyokhin A.** Self-balancing equipment of drum-type washing machines. Young scientist USA, Vol. 1, Issue 5, 2014, p. 9-11.

[8] **Royzman V., Bubulis A., Drach I.** System analysis of automatic balancing (self-balancing) machine rotors with liquid working bodies. Solid State Phenomena, Vol. 147, Issue 149, 2009, p. 374-379.

[9] **Rankine W. J.** On the centrifugal whirling of shaft. The Engineer, Vol. 27, 1869, p. 249.

[10] **Stodola A.** Dampf und Gasturbinen. Auflage Edition, Springer, Berlin, 1924, p. 1157.

[11] **Royzman V., Drach I., Bubulis A.** Movement of working fluid in the field of centrifugal forces and forces of weight. Proceedings of the 21st International Scientific Conference: Mechanika, Kaunas, 2016.

[12] **Kushul Ya M.** Self-Oscillations of Rotor. AS USSR, 1963, p. 168.

[13] **Anikeev G. I.** Transitional Almost Periodical Oscillations of Rotors. Nauka, Moscow, 1979, p. 136.

[14] **Ragulskis K. M., Ionushas R. D., Bakshis A. K.** Vibrations of Rotor Systems. Mokslas, Vilnius, 1976, p. 413.

[15] **Siminovskiy V. I.** Steadiness and Nonlinear Oscillations of Rotors of Centrifugal Machines. Kharkiv University, Kharkiv, 1986, p. 120.

[16] **Kalmens Ya V.** Provision of Vibrostability of Rotor Machines on the Basis of Similitude and Modeling Methods. RAN StP., 1992, p. 372.

[17] **Kelzon A. S., Malinin L. M.** Controlling Oscillations of Rotor. Polytechnics, 1992, p. 118.

[18] **Kim Keunjoo, Park Seungchul, Kim Jongryong** Balancing Unit and Laundry Treatment Apparatus. Patent No. EP3085827A1, LG Electronics, 2016.

[19] **Ostdiek Stephen D., Vishal Verma** Laundry Treating Appliance with Balancing System. Patent No. US20120144598A1, Whirlpool Corporation, 2012.

[20] SKF – Automatic balancing units, http://www.skf.com/us/industry-solutions/portable-power-tools/applications/grinders-planners-and-sanders/automatic-balancing-unit/index.html.

[21] **Kim Yong Kwon, Lee Kyu Chai, Ko Hong Seok, Lee Sang Up** Washing Machine, Inner Tub of Washing Machine and Balancer Connection and Assembly Method Thereof. Patent No. US8984918B2 Samsung Electronics Co., 2015.

[22] **Leblanc M.** Automatic balancer for rotating bodies. Patent No. US1209730, Expl Des Procedes Westinghouse Leblanc Sa, 1916.

[23] **Thearle E. L.** A new type of dynamic-balancing machine. Transactions ASME, Vol. 54, 1932, p. 131-141.

[24] **Den Hartor J.-P.** Mechanical Oscillations. Phismathgiz, Moscow, 1960, p. 574, (in Russian).

[25] **Dyer J. B.** Domestic Appliance. Patent No. US2375635A, Motors Liquidation Co, 1945.

[26] **Kasahara M., Kaneko S., Oshita K., Ishii H.** Experiments of liquid motion in a whirling ring. Proceedings of the Dynamics and Design Conference, Tokyo, Japan, 2000.

[27] **Nakamura T.** Study on the improvement of the fluid balancer of washing machines. Proceedings of the 13th Asia-Pacific Vibrations Conference, New Zealand, 2009.

[28] **Bae S., Lee J. M., Kang Y. J., Kang J. S., Yun J. R.** Dynamic analysis of an automatic washing machine with a hydraulic balancer. Journal of Sound and Vibration, Vol. 257, 2002, p. 3-18.

[29] **Majewski T.** Fluid balancer for a washing machine. Proceedings of the 16th International Congress, 2010.

[30] **Urbiola Soto L., Lopez Parra M.** Dynamic performance of the Leblanc balancer for automatic washing machines. Journal of Vibration and Acoustics, Vol. 133, Issue 4, 2011, p. 41014.

[31] **Gusarov A. A.** Balancing Machine Rotors. Book 2, Nauka, Moscow, 2004, p. 266.

[32] **Nesterenko V. P.** Theory and practice of devices for automatic balancing of rotors. Thesis, Novosibirsk Electrical Engineering Institute, Novosibirsk, 1990, p. 24-30.

[33] **Pashkov E., Martyushev N., Ponomarev A.** Efficiency of balancing by liquid-type automatic balancing devices. Advanced Materials Research, Vol. 1040, 2014, p. 858-863.
[34] **Langthjem M. A., Nakamura T.** Dynamics of the fluid balancer: perturbation solution of a forced Korteweg-de Vries-Burgers equation. RIMS, Kyoto University, Vol. 1847, 2013, p. 73-85.
[35] **Marlon Wesley Machado Cunico** Characterization and modelling of Leblanc hydrodynamic stabilizer: a novel approach for steady and transient state models. Modelling and Simulation in Engineering, Vol. 2015, 2015, p. 729582.
[36] **Dimentberg F. M., Shatalov K. T., Husarov A. A.** Oscillations of Machines. Mashinostroenie, Moscow, 1964, p. 256-291.
[37] **Pars L. A.** Analytical Dynamics. Nauka, Moscow, 1971, p. 636.
[38] **Moiseev N., Rumyantsev V.** Dynamics of the Body with Cavities Containing Liquid. Nauka, Moscow, 1965, p. 440, (in Russian).

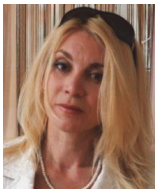

Ilona Drach Ph.D., Associate Professor of the Software Engineering Department of the Khmelnytsky National University. After graduation from Ivan Franko Lviv State University she was qualified as a mathematician. In 2008 she defended his thesis. In 2010 awarded the title of Associate Professor. Scientific interests: engineering (balancing, reducing vibration), mathematics, mathematical modelling.

Vilen Royzman received Doctoral degree in Machine Engineering Institute of Science Academy of USSR, Moscow, Russia, in 1979. In 1980 he received title of Professor. Now he works at Khmelnytsky National University as Head of Department of Telecommunication and Radio Engineering. His current research interests include vibrations, rotor balancing, inverse problems and strength in electronics.

Vitalii Tkachuk Ph.D. of the Engineering. Born in 1981 in the Khmelnytsky region. In the period of 1998-2003 he studied at the Khmelnytsky National University. In 2011 he defended his thesis. In 2014 awarded the title of Associate Professor. Works as the Associate Professor of Department of Engineering Techniques, Khmelnitskiy National University. Scientific interests: balancing, reducing vibration, engineering analysis, CNC machines

Andrii Goroshko received Doctoral degree of dynamics and strength of machines in Lviv Polytechnic National University in 2017. Now he works at Khmelnytsky National University as Professor of Department of Physics and Electrical Engineering. His current research interests include vibrations, rotor balancing, strength, inverse problems, statistics.

2.2. Spindle units on rolling bearings diagnostics by indirect measurement of spindle vibration

Yuriy Danylchenko[1], Andriy Petryshyn[2]
National Technical University of Ukraine "Igor Sikorsky Kyiv Polytechnic Institute", Kyiv, Ukraine
E-mail: [1]*yumd@i.ua*, [2]*m.p3shka.a.i@gmail.com*

Abstract. A method of indirect measurement of spindle vibrations based on the results of measuring the vibrations of the spindle unit housing and theoretical compliance function has been developed. Method is based on performing experimental and theoretical studies of the spindle unit dynamic behavior, mounted on a special test rig with a low natural frequency. Test rig consists of the frame, elastically fixed on a massive foundation and spindle unit that is attached to the frame. Dynamic model of the test rig is presented in a form of a complex vibratory mechanical system which consists of four subsystems. For system decomposition, method of dynamic compliance is used, and for subsystems dynamic characteristics calculation-transfer matrix method. Theoretical compliance function is considered as the ratio of dynamic compliances of the subsystems at the points of calculation and measurement of vibrations. This method was used for assembling and manufacturing faults diagnostic of spindle units on rolling bearings that cause low-frequency vibrations and its effectiveness has been confirmed.

Keywords: spindle unit, rolling bearings, assembling and manufacturing faults, vibration diagnostic, mechanical vibratory system, dynamical compliance.

1. Introduction

The most common methods for rotary machines technical condition evaluation, including spindle units, are methods of vibration diagnostic.

The advantages of these methods are explained by the sufficiently high degree of mechanical vibrations determinacy in frequency composition, which allows us to perform identification their causes and sources with sufficient confidence.

In the vibrations spectrum of the rotor mounted on rolling bearings, it is possible to distinguish 4 main ranges that characterize [1]: 1) the presence and magnitude of the imbalance (vibration with a frequency equal to the rotor running speed); 2) bearings misalignment due to assembling faults or external loads on the rotor (vibration with a rotor running speed and twice rotor running speed frequency); 3) quality of the rotary drive (vibration at the characteristic frequencies of rotary drive); 4) manufacturing defects of races and rolling elements (so-called "bearing vibrations" associated with frequencies, determined by the bearing kinematics). Vibration diagnostics methodology of rotor systems is based on the evaluation of the vibration magnitude at these frequencies.

Vibration diagnostics systems of spindle units (SU) of modern metal-cutting machines are aimed at spindle error motion control [2-4] and fault detection of its bearings [5, 6].

Modern methods of spindle error motion control are built on the patterns of non-contact measurement of spindle linear displacements on the reference surface for measurements of a spindle or artifact [3, 4]. In this case, it is necessary to extract from the measurement results a component, which is caused by the error on reference surface for measurements. The accuracy of the spindle error motion determining depends on the method of solving this problem [4]. This is especially true for precision SU, the error motion of which is commensurable with the error on reference surface for measurements [7]. Such a procedure for spindle error motion determination requires ensuring special conditions for the measurement, which makes it problematic to use for error motion determination of fixed in spindle workpiece or tool, in the cutting zone during machining. An alternative to direct measurement of spindle vibrations can be the measurement of vibrations on the spindle unit housing unit with subsequent identification of these vibrations according to the theoretically established compliance function.

The most commonly used type in SU are rolling bearings. The vibration signal of a faulty rolling bearing includes deterministic signals, bearing element defect signals and noise [8]. Deterministic signals are, as a rule, low-frequency signals caused manufacturing faults of recess and rolling elements of bearings. The fault signals of the bearing elements are periodic resonance vibrations of the carrier elements resulting from short pulses generated each time the defect hits its matched element [5]. It is this difference in signals that makes it possible to extract signals of bearing elements faults from the general signal. This difference also determines the effectiveness of methods for condition monitoring and fault diagnostics of rolling bearings [9].

The most effective methods for bearing faults diagnostics are methods of high-frequency excitation, known as high frequency resonance technique (HFRT), which is also known as envelope analysis, and shock pulse method (SPM) [5, 8, 9]. The use of low-frequency excitation to detect faults in of low-speed bearings elements is considered almost impossible. The main reason for this considered to be limitation on the energy level, generated by faults in the bearing elements [10].

The carried-out analysis indicates significant advantages of vibration diagnostics of the SU from measurements of vibrations in resonant zones and the prospects of creating tools and methods for conducting such diagnostics.

This study is devoted to the development of a method for indirect measurement of spindle vibrations and its application for estimating assembling and manufacturing faults of the SU on rolling supports.

2. The main idea of the method of indirect measurement of spindle vibrations

The method of indirect measurement of the spindle vibrations is based on measuring the vibrations on the spindle unit housing with the subsequent calculation of the spindle axis vibration (fixed in the spindle mandrel) according to the theoretical compliance function $W(\omega)$. For the measurement schemes shown in Fig. 1, compliance function $W(\omega)$ associates the spindle housing vibrations, at the place of measurement (position 1) and the axis of the tool mandrel (position 2).

In common case compliance function $W(\omega)$ is defined as:

$$W(\omega) = \frac{q_2(\omega)}{q_1(\omega)}, \tag{1}$$

where $q_2(\omega)$ and $q_1(\omega)$ – calculated functions of tool holder displacement at point 2 and the spindle housing at point 1 under unit harmonic force applied at point 3 (Fig. 1); ω – excitation frequency.

The position of point 3 is determined by the objective. In case of evaluating assembling and manufacturing faults of the SU on rolling-contact bearings, point 3 is located on the axis of the spindle under the leading bearing (Fig. 1(a)). In case of evaluating spindle error motion during machining, point 3 is placed on the axis of the tool holder under cutting zone, that is, the positions of points 2 and 3 coincide (Fig. 1(b)).

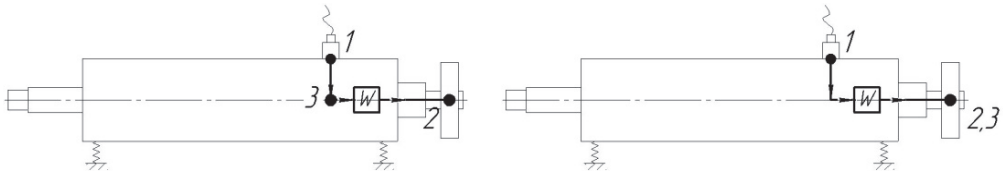

a) b)

Fig. 1. Measurement scheme for the assembling and manufacturing faults estimation of SU on rolling bearings a) and spindle vibrations b): 1 – point of vibration measurement of the spindle housing; 2 – point of vibration calculation of the spindle axis (tool-holder); 3 – point of the unit harmonic force application

Vibration spectrum calculation of the tool-holder from measured vibrations of the spindle housing is performed according to:

$$A_2(\omega_i) = A_1(\omega_i) \cdot W(\omega_i), \quad (2)$$

where $A_1(\omega_i)$ and $A_2(\omega_i)$ – amplitudes of the i-th spectral components of the experimental vibrations spectrum of the spindle housing and theoretical vibration spectrum tool-older axis, respectively.

These are the spectrums of absolute vibrations. Axis vibration spectrum of the tool-holder relative to the spindle housing is obtained as a result of vector subtraction of the corresponding spectrums of absolute vibrations taking into account phase angles of the spectral components.

Proposed theoretical-experimental method allows simplifying the procedure for spindle unit condition monitoring and evaluation. In addition, it does not require the use of high-precision measuring surfaces for spindle vibration determination.

3. Test rig

3.1. Test rig design

When evaluating level of vibrations at characteristic frequencies, it should not be forgotten that there is a complex interaction of disturbing forces in the bearing with natural frequencies of the entire unit [11].

However, this SU property can be used to detect the incipient faults of the rolling bearings [12]. For this, it is necessary that the frequencies of the shock pulses that occur when the faults of the bearing elements periodically enter the contact zone coincide with the same resonant frequency of the mechanical system.

In turn, it should be noted that the resonant frequencies of the spindle units are quite high. For example, for a vertical milling machine [13], the first natural frequency of the spindle head is 315 Hz, and the spindle frequency is 1410 Hz. Such values of natural frequencies do not allow using the results of measuring resonance vibrations of the machine units for diagnostic of faults that cause low-frequency vibrations. However, this can be realized on special test rigs, with sufficiently lower natural frequencies of the carrier elements [14].

Test rig [14] is a frame elastically mounted on a massive foundation, with the possibility of oscillating motion in a vertical plane. The angular stiffness of the frame is regulated by changing the working length of the spring or by installing a rigid beam instead. By adjusting the angular rigidity of the frame, it is possible to change the value of its first natural frequency in the range 5-37 Hz. Spindle unit is elastically mounted on the frame. Test rig design is shown in Fig. 2.

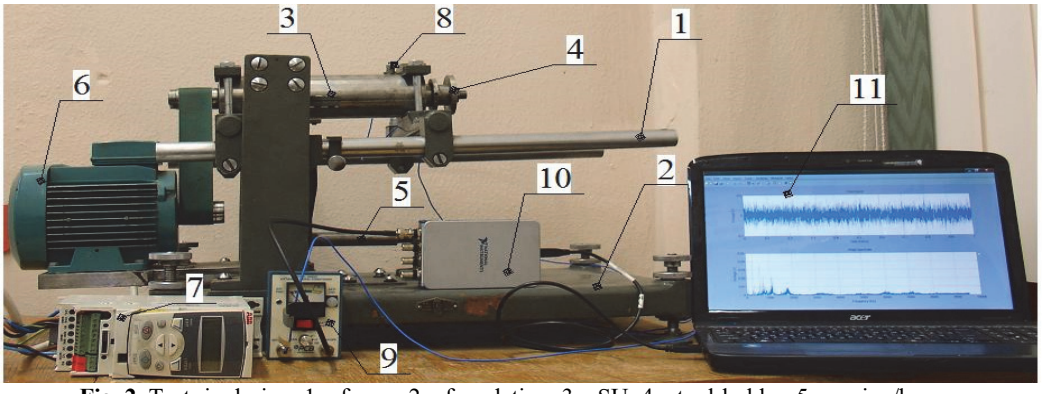

Fig. 2. Test rig design: 1 – frame; 2 – foundation; 3 – SU; 4 – tool-holder; 5 – spring/beam; 6 – motor; 7 – frequency converter; 8 – sensor; 9 – amplifier; 10 – AD converter; 11 – PC

4. Test rig dynamic model

The implementation of the method of indirect measuring of spindle vibrations on a test rig requires determination of its dynamic characteristics. In order to perform that, it is necessary to create its dynamic model and experimentally confirm its adequacy.

When studying the dynamic behavior of complex mechanical systems, it is considered reasonable to separate them (decomposition) into simpler subsystems [15, 16]. Separation of subsystems from each other is ensured either by the introduction of additional connections that prohibit movement of common points (nodes) of subsystems (dynamic stiffness method) or, on the contrary, by eliminating constrains between them (method of dynamic compliances).

For rotary machines dynamic characteristics calculation, where SU belongs to, it is more convenient to use the method of dynamic compliances [16]. When system is decomposed using the method of dynamic compliances, harmonic reactions are applied to the discarded constrains, which are then determined from the deformation compatibility condition of subsystems, that is, the conditions for the amplitude balance of generalized displacements (linear and angular) at the separation points of the subsystems.

The sequence of dynamic model development of the mechanical vibratory system that includes several subsystems is described in detail in [17].

Using the recommendations of [17], we will present a test rig with a mounted SU in the form of a mechanical vibratory system which consists of 4 subsystems (Fig. 3).

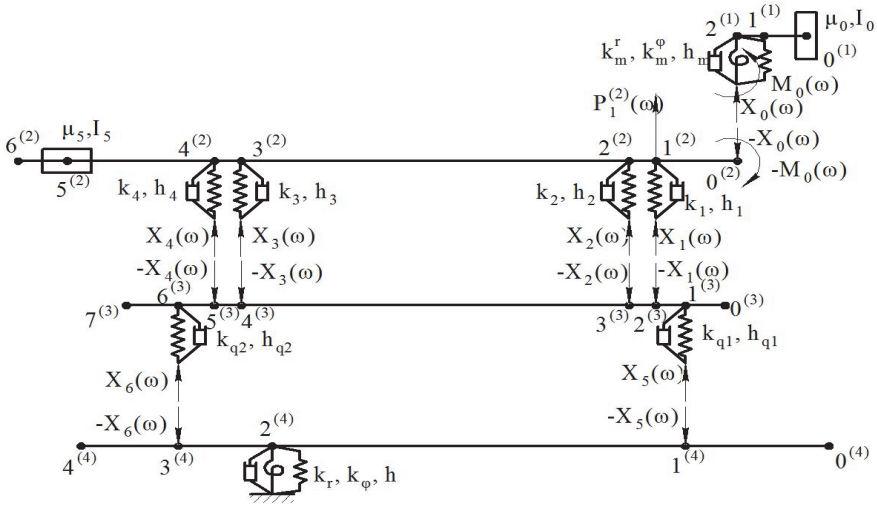

Fig. 3. Design models of test rig subsystems

First subsystem (tool-holder, index $s = 1$) is considered as a beam, that consists of two sections with distributed mass. On the front end of tool-holder (cross-section $0^{(1)}$) concentrated weight is located (disc). In section $2^{(1)}$ the tool-holder is connected with spindle (spindle cross-section $0^{(2)}$), which is taken into account by an elastic connection with radial k_m^r and angular k_m^ϕ stiffness.

Second subsystem (spindle, index $s = 2$) is considered as a beam, which consists of six sections with distributed mass. In cross-sections $1^{(2)}$, $2^{(2)}$, $3^{(2)}$ and $4^{(2)}$ bearings are located, which is taken into account by elastic connections of spindle and spindle housing with stiffness k_1, k_2, k_3 and k_4 accordingly. In cross-section $5^{(2)}$ concentrated weight is located (pulley wheel).

Third subsystem (spindle housing, index $s = 3$) is considered as a hollow beam, which consists of seven sections with distributed mass. In cross-sections $2^{(3)}$, $3^{(3)}$, $4^{(3)}$ and $5^{(3)}$ spindle housing is connected with spindle. In cross-sections $1^{(3)}$ and $6^{(3)}$ its connected to the frame, that

is taken into account by supports with stiffness k_{q1} and k_{q2}.

Fourth subsystem (frame, index $s = 4$) is considered as an equivalent beam, which consists of four sections with distributed mass. In cross-sections $1^{(4)}$, $3^{(4)}$ of the frame spindle unit is mounted, in cross-section $2^{(4)}$ radial and angular joins is located, which connect frame with test rig foundation, and taken into account by radial k_r and angular k_ϕ stiffness.

The connections of the subsystems are: connection of tool-holder with spindle for subsystems 1 and 2; spindle bearings for subsystems 2 and 3; fixtures for subsystems 3 and 4. All connections have elastic and dissipative properties.

To determine the compliance functions $W(\omega)$ for different system elements vibrations, design model (Fig. 3) should take into account the necessity of a unit harmonic load $P_i^{(s)}(\omega) = 1 \cdot \sin\omega t$ application at certain points of the subsystems. Thus, the scheme shown in Fig. 3 is designed to solve the problem of assembling and manufacturing faults estimation of SU (Fig. 1(a)). Therefore, in the design model (Fig. 3) a unit harmonic load $P_1^{(2)}(\omega) = 1 \cdot \sin\omega t$ is applied to the spindle section.

According to decomposition scheme (Fig. 3), deformation compatibility conditions in subsystem separation points are:

– For subsystems 1 and 2:

$$\begin{cases} \alpha_{00}^{12}X_0 + \gamma_{00}^{12}M_0 - \alpha_{01}^{(2)}X_1 - \alpha_{02}^{(2)}X_2 - \alpha_{03}^{(2)}X_3 - \alpha_{04}^{(2)}X_4 = \alpha_{0P}^{(2)}, \\ \beta_{00}^{12}X_0 + \phi_{00}^{12}M_0 - \beta_{01}^{(2)}X_1 - \beta_{02}^{(2)}X_2 - \beta_{03}^{(2)}X_3 - \beta_{04}^{(2)}X_4 = \beta_{0P}^{(2)}. \end{cases} \quad (3)$$

– For subsystems 2 and 3:

$$\begin{cases} -\alpha_{10}^{(2)}X_0 - \gamma_{10}^{(2)}M_0 + \alpha_{11}^{23}X_1 + \alpha_{12}^{23}X_2 + \alpha_{13}^{23}X_3 + \alpha_{14}^{23}X_4 - \alpha_{21}^{(3)}X_5 - \alpha_{26}^{(3)}X_6 = -\alpha_{1P}^{(2)}, \\ -\alpha_{20}^{(2)}X_0 - \gamma_{20}^{(2)}M_0 + \alpha_{21}^{23}X_1 + \alpha_{22}^{23}X_2 + \alpha_{23}^{23}X_3 + \alpha_{24}^{23}X_4 - \alpha_{31}^{(3)}X_5 - \alpha_{36}^{(3)}X_6 = -\alpha_{2P}^{(2)}, \\ -\alpha_{30}^{(2)}X_0 - \gamma_{30}^{(2)}M_0 + \alpha_{31}^{23}X_1 + \alpha_{32}^{23}X_2 + \alpha_{33}^{23}X_3 + \alpha_{34}^{23}X_4 - \alpha_{41}^{(3)}X_5 - \alpha_{46}^{(3)}X_6 = -\alpha_{3P}^{(2)}, \\ -\alpha_{40}^{(2)}X_0 - \gamma_{40}^{(2)}M_0 + \alpha_{41}^{23}X_1 + \alpha_{42}^{23}X_2 + \alpha_{43}^{23}X_3 + \alpha_{44}^{23}X_4 - \alpha_{51}^{(3)}X_5 - \alpha_{56}^{(3)}X_6 = -\alpha_{4P}^{(2)}. \end{cases} \quad (4)$$

– For subsystems 3 and 4:

$$\begin{cases} -\alpha_{12}^{(3)}X_1 - \alpha_{13}^{(3)}X_2 - \alpha_{14}^{(3)}X_3 - \alpha_{15}^{(3)}X_4 + \alpha_{11}^{34}X_5 + \alpha_{16}^{34}X_6 = 0, \\ -\alpha_{62}^{(3)}X_1 - \alpha_{63}^{(3)}X_2 - \alpha_{64}^{(3)}X_3 - \alpha_{65}^{(3)}X_4 + \alpha_{61}^{34}X_5 + \alpha_{66}^{34}X_6 = 0, \end{cases} \quad (5)$$

or in a matrix form:

$$[\mathbf{D}(\omega)] \cdot \mathbf{F} = \Delta_{\mathbf{P}}, \quad (6)$$

where X_i, M_i – harmonic reactions in discarded connections; $\alpha_{ij}^{(s)}$, $\beta_{ij}^{(s)}$, $\gamma_{ij}^{(s)}$, $\phi_{ij}^{(s)}$ – dynamic compliances of subsystems s: $\alpha_{ij}^{(s)}$ and $\beta_{ij}^{(s)}$ – accordingly displacement and angle of rotation in point i from unit harmonic force applied in point j; $\gamma_{ij}^{(s)}$ and $\phi_{ij}^{(s)}$ – accordingly displacement and angle of rotation in point i from unit harmonic moment applied in point j; $\alpha_{iP}^{(2)}$ and $\beta_{iP}^{(2)}$ – generalized displacements (linear and angular) from unit harmonic load $P_1^{(2)}$, $\alpha_{iP}^{(2)} = \alpha_{i1}^{(2)}P_1^{(2)}$, $\beta_{0P}^{(2)} = \beta_{01}^{(2)}P_1^{(2)}$, $i = 0, 1, 2, 3, 4$; $\mathbf{R}$ – vector of harmonic reactions in discarded connections, $\mathbf{R} = (X_0, M_0, X_1, X_2, X_3, X_4, X_5, X_6)^T$; $\Delta_{\mathbf{P}}$ – generalized displacements vector:

$$\Delta_{\mathbf{P}} = \left(\alpha_{0P}^{(2)}, \beta_{0P}^{(2)}, -\alpha_{1P}^{(2)}, -\alpha_{2P}^{(2)}, -\alpha_{3P}^{(2)}, -\alpha_{4P}^{(2)}, 0, 0\right)^T,$$

and $[\mathbf{D}(\omega)]$ – dynamic compliance martix:

$$\mathbf{D}(\omega)=\begin{pmatrix} \alpha_{00}^{12} & \gamma_{00}^{12} & -\alpha_{01}^{(2)} & -\alpha_{02}^{(2)} & -\alpha_{03}^{(2)} & -\alpha_{04}^{(2)} & 0 & 0 \\ \beta_{00}^{12} & \phi_{00}^{12} & -\beta_{01}^{(2)} & -\beta_{02}^{(2)} & -\beta_{03}^{(2)} & -\beta_{04}^{(2)} & 0 & 0 \\ -\alpha_{10}^{(2)} & -\gamma_{10}^{(2)} & \alpha_{11}^{23} & \alpha_{12}^{23} & \alpha_{13}^{23} & \alpha_{14}^{23} & -\alpha_{21}^{(3)} & -\alpha_{26}^{(3)} \\ -\alpha_{20}^{(2)} & -\gamma_{20}^{(2)} & \alpha_{21}^{23} & \alpha_{22}^{23} & \alpha_{23}^{23} & \alpha_{24}^{23} & -\alpha_{31}^{(3)} & -\alpha_{36}^{(3)} \\ -\alpha_{30}^{(2)} & -\gamma_{30}^{(2)} & \alpha_{31}^{23} & \alpha_{32}^{23} & \alpha_{33}^{23} & \alpha_{34}^{23} & -\alpha_{41}^{(3)} & -\alpha_{46}^{(3)} \\ -\alpha_{40}^{(2)} & -\gamma_{40}^{(2)} & \alpha_{41}^{23} & \alpha_{42}^{23} & \alpha_{43}^{23} & \alpha_{44}^{23} & -\alpha_{51}^{(3)} & -\alpha_{56}^{(3)} \\ 0 & 0 & -\alpha_{12}^{(3)} & -\alpha_{13}^{(3)} & -\alpha_{14}^{(3)} & -\alpha_{15}^{(3)} & \alpha_{11}^{34} & \alpha_{16}^{34} \\ 0 & 0 & -\alpha_{62}^{(3)} & -\alpha_{63}^{(3)} & -\alpha_{64}^{(3)} & -\alpha_{65}^{(3)} & \alpha_{61}^{34} & \alpha_{66}^{34} \end{pmatrix}, \quad (7)$$

where:

$$\alpha_{00}^{12}=\alpha_{22}^{(1)}+\alpha_{00}^{(2)}+\frac{1}{k_m^r},\quad \beta_{00}^{12}=\beta_{22}^{(1)}+\beta_{00}^{(2)},\quad \gamma_{00}^{12}=\gamma_{22}^{(1)}+\gamma_{00}^{(2)},$$
$$\phi_{00}^{12}=\phi_{22}^{(1)}+\phi_{00}^{(2)}+\frac{1}{k_m^{\phi}},\quad \alpha_{11}^{23}=\alpha_{11}^{(2)}+\alpha_{22}^{(3)}+\frac{1}{k_1},\quad \alpha_{12}^{23}=\alpha_{12}^{(2)}+\alpha_{23}^{(3)},$$
$$\alpha_{13}^{23}=\alpha_{13}^{(2)}+\alpha_{24}^{(3)},\quad \alpha_{14}^{23}=\alpha_{14}^{(2)}+\alpha_{25}^{(3)},\quad \alpha_{21}^{23}=\alpha_{21}^{(2)}+\alpha_{32}^{(3)},$$
$$\alpha_{22}^{23}=\alpha_{22}^{(2)}+\alpha_{33}^{(3)}+\frac{1}{k_2},\quad \alpha_{23}^{23}=\alpha_{23}^{(2)}+\alpha_{34}^{(3)},\quad \alpha_{24}^{23}=\alpha_{24}^{(2)}+\alpha_{35}^{(3)},$$
$$\alpha_{31}^{23}=\alpha_{31}^{(2)}+\alpha_{42}^{(3)},\quad \alpha_{32}^{23}=\alpha_{32}^{(2)}+\alpha_{43}^{(3)},\quad \alpha_{33}^{23}=\alpha_{33}^{(2)}+\alpha_{44}^{(3)}+\frac{1}{k_3},$$
$$\alpha_{34}^{23}=\alpha_{34}^{(2)}+\alpha_{45}^{(3)},\quad \alpha_{41}^{23}=\alpha_{41}^{(2)}+\alpha_{52}^{(3)},\quad \alpha_{42}^{23}=\alpha_{42}^{(2)}+\alpha_{53}^{(3)},$$
$$\alpha_{43}^{23}=\alpha_{43}^{(2)}+\alpha_{54}^{(3)},\quad \alpha_{44}^{23}=\alpha_{44}^{(2)}+\alpha_{55}^{(3)}+\frac{1}{k_4},\quad \alpha_{11}^{34}=\alpha_{11}^{(3)}+\alpha_{11}^{(4)}+\frac{1}{k_{q1}},$$
$$\alpha_{16}^{34}=\alpha_{16}^{(3)}+\alpha_{13}^{(4)},\quad \alpha_{61}^{34}=\alpha_{61}^{(3)}+\alpha_{31}^{(4)},\quad \alpha_{66}^{34}=\alpha_{66}^{(3)}+\alpha_{33}^{(4)}+\frac{1}{k_{q2}}.$$

Dynamic compliances $\alpha_{ij}^{(s)}$, $\beta_{ij}^{(s)}$, $\gamma_{ij}^{(s)}$, $\phi_{ij}^{(s)}$ are determined according to methodology, presented in [17] using the transfer matrix method [18, 19].

Subsystems transfer matrices $\Pi^{(s)}$ are written in accordance with decomposition scheme (Fig. 3) by the methodology [17]:

For tool-holder ($s=1, u=2$):

$$\Pi^{(1)}=\prod_{i=2}^{0}\Pi_i^{(1)}=\mathbf{U}_2^{(1)}\cdot\mathbf{U}_1^{(1)}\cdot\mathbf{G}_0^{(1)}. \quad (8)$$

For spindle ($s=2, u=6$):

$$\Pi^{(2)}=\prod_{i=6}^{0}\Pi_i^{(2)}=\mathbf{U}_6^{(2)}\cdot\mathbf{G}_5^{(2)}\cdot\mathbf{U}_5^{(2)}\cdot\mathbf{U}_4^{(2)}\cdot\mathbf{U}_3^{(2)}\cdot\mathbf{U}_2^{(2)}\cdot\mathbf{U}_1^{(2)}. \quad (9)$$

For spindle housing ($s=3, u=7$):

$$\Pi^{(3)} = \prod_{i=7}^{0} \Pi_i^{(3)} = \mathbf{U}_7^{(3)} \cdot \mathbf{U}_6^{(3)} \cdot \mathbf{U}_5^{(3)} \cdot \mathbf{U}_4^{(3)} \cdot \mathbf{U}_3^{(3)} \cdot \mathbf{U}_2^{(3)} \cdot \mathbf{U}_1^{(3)}. \quad (10)$$

For frame ($s = 4$, $u = 4$):

$$\Pi^{(4)} = \prod_{i=4}^{0} \Pi_i^{(4)} = \mathbf{U}_4^{(4)} \cdot \mathbf{U}_3^{(4)} \cdot \mathbf{R}_2^{(4)} \cdot \mathbf{U}_2^{(4)} \cdot \mathbf{U}_1^{(4)}, \quad (11)$$

where $\Pi^{(s)}$ – transfer matrix of the beam system, equal to the product of transfer matrices of all sections between the u-th and the 0-th sections of the system's beam, $\Pi^{(s)} = \prod_{i=u}^{0} \Pi_i^{(s)}$; $\Pi_i^{(s)}$ - transfer matrix of the i-th section, equal to the product of all transfer matrices on this section, $\Pi_i^{(s)} = \mathbf{G}_i^{(s)} \cdot \mathbf{R}_i^{(s)} \cdot \mathbf{U}_i^{(s)}$; $\mathbf{G}_i$ – mass-inertia matrix of the concentrated weight; $\mathbf{R}_i$ – matrix of elastic-dissipative linear and angular support; $\mathbf{U}_i$ – matrix of the beam section with distributed mass, i – number of the subsystem section; u– general number of subsystem sections. Transfer matrices $\mathbf{G}_i$, $\mathbf{R}_i$ and $\mathbf{U}_i$ are determined by dependencies [18, 19].

From the system of equations (6), the reactions of the discarded connections are determined, and then the amplitudes $q_i^{(s)}$ ($i = 0,\ldots,u$) of the transverse (radial) displacements of the characteristic points of the subsystems:

Tool-holder ($s = 1$, $i = 0,\ldots,2$):

$$q_i^{(1)} = \alpha_{i2}^{(1)} X_0 + \gamma_{i2}^{(1)} M_0. \quad (12)$$

Spindle ($s = 2$, $i = 0,\ldots,6$):

$$q_{\mathrm{i}}^{(2)} = -\alpha_{\mathrm{i}0}^{(2)} X_0 - \gamma_{\mathrm{i}0}^{(2)} M_0 + \alpha_{\mathrm{i}1}^{(2)} X_1 + \alpha_{\mathrm{i}2}^{(2)} X_2 + \alpha_{\mathrm{i}3}^{(2)} X_3 + \alpha_{\mathrm{i}4}^{(2)} X_4 + \alpha_{\mathrm{i}1}^{(2)} P_1^{(2)}. \quad (13)$$

Spindle housing ($s = 3$, $i = 0,\ldots,7$):

$$q_i^{(3)} = -\alpha_{i2}^{(3)} X_1 - \alpha_{i3}^{(3)} X_2 - \alpha_{i4}^{(3)} X_3 - \alpha_{i5}^{(3)} X_4 + \alpha_{i5}^{(3)} X_5 + \alpha_{i6}^{(3)} X_6. \quad (14)$$

Frame ($s = 4$, $i = 0,\ldots,4$):

$$q_i^{(4)} = -\alpha_{i1}^{(4)} X_5 - \alpha_{i3}^{(4)} X_6. \quad (15)$$

Compliance function $W(\omega)_{13}$, connecting the vibration of the point $0^{(1)}$ of the tool-holder subsystem ($s = 1$) with the vibrations of the spindle housing ($s = 3$) at the point $2^{(3)}$ under unit harmonic load applied at this point (Fig. 3) is determined as:

$$W(\omega)_{13} = \frac{q_0^{(1)}(\omega)}{q_2^{(3)}(\omega)} = \frac{\alpha_{02}^{(1)} X_0 + \gamma_{02}^{(1)} M_0}{-\alpha_{22}^{(3)} X_1 - \alpha_{23}^{(3)} X_2 - \alpha_{24}^{(3)} X_3 - \alpha_{25}^{(3)} X_4 + \alpha_{25}^{(3)} X_5 + \alpha_{26}^{(3)} X_6}. \quad (16)$$

4.1. Experimental verification of the test rig dynamic model adequacy

As the tested SU grinding head were taken. The SU housing is made in the form of a quill with an external diameter of 65 mm and a length of 250 mm. The spindle shaft is mounted on duplex angular-contact ball bearings type 7004, assembled according to the "tandem-X" scheme.

Measurement of vibration at the test rig was carried out using a piezoelectric accelerometer. PCB 353B15 and amplifier PCB 480E09. The signal was registered using the NI USB-9215 AD

converter and processed in Matlab.

The experimental verification consists in obtaining and analyzing of system harmonic response to the impact load. Studies were carried out for four different versions of the system: 1) test rig with mounted SU and attached tool-holder, the angular rigidity of the system is set by an extension spring; 2) test rig without SU, angular rigidity of system is set by an extension spring; 3) stand with mounted SU and attached tool-holder, the angular rigidity of the system is set by a rigid beam, installed instead of a spring; 4) stand without SU, angular rigidity of system is set by a rigid beam, installed instead of a spring.

For the first and third versions, measurement were taken at the end of the tool-holder (Fig. 4(a)), the impulse load was applied to the frame.

For the second and fourth variants, measurements were taken at the place where the spindle unit was attached to the frame (Fig. 4(b)).

The natural frequencies values of the test rig with mounted SU (Fig. 4(a)) are determined using Eq. (7) from the condition $det[\mathbf{D}(\omega)] = 0$. Natural frequencies of the frame (Fig. 4(b)) are determined from the calculation of frame transfer matrix Eq. (11) using the dependency given in [19].

The results of comparison are shown in Fig. 5. $P_i^{(s)}$ ith natural frequency of the subsystem s. The left values of the natural frequency correspond to the experimental values, the right ones – calculated.

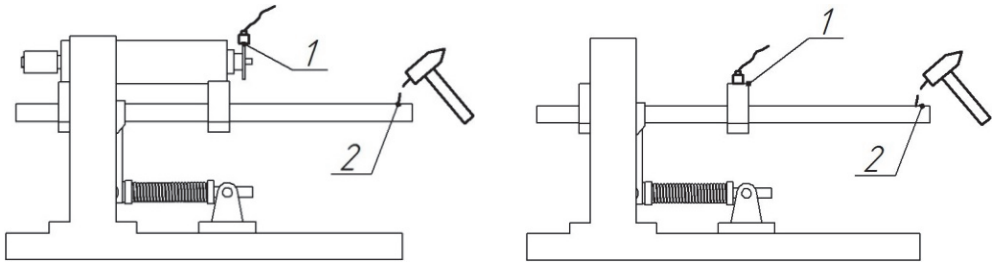

a) b)

Fig. 4. Schemes for the sensor installation and applied impact load for measuring natural frequencies spectrum of the system: 1 – sensor, 2 – place of load application

5. An example of using the method of indirect measurement of spindle vibrations

5.1. The research procedure at estimation of assembling and manufacturing faults of SU on rolling bearings

The use of the method involves experimental and theoretical studies of dynamic behavior of the SU, mounted on the test rig.

The experimental part of the study (Fig. 1(a)) provides:

1. Determination of the first natural frequency $P_1^{(4)}$ of the test rig frame ($P_1^{(4)} = 33$ Hz, Fig. 5(c)).

2. Determination of the spindle rotation frequencies corresponding to the conditions for the resonance vibrations of the frame due to occurrence of assembling and manufacturing faults of the SU.

3. Measurement of spindle housing vibrations at these speeds.

The spindle rotation frequencies at which the resonance vibrations of the frame occurs are determined by the condition of the frame first natural frequency matching with the frequencies of the forced vibrations caused by assembling and manufacturing faults of the SU on rolling bearings. The characteristic frequencies of forced vibrations and rotational speeds of the spindle, corresponding to the conditions of frame resonance vibrations, are given in Table 1.

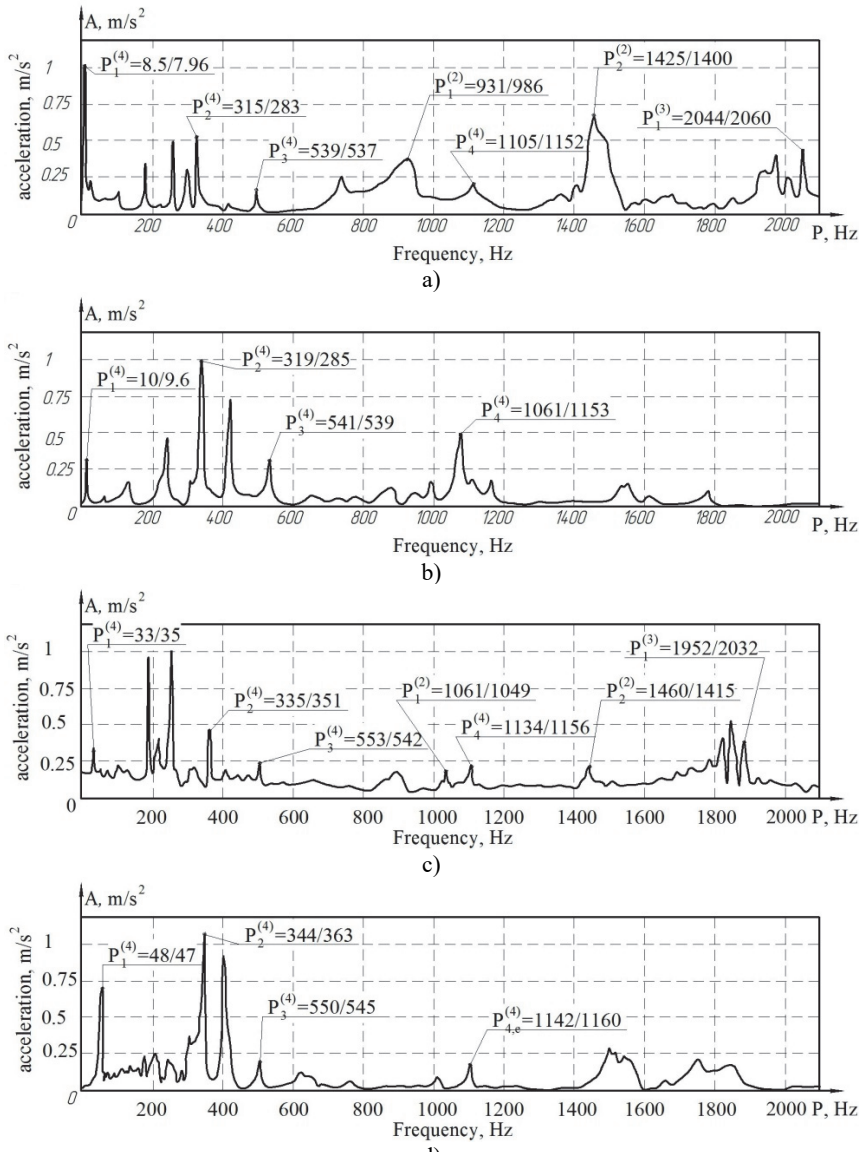

Fig. 5. Natural frequencies spectrums of the test rig for different variants of test rig:
a) with extension spring and SU; b) with extension spring without SU;
c) with rigid beam and SU; d) with rigid beam without SU

Theoretical part of the study:

1. Calculation of the displacement functions of $q_0^{(1)}(\omega)$ and $q_2^{(3)}(\omega)$ of point $0^{(1)}$ (tool-holder) and point $2^{(3)}$ (spindle housing) under unit harmonic load applied to the spindle at the location of the front support leading bearing (point $1^{(2)}$). These functions, in fact, are dynamic compliances of the tool-holder and spindle housing subsystems and can be calculated from the Eq. (12) and Eq. (14).

2. Calculation of the compliance function $W(\omega)_{13}$ that connects vibration of points $0^{(1)}$of the tool-holder and point $2^{(3)}$of the spindle housing Eq. (16).

3. Calculation of tool-holder axis vibration spectrum at characteristic frequencies of spindle

(Table 1), according to experimental vibration spectrum of spindle housing Eq. (2).

4. Calculation of the spectrum of tool-holder and spindle housing relative vibration and determination of relative vibration amplitudes of tool-holder point $0^{(1)}$ at characteristic frequencies of forced vibrations.

Table 1. Main frequencies of forced vibrations caused by assembling and manufacturing faults of SU on rolling bearings

No.	Forced vibration frequency	Spindle rotation frequency f_r corresponding to the frame resonance vibrations $P_1^{(4)}$, Hz
1	Spindle rotation frequency, f_r	$f_{r1} = 33$
2	Spindle double rotation frequency, $2f_r$	$f_{r2} = 16.5$
3	Spindle triple rotation frequency,$3f_r$	$f_{r3} = 11$
4	FTF, $f_{FTF} = \frac{1}{2} \cdot f_r \cdot \left(1 - \frac{d_{Bd}}{d_{Pd}} \cdot \cos\theta\right)$	$f_{r4} = 85.77$
5	BPFO, $f_{BPFO} = f_{FTF} \cdot Nb$	$f_{r5} = 9.55$
6	BPFI, $f_{BPFI} = (f_r - f_{FTF}) \cdot Nb$	$f_{r6} = 5.96$
7	BSF, $f_{BSF} = \frac{1}{2} \cdot f_r \cdot \frac{d_{Pd}}{d_{Bd}} \cdot \left(1 - \frac{d_{Bd}^2}{d_{Pd}^2} \cdot \cos^2\theta\right)$	$f_{r7} = 16.1$
Note: d_{Bd} – ball or roller diameter, mm; Nb – number of rolling elements in one row; d_{Pd} – bearing pitch diameter, mm; θ – bearing contact angle.		

5.2. Research results

Results of theoretical determination of tool-holder and spindle housing dynamic characteristics are shown in Figs. 6-9.

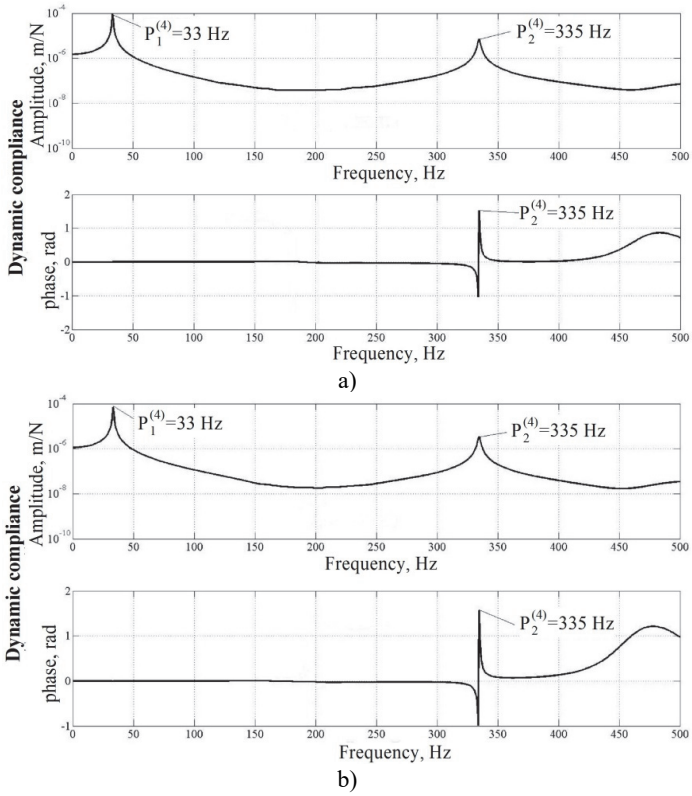

Fig. 6. a) Dynamic compliances of tool-holder and b) spindle housing

Fig. 6 presents the amplitude-frequency and phase-frequency characteristics of the tool-holder $q_0^{(1)}(\omega)$ and spindle housing $q_2^{(3)}(\omega)$ dynamic compliances. Fig. 7 illustrates the amplitude-frequency and phase-frequency characteristics of the compliance function. Fig. 8 illustrates experimentally obtained spectrum of the spindle housing absolute vibrations at point $2^{(3)}$ and the corresponding calculated spectrum of the tool-holder absolute vibrations at point $1^{(2)}$ and obtained at spindle speed $n = 660$ RPM ($f_r = 11$ Hz). Fig. 9 shows the calculated spectrum of the relative vibrations of the tool-holder end at spindle speed corresponding to the frame resonances at characteristic frequencies of assembling and manufacturing faults of the SU.

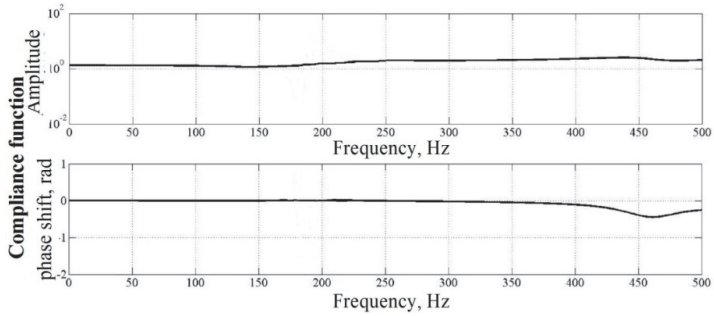

Fig. 7. Compliance function $W(\omega)_{13}$

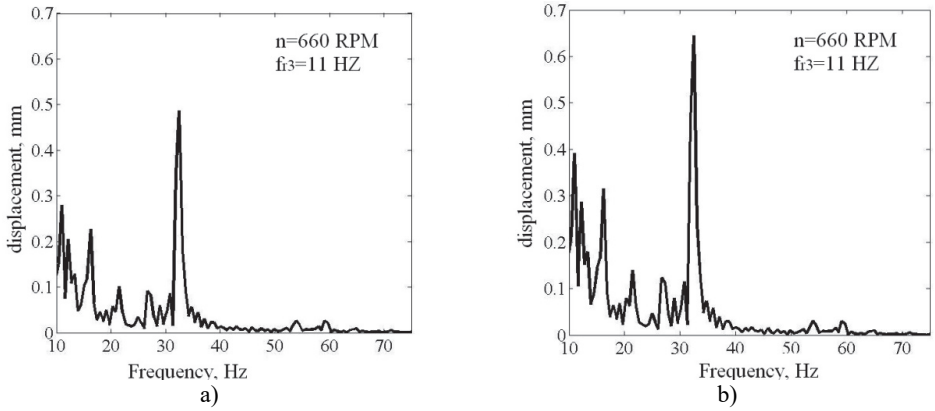

Fig. 8. Absolute vibration spectrums: a) spindle housing – experimental; b) tool-holder – calculated

5.3. Discussion

As can be seen from Fig. 7, in the low-frequency range (up to 70 Hz) there are two resonance zones corresponding to the first $P_1^{(4)} = 33$ Hz and second $P_2^{(4)} = 335$ Hz natural frequencies of the test rig frame. In this case, the compliance function $W(\omega)_{13}$ (Fig. 7) is practically linear. This means that the nature of the absolute vibrations of spindle housing and tool-holder is determined by the vibrations of the frame. This is confirmed by the similarity of the absolute vibration experimental spectrum of the spindle housing and the corresponding calculated tool-holder absolute vibration spectrum (Fig. 8).

From the calculated spectrum of the tool-holder relative vibration (Fig. 10), we can make the following conclusions:

– in the non-resonance mode at low spindle speeds, the effect of assembling and manufacturing faults of spindle units on the formation of tool-holder vibration spectrum is not observed (Fig. 9(a));

– high amplitudes of resonance vibrations at first f_r (Fig. 10(f)), second $2f_r$ (Fig. 10(e)) and

third $3f_r$ (Fig. 10, d) harmonics of spindle rotation frequency indicate the presence of a significant spindle imbalance and misalignment of bearing seats [20];

– a high amplitude of resonance vibrations at f_{BPFO} frequency indicate the presence of a significant defect on the bearing outer ring (Fig. 10(c));

– there are no significant defects on the bearing inner ring (Fig. 10(b)).

This confirms the high information value of the compliance function $W(\omega)_{13}$ and prospective of developed method of indirect measurement of spindle vibrations for the assembling and manufacturing faults diagnostics of SU on rolling bearings that cause low-frequency vibrations.

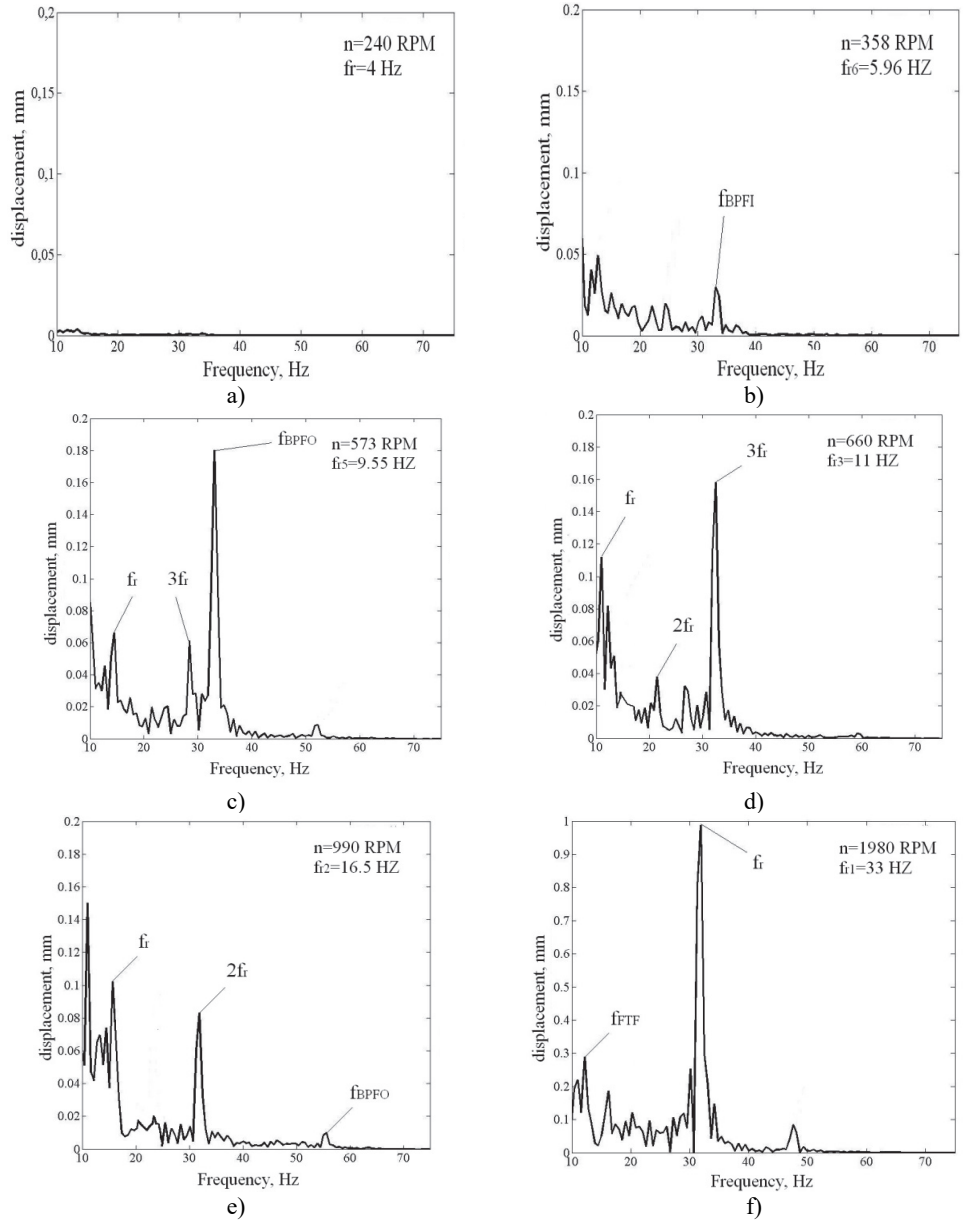

Fig. 9. Calculated spectrums of tool-holder relative vibrations at spindle speeds, corresponding to frame resonance at characteristic frequencies of forced vibrations: a) non-resonance mode, b) f_{BPFI}, c) f_{BPFO}, d) $3f_r$; e) $2f_r$; f) f_r

6. Conclusions

1) An alternative to direct measurement of spindle vibrations (or tool-holder) may be their identification based on the results of measuring the vibrations of the spindle housing using the calculated compliance function characterizing the ratio of vibrations at the points of measurement and identification. It was this idea that formed the basis for creating a method for indirect measurement of spindle vibrations.

2) When developing a design scheme of a spindle unit mounted on the test rig as a complex mechanical vibratory system, the theoretical compliance function will be the ratio of the dynamic compliances of the corresponding subsystems at the points of calculation and vibration measurement.

3) The application of the dynamic compliance method for the decomposition of a complex mechanical vibratory system, which contains a spindle unit, in combination with the transfer matrix method, used for calculation of subsystems dynamic characteristics, makes it possible to obtain acceptable modeling results with the relative simplicity of design schemes and algorithms computation.

4) The results of the study indicate a high degree of information value of compliance function and prospects of developed method application for the assembling and manufacturing faults diagnostics of SU on rolling bearings in the low-frequency region. It is established that the compliance function gives a clear idea of the relationship between the displacements at measurement and identification points, as well as reasons of these relations variation.

References

[1] Vibration Diagnostic Guide. SKF Condition Monitoring, CM5003, 2000, p. 28.

[2] Axes of Rotation, Methods for Specifying and Testing. An American National Standard, ASME B89.3.4, 2010.

[3] **Graham T.** Smith Machine Tool Metrology. An Industrial Handbook. Springer International Publishing Switzerland, 2016, p. 700.

[4] **Kok You Cheng** Review of Machine Tool Metrology (Spindle). National University of Singapore, Department of Mechanical Engineering, 2011/2012, p. 40.

[5] **Trivedi P., Bharti P. K.** Study of bearing rolling element defect using empirical mode decomposition technique. International Journal of Engineering Development and Research (IJEDR), Vol. 5, Issue 2, 2017, p. 553-565.

[6] **Shakya P., Darpe A. K., Kulkarni M. S.** Vibration based fault diagnosis in rolling element bearings: ranking of various time, frequency and time-frequency domain data-based damage identification parameters. International Journal of Condition Monitoring, Vol. 3, Issue 2, 2013, p. 53-62.

[7] **Nahata S., Anandan K. P., Ozdoganlar O. B.** LDV-based spindle metrology for ultra-high-speed micromachining spindles. North American Manufacturing Research Conference, 2013.

[8] **Barszcz T., Sawalhi N.** Fault detection enhancement in rolling element bearings using the minimum entropy deconvolution. Archives of Acoustics, Vol. 37, Issue 2, 2012, p. 131-141.

[9] **Barzdaitis V., Zemaitis V., Zebelys K., Pocius Z., Mazeika P.** Condition monitoring of roller bearings using different diagnostic methods. Diagnostyka, Vol. 30, Issue 1, 2004, p. 53-60.

[10] **Jamaludin N., Mba D., Bannister R. H.** Condition monitoring of slow-speed rolling element bearings using stress waves. Proceedings of the Institution of Mechanical Engineers, Part E: Journal of Process Mechanical Engineering, Vol. 215, Issue 4, 2001, p. 245-271.

[11] **Kozochkin M. P., Sabirov F. S.** Detection of spindle units defects by vibration acoustic methods. Vestnik UGATU – Ufa: UGATU, Vol. 13, Issue 1, 2009, p. 133-137.

[12] **Denisenko A. F., Gasparov E. S.** Vibration characteristics analysis of spindle unit bearings. Vestnik Samarskoko GTU, Technical Science, Vol. 2, Issue 34, 2012, p. 103-108.

[13] **Jui Hung P., Yuan Lai L., Tzuo Luo L., Hsi Hsiao H.** Prediction of the dynamic characteristics of a milling machine using the integrated model of machine frame and spindle unit. World Academy of Science, Engineering and Technology, Vol. 6, 2012, p. 626-632.

[14] **Danylchenko Yu M., Petryshyn A. I., Danylchenko M. A.** Test Bench for Assembling and Manufacturing Faults Diagnostics of Spindle Sleeve. Patent No. UA112210U, 2016.

[15] **Banakh L. Y., Kempner M. L.** Vibrations of Mechanical Systems with Regular Structure. Springer, 2010, p. 250.
[16] **Biderman V. L.** Applied Theory of Mechanical Vibrations. Mashinostroenie, Moscow, 1972, p. 416.
[17] **Danylchenko Yu M., Dorozhko A. O., Petryshyn A. I.** Research of the dynamical characteristics of "spindle unit" mechanical system. Vestnik MSTU STANKIN, Vol. 28, Issue 1, 2014, p. 81-91.
[18] **Hatter D. J.** Matrix Computer Methods of Vibration Analysis. Butterworth, London, 1973, p. 206.
[19] **Ivovych V. A.** Transfer Matrices in Elastic Systems Dynamic. Handbook, Mashinostroenie, Moscow, 1981, p. 183.
[20] **Balitckiy A. V., Barkov A. V., Barkov N. A., et al.** Vibration-Based Diagnostics. Non-destructive testing: Handbook, Vol. 7, Book 2, Mashinostroenie, Moscow, 2005, p. 829.

Yuriy Danylchenko received Doctor of Science in engineering in National Technical University of Ukraine "Kyiv Politechnic Institute", Kyiv, Ukraine, in 2004, where he works to the present day. His current research interests include dynamic and spindle units accuracy, rolling bearings rotating accuracy, vibration monitoring of spindle units on rolling bearings.

Andriy Petryshyn received Ph.D. degree in National Technical University of Ukraine "Kyiv Politechnic Institute", Kyiv, Ukraine, in 2016, where he works to the present day. His current research interests include control, spindle units dynamics and fault diagnosis.

2.3. Methods of ensuring the required dynamics of an AMB supported axial LVAD rotor

Yulia Bogdanova[1], Alexander Gouskov[2]
[1, 2]Bauman Moscow State Technical University, Moscow, Russia
[1]National Research Center "Kurchatov Institute", Moscow, Russia
[2]Vibrations Laboratory, RAS Institute of Machine Science, Moscow, Russia
E-mail: [1]*bogdanova.bmstu@gmail.com*, [2]*gouskov_am@mail.ru*

Abstract. Left ventricular assist device is a main alternative to donor heart transplantation today. The third-generation of devices includes continuous-flow pumps with an impeller or rotor suspended in the blood flow path using a magnetic bearing design. Magnetic bearings offer the advantages of non-contact suspension, thus, there is no wear over time and no friction, and large clearances. Active magnetic bearings are a mechatronic product in which the rotor dynamics can be controlled actively through the bearings. The main problem of non-contact suspension is to ensure a stability of rotor position. Besides researches of the last years have shown that with prolonged use of pumps with the constant blood flow, i.e. without pulsations, patients have complications associated with a cardiac atrophy, a coronary artery disorder, an embrittlement of vessels and, as a result, an internal bleeding. In this regard, the creation of blood flow pulsations and the provision of the stable controlled behavior of the rotor in pulsating modes of functioning of the axial LVAD with magnetic bearings are relevant and proposed in this article.

Keywords: nonlinear dynamics, rotor stabilization, attractor, invariant, synergetic control theory, left ventricular assist device.

1. Introduction

Cardiovascular diseases are a major cause of death worldwide. If medical treatments fail to restore an adequate blood flow in a patient, a mechanical support is needed.

Left ventricular assist device (LVAD) re-establish sufficient perfusion in patients with advanced heart failure when medication and other surgical therapies, such as valve replacement or ventricular reconstruction, have reached their limits. An implanted device draws blood from the left ventricle into the aorta. Energy is supplied from an external battery and transferred to the LVAD through a percutaneous cable [1].

Unfortunately, the base of donor hearts is small even in the most developed countries. Annually in the countries of Europe and the USA about 3500 transplantations are performed, whereas in Russia the number of transplantations per year is about 165 [2]. Today LVAD is the basic alternative to heart transplantation [3].

Patients are forced to be with implanted blood pumps for a long time. Increasingly, patients abandon the donor heart in favor of mechanical support [4]. Therefore, the main task of the development of LVAD is to improve the quality of the device.

To date, different types of blood pumps have been developed, but only a few are clinically available. The development of LVAD is a highly complex and interdisciplinary process with many requirements to be fulfilled [1]. Generally, LVADs can broadly be divided into first-, second and third-generation devices.

The first-generation of devices includes pulsatile membrane displacement pumps. These devices are engineered with a pumping chamber and two valves that fill and empty cyclically. Disadvantages of such blood pumps are large size, unreliable and an external position [5].

The second-generation devices include implantable, continuous flow, rotary pumps that offer several advantages over pulsatile flow pumps. Some of the advantages are the smaller size that reduces the risk of infections and simpler implantation. These pumps have an internal rotor within the blood flow path that is suspended by contact bearings [5, 6].

But in this design, there are some problems. Ball bearings are lubricated directly with blood

that leading to extensive damage to the red blood cells, called hemolysis [7, 8]. Seal failures resulted in many early pump failures. Additionally, seals accumulate thrombosis. Blood-lubricated bearings tend to be subject to high shear due to the high rotational speeds and small clearances [9]. So the most important problems associated with the development of the LVAD are the blood trauma (hemolysis), thrombosis, unreliability of the devices, lack of pulsations.

The third-generation of devices includes continuous-flow pumps with an impeller or rotor suspended in the blood flow path using a magnetic bearing design. Magnetic bearings offer the advantages of non-contact suspension, thus, there is no wear over time and no friction, and large clearances [10, 11].

The large clearance allows the rotor to rotate at high speeds with the appearance of low shear stresses that reduces the rate of hemolysis and thrombosis. The magnetic bearings provide the durability and the operational reliability of the blood pump. Moreover, there is no need for maintenance. In addition, active magnetic bearings (AMB) are controlled by electronic control scheme with feedback. This provides a higher positioning accuracy of the rotor [12]. The development of LVAD of axial type with magnetic bearings suspension becomes perspective.

Currently the most popular blood pump of axial type with magnetic bearings introduced into medical practice is Incor (BerlinHeart Company). Incor as well as other pumps of the second and third generation has a continuous blood flow. But researches of the last years have shown that with prolonged use of pumps with the constant blood flow, i.e. without pulsations, patients have complications associated with a cardiac atrophy, a coronary artery disorder, an embrittlement of vessels and, as a result, an internal bleeding [13, 14]. In this regard, a task of the creation of pulsations at the outflow from the pump chamber becomes one of the priority when developing the pump of a new generation.

There is not the axial blood pump of pulsating type in the world market yet. In contrast to the huge number of researches devoted to the study of the blood flow in the pump chamber, the influence of shear stresses on erythrocytes, the design of the geometry of the flow part, there are practically no studies related to the dynamics of the rotor with active magnetic supports in conditions of blood flow and pump functioning regimes. The problem of absence of mathematical models of the nonlinear rotor dynamics of the LVAD with magnetic bearings remains open. AMB are widely used in machine-tool constructions, in vacuum systems, in high-speed engineering [15-17]. As a rule, objects have a small gap, and in most works the magnetic suspension model linearized at the equilibrium position is used. However, the nonlinear properties of magnetic bearings can lead to the dynamics of the rotor, whose motion is completely different from that predicted by the linear model [18-22].

The development of reliable, designed for long-term mechanical support, domestic LVAD of the new generation seems perspective. The analysis of researches allows to state that to date there are still no scientifically based methodologies for designing such complex system as blood pump. Especially it concerns the design techniques of the rotor-magnetic part of the pump. Therefore, the creation of blood flow pulsations and the provision of the stable controlled behavior of the rotor in pulsating modes of functioning of the axial LVAD with AMB are relevant.

2. Equations of motion

The rigid rotor with mass m of the axial LVAD rotates with the constant angular velocity Ω in two radial active magnetic bearings AMB A and AMB B (Fig. 1(a)). Magnetic bearings consist of four identical contours (Fig. 1(b)), which are located symmetrically opposite each other.

The small motions of the rotor are described by the displacements x^o and y^o of its geometric center O with respect to the inertial reference $IXYZ$ and by inclinations of axes $Ox^oy^oz^o$ (Fig. 2). These inclinations are described by two angles α and β. The axis Oz^o coincides with the geometrical longitudinal axis of the rotor and the axis Ox^o passes through the center of mass of the rotor C. $Cx'y'z'$ is the rotor-fixed system of principal axes with $I_{x'} = I_{y'} = I_x$ and $I_{z'} = I_z$

moments of inertia. The rotor motion in the longitudinal direction is fixed by permanent magnets and therefore is not considered. Rotor has a static and dynamic unbalances. The static unbalance is characterized by the eccentricity $OC = e$. The dynamic unbalance is characterized by the angle $\gamma_x = \gamma$ [23, 24]. In the nominal reference position of the rotor, axes of $Ox^o y^o z^o$ system coincide with the origin of the inertially fixed coordinate system $IXYZ$.

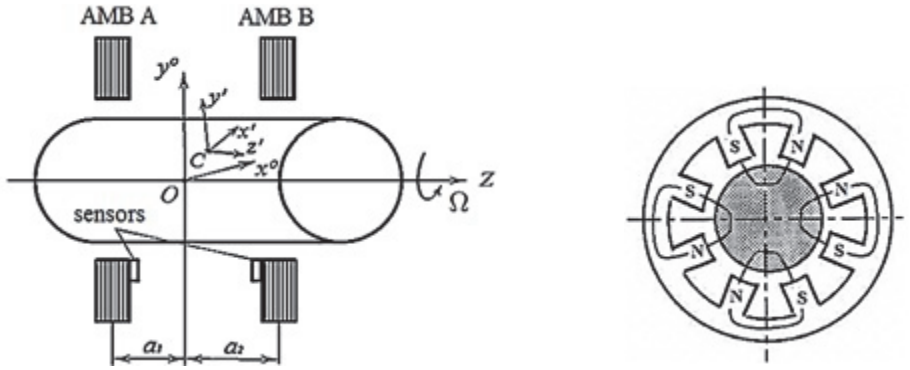

Fig. 1. a) Symmetrical rigid rotor in two radial active magnetic bearings, b) geometry of the radial bearing magnet

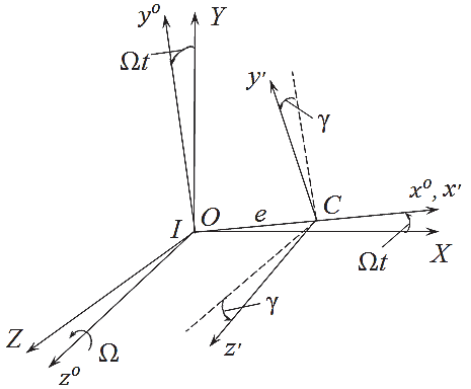

Fig. 2. Relationship of coordinate systems

The angular velocity Ω of the rotor about its longitudinal axis is assumed to be constant. The equations of motion for the variables:

$$\mathbf{q} = \{x_o, y_o, \alpha, \beta\}^T. \tag{17}$$

Follow from Lagrange's equations:

$$\frac{d}{dt}\left(\frac{\partial T}{\partial \dot{q}_i}\right) - \frac{\partial T}{\partial q_i} = Q_i, \quad i = 1, \ldots, 4. \tag{18}$$

With the kinetic energy T and the generalized forces Q_i.
The kinetic energy T is:

$$T = \frac{1}{2} m(x_0^2 + y_0^2) + mWe(-x_o \sin Wt + y_0 \cos Wt) + \frac{1}{2}\, \mathbf{\Omega}^T \mathbf{I}_o \mathbf{\Omega}, \tag{19}$$

where $\mathbf{I}_o$ is the matrix of the inertia tensor and $\mathbf{\Omega}$ is expressed [17]:

$$\mathbf{\Omega} = \begin{Bmatrix} \Omega_{x^o} \\ \Omega_{y^o} \\ \Omega_{z^o} \end{Bmatrix} = \begin{bmatrix} \dot{\alpha}\cos(\Omega t) + \dot{\beta}\sin(\Omega t) \\ -\dot{\alpha}\sin(\Omega t) + \dot{\beta}\cos(\Omega t) \\ \Omega - \alpha\dot{\beta} \end{bmatrix}. \tag{20}$$

Hence, the equations of motion follow in the form [17]:

$$\begin{aligned} &m\ddot{x}_o = F_1 + F_{ext1} + m\Omega^2 e\cos(\Omega t), \\ &m\ddot{y}_o = F_2 + F_{ext2} + m\Omega^2 e\sin(\Omega t), \\ &I_x\ddot{\alpha} + I_z\Omega\dot{\beta} = F_3 + F_{ext3} + \Omega^2\gamma(I_x - I_z)\cos(\Omega t), \\ &I_x\ddot{\beta} - I_z\Omega\dot{\alpha} = F_4 + F_{ext4} + \Omega^2\gamma(I_x - I_z)\sin(\Omega t). \end{aligned} \tag{21}$$

The first two equations in Eq. (5) describe the translational motion of the rotor. The last two represent angular motions, with the second terms in the left-hand sides characterizing the gyroscopic effects. As can be seen from equations Eq. (5), the parameters of unbalances play the role of an external periodic load.

In matrix form the equations of motion are:

$$\mathbf{M}\,\ddot{\mathbf{q}} + \Omega\mathbf{G}\dot{\mathbf{q}} = \mathbf{F} + \mathbf{F}_{ext} + \Omega^2\mathbf{Q}_v(t), \tag{22}$$

where $\mathbf{M} = \mathrm{diag}(m, m, I_x, I_x)$ is the inertia matrix, $\mathbf{G}$ is the skew-symmetric gyroscopic matrix with two non-zero elements $(\mathbf{G})_{34} = -(\mathbf{G})_{43} = I_z$, $\mathbf{F} = \{F_1, \dots, F_4\}^T$, $\mathbf{F}_{ext} = \{F_{ext1}, \dots, F_{ext4}\}^T$ are the electromagnetic reactions of the suspension and the generalized external forces respectively, $\mathbf{Q}_v(t)$ is the generalized excitation loads which expressed:

$$\mathbf{Q}_v(t) = \begin{Bmatrix} me\cos(\Omega t) \\ me\sin(\Omega t) \\ \gamma(I_x - I_z)\cos(\Omega t) \\ \gamma(I_x - I_z)\sin(\Omega t) \end{Bmatrix}. \tag{23}$$

The generalized electromagnetic reactions of the suspension are created by controlling magnetic bearings forces:

$$\mathbf{F}_{AMB} = \{F_{Ax}, F_{Ay}, F_{Bx}, F_{By}\}^T, \tag{24}$$

which are applied to the rotor in the control points of AMB A and AMB B at the distance a_1 and a_2 from the geometric center O. The sensors have the same longitudinal coordinates as the centers of the support points of the rotor, that is, the control points coincide with the measurement points.

Vectors $\mathbf{F}$ and $\mathbf{F}_{AMB}$ are related by:

$$\mathbf{F} = \mathbf{T}_b{}^T\mathbf{F}_{AMB}, \tag{25}$$

where $\mathbf{T}_b$ is the transformation matrix:

$$\mathbf{T}_b = \begin{bmatrix} 1 & 0 & 0 & -a_1 \\ 0 & 1 & a_1 & 0 \\ 1 & 0 & 0 & a_2 \\ 0 & 1 & -a_2 & 0 \end{bmatrix}. \tag{26}$$

This leads to the following form for the equations of motion:

$$\mathbf{M}\,\ddot{\mathbf{q}} + \Omega\mathbf{G}\dot{\mathbf{q}} = \mathbf{T}_b^T\mathbf{F}_{AMB} + \mathbf{F}_{ext} + \Omega^2\mathbf{Q}_v(t). \tag{27}$$

As a rule, the magnetic suspension equations are linearized at the equilibrium position [25]. Then the linear model is adequate only for small deviations of the variables from their nominal values or displacement values. In fact, these deviations can be considerable. In some works, it is shown, if the deflections of the rotor exceed half of the gap, the net magnetic force which is produced by a pair of opposite electromagnets changes more than 44 % from the linear approximation of itself [20]. Therefore, the magnetic bearings operation changes from the equilibrium point. For small air gaps and large control currents the nonlinear characteristics become very significant. Dynamic behavior of the rotor can be changed from the linear model result because of the nonlinear characteristics of magnetic bearings. The nonlinear model of bearings forces has a form:

$$\begin{aligned}
F_{Ax} &= F_{Ax1} - F_{Ax2} = k_A\left[\left(\frac{i_0 + i_{Ax}}{\delta - x_{bA}}\right)^2 - \left(\frac{i_0 - i_{Ax}}{\delta + x_{bA}}\right)^2\right],\\
F_{Ay} &= F_{Ay1} - F_{Ay2} = k_A\left[\left(\frac{i_0 + i_{Ay}}{\delta - y_{bA}}\right)^2 - \left(\frac{i_0 - i_{Ay}}{\delta + y_{bA}}\right)^2\right],\\
F_{Bx} &= F_{Bx1} - F_{Bx2} = k_B\left[\left(\frac{i_0 + i_{Bx}}{\delta - x_{bB}}\right)^2 - \left(\frac{i_0 - i_{Bx}}{\delta + x_{bB}}\right)^2\right],\\
F_{By} &= F_{By1} - F_{By2} = k_B\left[\left(\frac{i_0 + i_{By}}{\delta - y_{bB}}\right)^2 - \left(\frac{i_0 - i_{By}}{\delta + y_{bB}}\right)^2\right],
\end{aligned} \tag{28}$$

with the bias current i_0, the constructive parameter $k_A = k_B = \frac{\mu_0 n^2 A}{2}\cos(\chi)$ (μ_0 – magnetic constant, n – number of winding turns, A – winding area, χ – angle of deviation of magnetic force from vertical/horizontal equal to 22.5°) and the radial gap δ. The currents i_{Ax} and i_{Bx} create the magnetic forces F_{Ax} and F_{Bx} in the X direction and the currents i_{Ay}, i_{By} create the magnetic forces F_{Ay} and F_{By} in the direction of the axis Y (Fig. 3).

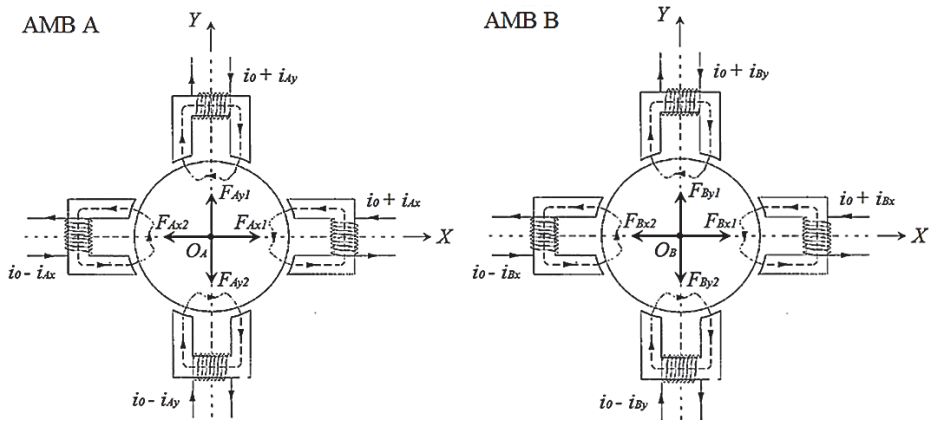

Fig. 3. Principle of radial force generation

The vector:

$$\mathbf{q}_b = \begin{Bmatrix} x_{bA} \\ y_{bA} \\ x_{bB} \\ y_{bB} \end{Bmatrix} = \begin{Bmatrix} x_o - a_1\beta \\ y_o + a_1\alpha \\ x_o + a_2\beta \\ y_o - a_2\alpha \end{Bmatrix}. \tag{29}$$

Comprises the rotor displacements within the magnetic bearings, whereas the vector $\mathbf{i} = \{i_{Ax}, i_{Bx}, i_{Ay}, i_{By}\}^T$ contains the individual coil control currents of all four bearing magnets.

At a switched-on electric motor the right-hand side of the equations of motion Eq. (11) will include a matrix of positional forces $\mathbf{C}_m$ [17]:

$$\mathbf{M}\,\ddot{\mathbf{q}} + \Omega\mathbf{G}\dot{\mathbf{q}} = \mathbf{T}_b^T\mathbf{F}_{AMB} + \mathbf{C}_m\,\mathbf{q} + \mathbf{F}_{ext} + \Omega^2\mathbf{Q}_v(t). \tag{30}$$

For the motor with a length l_m arranged in a symmetrical suspension, the matrix, taking into account its effect on the suspension, has the form:

$$\mathbf{C} = \frac{c_m}{4}\begin{bmatrix} 1+k_m & 0 & 1-k_m & 0 \\ 0 & 1+k_m & 0 & 1-k_m \\ 1-k_m & 0 & 1+k_m & 0 \\ 0 & 1-k_m & 0 & 1+k_m \end{bmatrix}, \tag{31}$$

where c_m is the motor stiffness, $k_m = \frac{l_m^2}{3(a_1+a_2)^2}$ is the motor design parameter (constant value). Matrices $\mathbf{C}$ and $\mathbf{C}_m$ are related by:

$$\mathbf{C}_m = \mathbf{T}_b^T\mathbf{C}\mathbf{T}_b. \tag{32}$$

Then the equations of motion follow in the form:

$$\mathbf{M}\,\ddot{\mathbf{q}} + \Omega\mathbf{G}\dot{\mathbf{q}} + (-\mathbf{T}_b^T\mathbf{C}\mathbf{T}_b)\mathbf{q} = \mathbf{T}_b^T\mathbf{F}_{AMB} + \mathbf{F}_{ext} + \Omega^2\mathbf{Q}_v(t). \tag{33}$$

Rotation in the blood flow is associated with the hydrodynamic resistance. Since the rotor is screw and has a non-constant shape, the standard theory of hydrodynamic lubrication cannot be applied. From the theory of similarity and dimension vector of hydrodynamic resistance can take the form:

$$\begin{Bmatrix} M_{Hx} \\ M_{Hy} \\ M_{Hz} \end{Bmatrix} = c_w\eta\pi r^2 l \begin{Bmatrix} -\dot{\alpha} - \Omega\beta \\ -\dot{\beta} + \Omega\alpha \\ -\Omega \end{Bmatrix} \tag{34}$$

with the coefficient of medium resistance c_w and the dynamic viscosity of blood η. The radius and the length of the rotor are indicated r and l respectively. The relation (18) can be written in the form:

$$\mathbf{M}_H = \mathbf{H}_D\dot{\mathbf{q}} + \Omega\mathbf{H}_S\mathbf{q},$$
$$\mathbf{H}_D = \begin{bmatrix} 0 & 0 & 0 & 0 \\ 0 & 0 & 0 & 0 \\ 0 & 0 & -c_w\eta\pi r^2 l & 0 \\ 0 & 0 & 0 & -c_w\eta\pi r^2 l \end{bmatrix}, \quad \mathbf{H}_S = \begin{bmatrix} 0 & 0 & 0 & 0 \\ 0 & 0 & 0 & 0 \\ 0 & 0 & 0 & -c_w\eta\pi r^2 l \\ 0 & 0 & c_w\eta\pi r^2 l & 0 \end{bmatrix}. \tag{35}$$

With considering Eq. (19) the equations of motion are expressed:

$$\mathbf{M}\ddot{\mathbf{q}} + (\Omega\mathbf{G} - \mathbf{H}_D)\dot{\mathbf{q}} + (-\mathbf{T}_b^T\mathbf{C}\mathbf{T}_b - \Omega\mathbf{H}_S)\mathbf{q} = \mathbf{T}_b^T\mathbf{F}_{AMB} + \mathbf{F}_{ext} + \Omega^2\mathbf{Q}_v(t). \tag{36}$$

Influence of the various accelerations that a person experiences in everyday life and in professional activity is taken into account in the vector of the generalized external forces. External inertial loads can be either piecewise-constant or harmonic:

$$\mathbf{F}_{ext} = \begin{Bmatrix} F_x + A_x \sin(pt) \\ F_y + A_y \sin(pt) \\ M_x + B_x \sin(pt) \\ M_y + B_y \sin(pt) \end{Bmatrix}, \tag{37}$$

where F_x, F_y, M_x, M_y – external piecewise-constant loads, A_x, A_y, B_x, B_y, p – amplitudes and frequency of external harmonic influence.

There is interest to present the equations of motion in a dimensionless form [26, 27], highlighting the dimensionless complexes (similarity criteria), that characterize a whole class of an artificial circulatory supports. Applying the change of variables:

$$\begin{aligned} &x_1 = x_o, \quad y_1 = y_o, \quad \alpha_1 = \alpha, \quad \beta_1 = \beta, \\ &x_2 = \dot{x}_1, \quad y_2 = \dot{y}_1, \quad \alpha_2 = \dot{\alpha}_1, \quad \beta_2 = \dot{\beta}_1, \end{aligned} \tag{38}$$

and formulas for the transition to dimensionless quantities $t = \bar{t}S_t$, $x_1 = \bar{x}_1 S_x$, $y_1 = \bar{y}_1 S_x$, $\alpha_1 = \bar{\alpha}_1 S_\beta$, $\beta_1 = \bar{\beta}_1 S_\beta$, $a_1 = \bar{a}_1 S_L$, $a_2 = \bar{a}_2 S_L$, $i_0 = \bar{\imath}_0 S_i$, $i_{Ax} = \bar{\imath}_{Ax} S_i$, $i_{Ay} = \bar{\imath}_{Ay} S_i$, $i_{Bx} = \bar{\imath}_{Bx} S_i$, $\delta = \bar{\delta} S_x$, $k_m = \bar{k}_m$, $F_x = \bar{F}_x S_F$, $F_y = \bar{F}_y S_F$, $M_x = \bar{M}_x S_M$, $M_y = \bar{M}_y S_M$, $r = \bar{r} S_L$, $l = \bar{l} S_L$, $e = \bar{e} S_x$, $A_x = \bar{A}_x S_F$, $A_y = \bar{A}_y S_F$, $B_x = \bar{B}_x S_M$, $B_y = \bar{B}_y S_M$, $\Omega = \bar{\Omega} S_\Omega$, $p = \bar{p} S_\Omega$, $\gamma = \bar{\gamma} S_\beta$ lead to the equations of motion in the dimensionless form (dimensionless quantities are with a dash, $(\,)' = d/d\bar{t}$):

$$\begin{aligned}
&\bar{x}_1' = \bar{x}_2, \\
&\bar{x}_2' = \bar{x}_1 + \frac{(-\bar{a}_1 + \bar{a}_2)}{2}\bar{\beta}_1 + \bar{F}_{Ax} + \bar{F}_{Bx} + \bar{F}_x + \bar{A}_x \sin(\bar{p}\bar{t}) + \bar{\Omega}^2 \bar{e}\cos(\bar{\Omega}\bar{t}), \\
&\bar{y}_1' = \bar{y}_2, \\
&\bar{y}_2' = \bar{y}_1 + \frac{(\bar{a}_1 - \bar{a}_2)}{2}\bar{\alpha}_1 + \bar{F}_{Ay} + \bar{F}_{By} + \bar{F}_y + \bar{A}_y \sin(\bar{p}\bar{t}) + \bar{\Omega}^2 \bar{e}\sin(\bar{\Omega}\bar{t}), \\
&\bar{\alpha}_1' = \bar{\alpha}_2, \\
&\bar{\alpha}_2'' = -\Pi_H \bar{\alpha}_2 - \Pi_1 \bar{\Omega}\bar{\beta}_2 + \frac{\Pi_2}{2}(\bar{a}_1 - \bar{a}_2)\bar{y}_1 - \Pi_H \bar{\Omega}\bar{\beta}_1 + \bar{a}_1 \Pi_2 \bar{F}_{Ay} - \bar{a}_2 \Pi_2 \bar{F}_{By} + \dots \\
&\quad + \frac{\Pi_2}{4}\left((\bar{a}_1^2 + \bar{a}_2^2)(1 + \bar{k}_m) - 2\bar{a}_1\bar{a}_2(1 - \bar{k}_m)\right)\bar{\alpha}_1 + \bar{M}_x + \bar{B}_x \sin(\bar{p}\bar{t}) \\
&\quad + \bar{\Omega}^2 \bar{\gamma}(1 - \Pi_1)\cos(\bar{\Omega}\bar{t}), \\
&\bar{\beta}_1' = \bar{\beta}_2, \\
&\bar{\beta}_2' = -\Pi_H \bar{\beta}_2 + \Pi_1 \bar{\Omega}\bar{\alpha}_2 + \frac{\Pi_2}{2}(-\bar{a}_1 + \bar{a}_2)\bar{x}_1 + \Pi_H \bar{\Omega}\bar{\alpha}_1 - \bar{a}_1 \Pi_2 \bar{F}_{Ax} + \bar{a}_2 \Pi_2 \bar{F}_{Bx} + \dots \\
&\quad + \frac{\Pi_2}{4}\left((\bar{a}_1^2 + \bar{a}_2^2)(1 + \bar{k}_m) - 2\bar{a}_1\bar{a}_2(1 - \bar{k}_m)\right)\bar{\beta}_1 + \bar{M}_y + \bar{B}_y \sin(\bar{p}\bar{t}) \\
&\quad + \bar{\Omega}^2 \bar{\gamma}(1 - \Pi_1)\sin(\bar{\Omega}\bar{t}),
\end{aligned} \tag{39}$$

where:

$$\bar{F}_{Ax} = \Pi_K \left[\left(\frac{\bar{\imath}_0 + \bar{\imath}_{Ax}}{\bar{\delta} - (\bar{x}_1 - \bar{a}_1\bar{\beta}_1)} \right)^2 - \left(\frac{\bar{\imath}_0 - \bar{\imath}_{Ax}}{\bar{\delta} + (\bar{x}_1 - \bar{a}_1\bar{\beta}_1)} \right)^2 \right],$$

$$\bar{F}_{Bx} = \Pi_K \left[\left(\frac{\bar{\imath}_0 + \bar{\imath}_{Bx}}{\bar{\delta} - (\bar{x}_1 + \bar{a}_2\bar{\beta}_1)} \right)^2 - \left(\frac{\bar{\imath}_0 - \bar{\imath}_{Bx}}{\bar{\delta} + (\bar{x}_1 + \bar{a}_2\bar{\beta}_1)} \right)^2 \right],$$

$$\bar{F}_{Ay} = \Pi_K \left[\left(\frac{\bar{\imath}_0 + \bar{\imath}_{Ay}}{\bar{\delta} - (\bar{y}_1 + \bar{a}_1 \bar{\alpha}_1)} \right)^2 - \left(\frac{\bar{\imath}_0 - \bar{\imath}_{Ay}}{\bar{\delta} + (\bar{y}_1 + \bar{a}_1 \bar{\alpha}_1)} \right)^2 \right],$$

$$\bar{F}_{By} = \Pi_K \left[\left(\frac{\bar{\imath}_0 + \bar{\imath}_{By}}{\bar{\delta} - (\bar{y}_1 - \bar{a}_2 \bar{\alpha}_1)} \right)^2 - \left(\frac{\bar{\imath}_0 - \bar{\imath}_{By}}{\bar{\delta} + (\bar{y}_1 - \bar{a}_2 \bar{\alpha}_1)} \right)^2 \right].$$

As independent units of dimension, the following scales were chosen:

$$S_x = \delta, \quad S_L = l, \quad S_t = \sqrt{\frac{m}{c_m}}, \quad S_i = \sqrt{\frac{P}{R}}, \tag{40}$$

where P is the electric power and R is the resistance. Two scales – meter-introduced because of the presence of anisotropy in the longitudinal and transverse dimensions of the research object and are related to each other by the ratio $\frac{S_x}{S_L} = \frac{\delta}{l} = \varepsilon$. The remaining scales are dependent on the dimension and are expressed through the selected ones and listed above. In the process of reducing the rotor model to a dimensionless form, dimensionless complexes were identified – the similarity criteria:

$$\Pi_1 = \frac{I_z}{I_x}, \quad \Pi_2 = \frac{ml^2}{I_x}, \quad \Pi_H = \frac{c_w \eta \pi l^3 \bar{r}^2 \bar{l} \sqrt{m/c_m}}{I_x}, \quad \Pi_K = \frac{k_A P}{c_m R \delta^3}. \tag{41}$$

It is necessary to create the blood flow pulsations as it was said earlier. From Pressure-Flow characteristic it can be seen that different rotational speeds can provide the same flow rate, depending on what pressure rise is required [28]. As is known a pressure of 120 to 80 mmHg is normal. The idea of the approach to create the blood flow pulsations is to change pressure rise in accordance with the change in the rotational speed. To approbate this method let change the rotational speed vary according to the harmonic law $\bar{\Omega} = \bar{A}\sin(\bar{\omega}\bar{t}) + \bar{\Omega}_0$ with a given amplitude and frequency. It should be noted, that the non-constant rotational speed can lead to additional accelerations and as a result other equations of motion. However, it was shown that the influence of these additional accelerations on the results of calculations is infinitely small and may not be taken into account.

3. Synergetic synthesis of control

The LVAD system is characterized by the following features: structural complexity (nonlinearity, large dimension, multiply connection and parametric uncertainty); multi-mode operation and lack of time for reconfiguration; nonlinear properties in modes of large deviations; the presence of external disturbances, which can lead to emergency situations; the requirement of energy efficiency.

The most appropriate method has been chosen, which makes it possible to solve immediately a set of stated problems. This is a method of analytical design of aggregated regulators (ADAR) of synergetic control theory (SCT) [29-36].

SCT is a new direction in control science. In general, SCT provides methods for designing optimal controllers for dynamical systems, where the controllers are coordinated with internal expectations of the systems. In SCT control goals are written in the form of invariants (technological, energy, chemical etc.). For the control goals were fulfilled, it is necessary that these invariants become attractors of the dynamical system. An attractor is a region in the state space of a dynamical system that pulls the trajectories from nearby areas of the state space. Whatever the initial conditions are, the system moves towards one of the attractors and remains

there infinitely. So, the control goals are fulfilled on this attractor. Procedure of synergetic synthesis is the search for control laws under which these invariants become attractors of the dynamical system. Introducing such areas of attraction, or attractors, to the dynamical system, is one of the main concepts of the SCT. The resulting dynamical systems with their controllers have areas of attraction that correspond to the control goals.

The model of the rotor dynamics in active magnetic bearings Eq. (23) includes external disturbances, which can lead to malfunctioning or failure of the system. Thus, effective control of the magnetic suspension should have the ability to compensate for their undesirable effect. For this, the principle of integral adaptation of ADAR method can be applied. The integral adaptation implies that to parry external disturbances it is necessary to represent each of them in the form of a dynamic model at the output of which an approximate perturbation of the corresponding class is formed. The original system Eq. (23) can be extended by introducing the perturbation estimates:

$$\begin{aligned}
\bar{z}_1 &= \bar{F}_x + \bar{A}_x \sin(\bar{p}\bar{t}) + \bar{\Omega}^2 \bar{e} \cos(\bar{\Omega}\bar{t}),\\
\bar{z}_2 &= \bar{F}_y + \bar{A}_y \sin(\bar{p}\bar{t}) + \bar{\Omega}^2 \bar{e} \sin(\bar{\Omega}\bar{t}),\\
\bar{z}_3 &= \bar{M}_x + \bar{B}_x \sin(\bar{p}\bar{t}) + \bar{\Omega}^2 \bar{\gamma}(1-\Pi_1)\cos(\bar{\Omega}\bar{t}),\\
\bar{z}_4 &= \bar{M}_y + \bar{B}_y \sin(\bar{p}\bar{t}) + \bar{\Omega}^2 \bar{\gamma}(1-\Pi_1)\sin(\bar{\Omega}\bar{t}),
\end{aligned} \tag{42}$$

and by introducing the perturbation model for each new variable in the form of integrators:

$$\frac{d\bar{z}_1}{d\bar{t}} = \mu_1 \Phi_{tech1}, \quad \frac{d\bar{z}_2}{d\bar{t}} = \mu_2 \Phi_{tech2}, \quad \frac{d\bar{z}_3}{d\bar{t}} = \mu_3 \Phi_{tech3}, \quad \frac{d\bar{z}_4}{d\bar{t}} = \mu_4 \Phi_{tech4}, \tag{43}$$

with μ_1, ..., μ_4 – constant coefficients. For the rotor stabilization the control goals can be written in the form of invariants (technological invariants):

$$\begin{aligned}
&\Phi_{tech1} = \bar{x}_1 - \bar{x}_1^0 = 0, \quad \Phi_{tech2} = \bar{y}_1 - \bar{y}_1^0 = 0,\\
&\Phi_{tech3} = \bar{\alpha}_1 - \bar{\alpha}_1^0 = 0, \quad \Phi_{tech4} = \bar{\beta}_1 - \bar{\beta}_1^0 = 0,
\end{aligned} \tag{44}$$

where $\bar{x}_1^0$, $\bar{y}_1^0$, $\bar{\alpha}_1^0$, $\bar{\beta}_1^0$ are desired values of the state coordinates. With Eq. (26) and Eq. (27) the system of equations Eq. (23) is expressed:

$$\begin{aligned}
\bar{x}_1' &= \bar{x}_2,\\
\bar{x}_2' &= \bar{x}_1 + \frac{(-\bar{a}_1 + \bar{a}_2)}{2}\bar{\beta}_1 + \bar{S}_{Ax} + \bar{S}_{Bx} + \bar{z}_1,\\
\bar{y}_1' &= \bar{y}_2,\\
\bar{y}_2' &= \bar{y}_1 + \frac{(\bar{a}_1 - \bar{a}_2)}{2}\bar{\alpha}_1 + \bar{S}_{Ay} + \bar{S}_{By} + \bar{z}_2,\\
\bar{\alpha}_1' &= \bar{\alpha}_2,\\
\bar{\alpha}_2' &= -\Pi_H \bar{\alpha}_2 - \Pi_1 \bar{\theta}_2 \bar{\beta}_2 + \frac{\Pi_2}{2}(\bar{a}_1 - \bar{a}_2)\bar{y}_1 - \Pi_H \bar{\theta}_2 \bar{\beta}_1 + \bar{a}_1 \Pi_2 \bar{S}_{Ay} - \bar{a}_2 \Pi_2 \bar{S}_{By} + \dots\\
&\quad + \frac{\Pi_2}{4}\left((\bar{a}_1^2 + \bar{a}_2^2)(1 + \bar{k}_m) - 2\bar{a}_1 \bar{a}_2 (1 - \bar{k}_m)\right)\bar{\alpha}_1 + \bar{z}_3,\\
\bar{\beta}_1' &= \bar{\beta}_2,\\
\bar{\beta}_2' &= -\Pi_H \bar{\beta}_2 + \Pi_1 \bar{\theta}_2 \bar{\alpha}_2 + \frac{\Pi_2}{2}(-\bar{a}_1 + \bar{a}_2)\bar{x}_1 + \Pi_H \bar{\theta}_2 \bar{\alpha}_1 - \bar{a}_1 \Pi_2 \bar{S}_{Ax} + \bar{a}_2 \Pi_2 \bar{S}_{Bx} + \dots\\
&\quad + \frac{\Pi_2}{4}\left((\bar{a}_1^2 + \bar{a}_2^2)(1 + \bar{k}_m) - 2\bar{a}_1 \bar{a}_2 (1 - \bar{k}_m)\right)\bar{\beta}_1 + \bar{z}_4,\\
\dot{\bar{z}}_1 &= \mu_1 \Phi_{tech1}, \quad \dot{\bar{z}}_2 = \mu_2 \Phi_{tech2}, \quad \dot{\bar{z}}_3 = \mu_3 \Phi_{tech3}, \quad \dot{\bar{z}}_4 = \mu_4 \Phi_{tech4},
\end{aligned} \tag{45}$$

where:

$$\bar{S}_{Ax} = \Pi_K \left[\left(\frac{\bar{\imath}_0 + \bar{u}_1}{\bar{\delta} - (\bar{x}_1 - \bar{a}_1\bar{\beta}_1)} \right)^2 - \left(\frac{\bar{\imath}_0 - \bar{u}_1}{\bar{\delta} + (\bar{x}_1 - \bar{a}_1\bar{\beta}_1)} \right)^2 \right],$$
$$\bar{S}_{Bx} = \Pi_K \left[\left(\frac{\bar{\imath}_0 + \bar{u}_2}{\bar{\delta} - (\bar{x}_1 + \bar{a}_2\bar{\beta}_1)} \right)^2 - \left(\frac{\bar{\imath}_0 - \bar{u}_2}{\bar{\delta} + (\bar{x}_1 + \bar{a}_2\bar{\beta}_1)} \right)^2 \right],$$
$$\bar{S}_{Ay} = \Pi_K \left[\left(\frac{\bar{\imath}_0 + \bar{u}_3}{\bar{\delta} - (\bar{y}_1 + \bar{a}_1\bar{\alpha}_1)} \right)^2 - \left(\frac{\bar{\imath}_0 - \bar{u}_3}{\bar{\delta} + (\bar{y}_1 + \bar{a}_1\bar{\alpha}_1)} \right)^2 \right],$$
$$\bar{S}_{By} = \Pi_K \left[\left(\frac{\bar{\imath}_0 + \bar{u}_4}{\bar{\delta} - (\bar{y}_1 - \bar{a}_2\bar{\alpha}_1)} \right)^2 - \left(\frac{\bar{\imath}_0 - \bar{u}_4}{\bar{\delta} + (\bar{y}_1 - \bar{a}_2\bar{\alpha}_1)} \right)^2 \right].$$

The control currents $\bar{\imath}_{Ax}, \bar{\imath}_{Bx}, \bar{\imath}_{Ay}, \bar{\imath}_{By}$ are control channels $\bar{u}_1 = \bar{\imath}_{Ax}$, $\bar{u}_2 = \bar{\imath}_{Bx}, \bar{u}_3 = \bar{\imath}_{Ay}$, $\bar{u}_4 = \bar{\imath}_{By}$. To further synthesize the control laws a parallel totality of macrovariables can be selected in the following form [32]:

$$\psi_1 = \bar{x}_2 - \varphi_1, \quad \psi_2 = \bar{y}_2 - \varphi_2, \quad \psi_3 = \bar{\alpha}_2 - \varphi_3, \quad \psi_4 = \bar{\beta}_2 - \varphi_4. \tag{46}$$

$\varphi_1, \varphi_2, \varphi_3, \varphi_4$ represent the internal controls and are determined in the course of further synthesis. For the macrovariables Eq. (30) to be invariant manifolds it is necessary that $\psi_{1,\dots,4} = 0$. For this the introduced set Eq. (30) must satisfy the solution of the system of basic functional equations of the ADAR method [32-34]:

$$T_1\dot{\psi}_1 + \psi_1 = 0, \quad T_2\dot{\psi}_2 + \psi_2 = 0, \quad T_3\dot{\psi}_3 + \psi_3 = 0, \quad T_4\dot{\psi}_4 + \psi_4 = 0, \tag{47}$$

where $T_1, T_2, T_3, T_4 > 0$ are time constants that affect the quality of the processes dynamics in a closed-loop system. Substituting expressions Eq. (30) and the complete derivatives of expressions Eq. (30) into equations Eq. (31) we have:

$$\begin{aligned} &T_1[\dot{\bar{x}}_2 - \dot{\varphi}_1] + \bar{x}_2 - \varphi_1 = 0, \quad T_2[\dot{\bar{y}}_2 - \dot{\varphi}_2] + \bar{y}_2 - \varphi_2 = 0, \\ &T_3[\dot{\bar{\alpha}}_2 - \dot{\varphi}_3] + \bar{\alpha}_2 - \varphi_3 = 0, \quad T_4\left[\dot{\bar{\beta}}_2 - \dot{\varphi}_4\right] + \bar{\beta}_2 - \varphi_4 = 0. \end{aligned} \tag{48}$$

The controls $\bar{u}_1, \bar{u}_2, \bar{u}_3, \bar{u}_4$ can be obtained from the system Eq. (32) when substituting the right-hand sides of the equations for variables $\dot{\bar{x}}_2, \dot{\bar{y}}_2, \dot{\bar{\alpha}}_2, \dot{\bar{\beta}}_2$ in Eq. (29). The obtained control laws depend on $\varphi_{1,\dots,4}$ and $\dot{\varphi}_{1,\dots,4}$. Under the control laws $\bar{u}_1, \bar{u}_2, \bar{u}_3, \bar{u}_4$ the represented point (RP) of the dynamical system hits the intersection of manifolds $\psi_{1,\dots,4} = 0$ and then moving along it to a given position of the phase space. When RP hits the intersection of manifolds Eq. (30), the system Eq. (29) is decomposed dynamically. The motion of the RP along the intersection of manifolds $\psi_{1,\dots,4} = 0$ is described by the equations of "internal" dynamics – the decomposed system:

$$\begin{aligned} &\dot{\bar{x}}_1 = \varphi_1, \quad \dot{\bar{z}}_1 = \mu_1(\bar{x}_1 - \bar{x}_1^0), \\ &\dot{\bar{y}}_1 = \varphi_2, \quad \dot{\bar{z}}_2 = \mu_2(\bar{y}_1 - \bar{y}_1^0), \\ &\dot{\bar{\alpha}}_1 = \varphi_3, \quad \dot{\bar{z}}_3 = \mu_3(\bar{\alpha}_1 - \bar{\alpha}_1^0), \\ &\dot{\bar{\beta}}_1 = \varphi_4, \quad \dot{\bar{z}}_4 = \mu_4\left(\bar{\beta}_1 - \bar{\beta}_1^0\right). \end{aligned} \tag{49}$$

For system Eq. (33), introduced earlier and called "internal" controls $\varphi_1, \varphi_2, \varphi_3, \varphi_4$ are external. Then, to find them explicitly, we introduce another parallel set of macrovariables:

$$\psi_5 = (\bar{x}_1 - \bar{x}_1^0) + h_1\bar{z}_1, \quad \psi_6 = (\bar{y}_1 - \bar{y}_1^0) + h_2\bar{z}_2,$$
$$\psi_7 = (\bar{\alpha}_1 - \bar{\alpha}_1^0) + h_3\bar{z}_3, \quad \psi_8 = (\bar{\beta}_1 - \bar{\beta}_1^0) + h_4\bar{z}_4, \tag{50}$$

where h_j, $j = 1, ..., 4$ – constant coefficients. The structure of macrovariables Eq. (34) includes the desired technological invariants Eq. (28), which determine the control goals. The introduced set of macrovariables must satisfy the solution of the system of basic functional equations of the ADAR method:

$$T_5\dot{\psi}_5 + \psi_5 = 0, \quad T_6\dot{\psi}_6 + \psi_6 = 0, \quad T_7\dot{\psi}_7 + \psi_7 = 0, \quad T_8\dot{\psi}_8 + \psi_8 = 0, \tag{51}$$

where T_5, T_6, T_7, $T_8 > 0$ are time constants. To explicitly define the functions φ_1, φ_2, φ_3, φ_4 it is necessary to differentiate the macrovariables Eq. (34) and substitute the expressions for $\psi_{5,\dots,8}$ and their derivatives with the right-hand sides of the system Eq. (33) into the functional equations Eq. (32). Under the control laws φ_1, φ_2, φ_3, φ_4 the RP of the dynamical system will fall on the intersection of manifolds $\psi_{5,\dots,8} = 0$ on which the control goals (technological invariants) will occur. A prerequisite for this is the tendency to zero $\bar{z}_i$, $i = 1, \dots, 4$. This is clearly seen from the decomposed system:

$$\dot{\bar{z}}_1 = -\mu_1 h_1 \bar{z}_1, \quad \dot{\bar{z}}_2 = -\mu_2 h_2 \bar{z}_2, \quad \dot{\bar{z}}_3 = -\mu_3 h_3 \bar{z}_3, \quad \dot{\bar{z}}_4 = -\mu_4 h_4 \bar{z}_4. \tag{52}$$

The stability of the degenerate system Eq. (36) is given by simple conditions: $\mu_1 h_1 > 0$, $\mu_2 h_2 > 0$, $\mu_3 h_3 > 0$ and $\mu_4 h_4 > 0$. The expressions for $\varphi_{1,\dots,4}$ obtained in explicit form are substituted into the $\bar{u}_1$, $\bar{u}_2$, $\bar{u}_3$,$\bar{u}_4$.

Table 1. Model data for dynamic analysis

Parameter	Symbol/ Value/ Unit
Diameter of the flow part	$D = 16{\cdot}10^{-3}$ m
Rotor diameter	$d = 15.6{\cdot}10^{-3}$ m
Radial gap	$\delta = 0.2{\cdot}10^{-3}$ m
Rotor length	$l = 22{\cdot}10^{-3}$ m
Rotor mass	$m = 12.42{\cdot}10^{-3}$ kg
Moments of inertia	$I_x = I_y = 6.9{\cdot}10^{-7}$ kg m^2, $I_z = 3.78{\cdot}10^{-7}$ kg m^2
Bearings coordinates	$a_1 = a_2 = 9{\cdot}10^{-3}$ m
Motor stiffness	$c_m = 6000$ N/m
Motor design parameter	$k_m = 0.202$
Unbalances parameters	$e = 4.27{\cdot}10^{-7}$ m, $\gamma = 2.15{\cdot}10^{-5}$ rad
Dimensionless complex	$\Pi_1 = I_z/I_x = 0.548$
Dimensionless complex	$\Pi_2 = ml^2/I_x = 8.714$
Dimensionless complex	$\Pi_K = k_A P/c_m R\delta^3 = 10^5$
Dimensionless complex	$\Pi_H = \frac{c_w \eta \pi l^3 \bar{r}^2 \bar{l}\sqrt{m/c_m}}{I_x} = 1.48{\cdot}10^{-7}$
Blood viscosity at 37 °C (non-Newtonian model of blood)	$\eta = 0.056$ Pa s
Coefficient of medium resistance	$c_w = 0.91$

4. Research results

Fig. 4 shows transients of the closed-loop system under external piecewise constant and harmonic loads. The transient time is 0.4 s and the output to the steady state occurs without additional oscillations and overregulation. The requirement of the accuracy of the rotor positioning is 4 μm and due to compensation of external disturbances is fulfilled. System parameters are given

by Table 1.

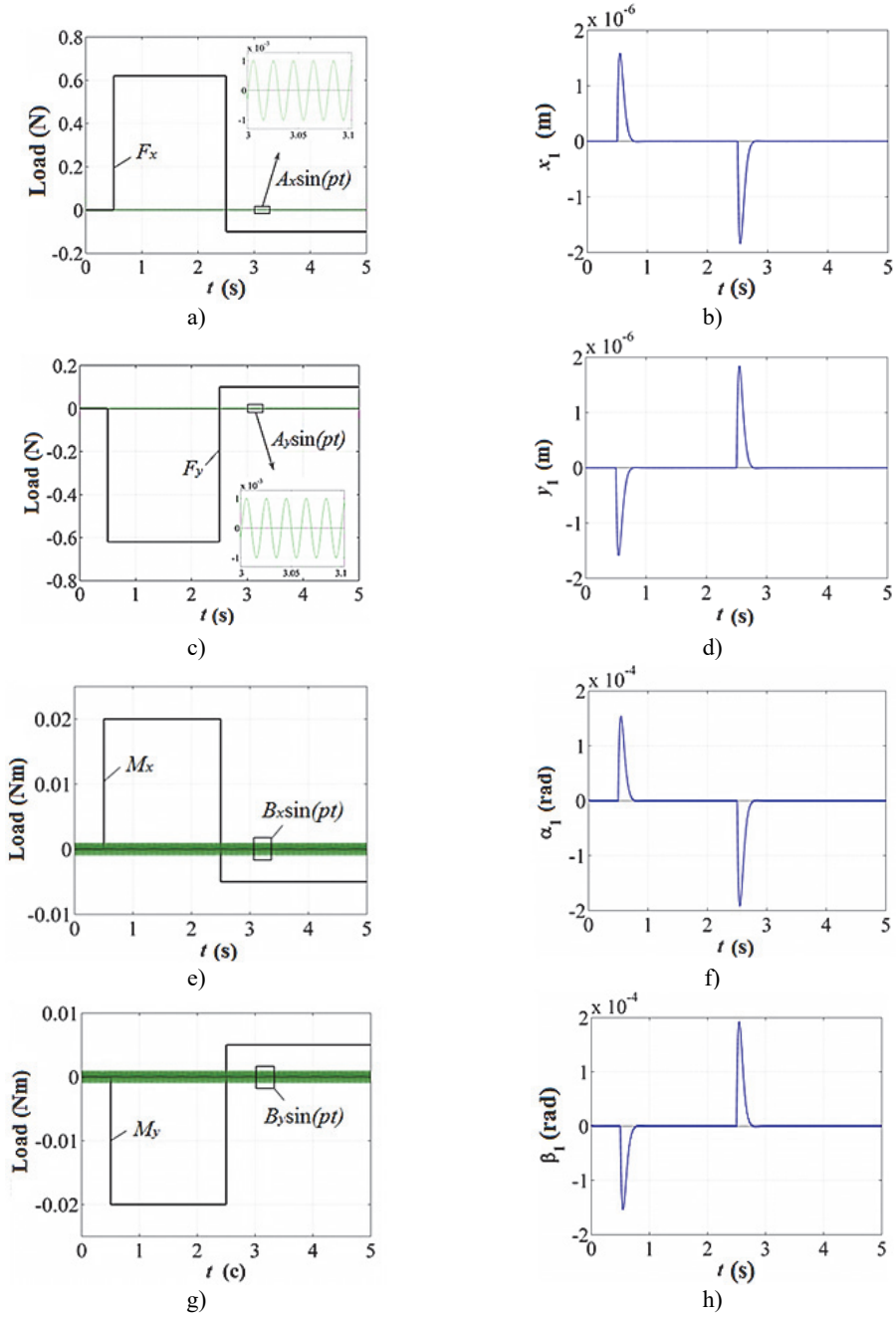

Fig. 4. State variables transients

Dynamic analysis was performed for the following coefficients of control: $T_{1,2,\ldots,8} = 35$, $h_{1,2,3,4} = 4000$, $\mu_1 = \mu_2 = 0.2$, $\mu_3 = \mu_4 = 1.2$ and zero initial values for the state coordinates. From the Pressure-Flow characteristic, constructed for the flow part optimal geometry of the blood pump [28], the following values of the rotational speed were received:

$A = \frac{700 \cdot \pi}{30}$ rad/s, $\omega = 2\pi$ rad/s, $\Omega_0 = \frac{9000 \cdot \pi}{30}$ rad/s. Values of the piecewise constant load are reference data and taken from the biomechanical analysis of human organism behavior at various accelerations [37]. Harmonic inertial load, to which the patient is exposed, for example, in transport, has low frequency (about 50 Hz).

Phase portraits (Fig. 5) demonstrate the contraction of the phase trajectories of the dynamical system to the target attractor under various initial conditions – something that is difficult to provide with other control methods. This fact also confirms the modeling of the "levitation startup" mode of the rotor from the safety bearings when the suspension is switched on, i.e. with the maximum possible deviation of the rotor from the zero-equilibrium position (Fig. 6(a)). The range of possible rotor positions is the region of attraction to the equilibrium position. The synthesized control laws guarantee the asymptotic stability of the closed-loop system and the parametric robustness of the dynamical system. The study of the parametric robustness was carried out by double increasing and decreasing each of the following parameters: Π_1, Π_2, Π_H, $\bar{a}_1$, $\bar{a}_2$, $\bar{e}$, $\bar{\gamma}$. The maximum value of the control currents is 5.4 mA (Fig. 6(b)). This is two times less than with linear PID control.

To test the effectiveness of the approach to creating the blood flow pulsations due to change in rotational speed computational fluid dynamics (CFD) analysis was carried out [38, 39]. Pressure rise changes in accordance with the change in the rotational speed (Fig. 7).

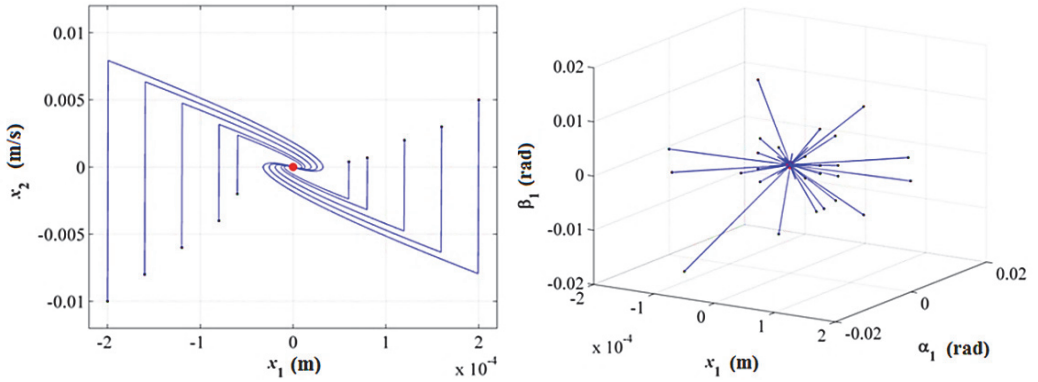

a) b)

Fig. 5. Phase portraits

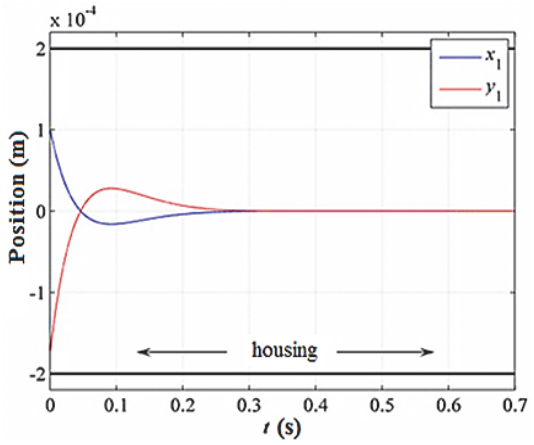

a)

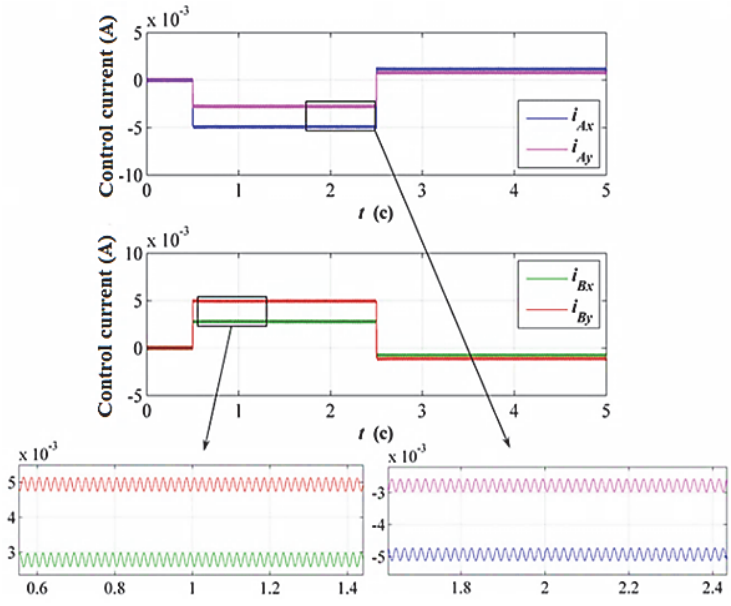

b)

Fig. 6. a) Levitation startup time history, b) value of control currents

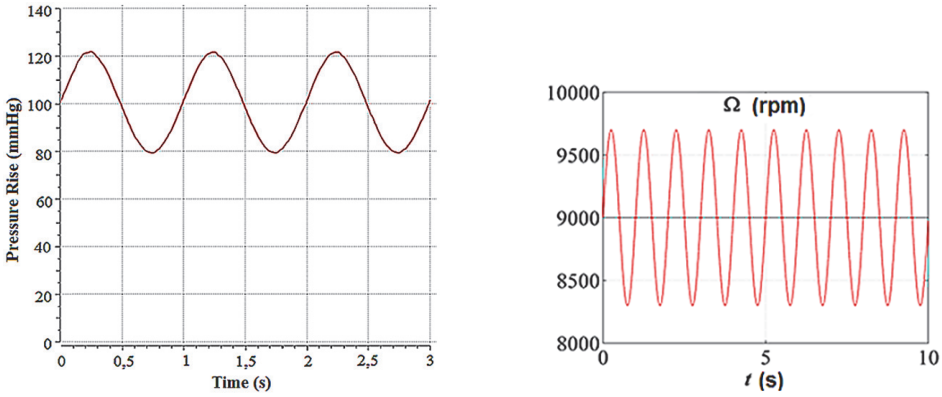

a) b)

Fig. 7. The change in pressure rise (CFD analysis result) a) according to change in rotational speed b)

5. Conclusions

The effective nonlinear control laws for stabilizing with high accuracy the rotor suspended by active magnetic bearings in axial LVAD that guarantee the provision of the required rotor dynamics under the conditions of various perturbations and changes in the internal parameters of the model were synthesized in this research. For this the basic method and principle of the synergetic control theory were applied. The developed methods for ensuring the required rotor dynamics are accurate, fast, economical in the sense of the values of control currents, and most importantly reliability, which in general ensures an increase in the safety of the life support system – left ventricular assist device. The designed synergetic control laws ensure the blood flow pulsations regime and compensate unwanted external disturbances as well as internal parametric perturbations. For the proposed LVAD with magnetic bearings of the new generation, which is the complex biomechanical system, with a wide spread of physical parameters and performance characteristics, the synergetic approach, unlike classical control methods, allows performing

highly efficient "non-power" control, consistent with a substantially nonlinear and multiply connected structure of control object.

Acknowledgements

This work was supported by the Russian Foundation for Basic Research (Grant No. 15-29-01085 ofi_m).

References

[1] **Finocchiaro T., et al.** Methods of design, simulation, and control for the development of new VAD/TAH concepts. Biomedical Engineering, Vol. 54, Issue 5, 2009, p. 269-281.
[2] **Gautier S. V., et al.** Donation and organ transplantation in the Russian federation in 2013. Bulletin of Transplantology and Artificial Organs, Vol. 2, 2014, p. 5-23.
[3] **Sajgalik P., et al.** Current status of left ventricular assist device therap. Mayo Clinic Proceedings, Vol. 91, Issue 7, 2016, p. 927-940.
[4] **Birks E. J.** The comparative use of ventricular assist device. 18th Annual THI Summit, 2010, p. 565-567.
[5] **Alba A. C., Delgado D. H.** The future is here: ventricular assist devices for the failing heart. Expert Review of Cardiovascular Therapy, Vol. 7, Issue 9, 2009, p. 1067-1077.
[6] **Rau G.** Research Report 2001/2002. Institute for Biomedical Technologies, Aachen University, 2002, p. 101.
[7] **Wurzinger L. J., Opitz R., Eckstein H.** Mechanical blood trauma: an overview. Angiology, Vol. 38, 1986, p. 81-97.
[8] **Allaire P. E., et al.** Design of a magnetic bearing-supported prototype centrifugal artificial heart pump. Tribology Transactions, Vol. 39, Issue 3, 1996, p. 663-669.
[9] **Yu J., Zhang X.** Hydrodynamic and hemolysis analysis on distance and clearance between impeller and diffuser of axial blood pump. Journal of Mechanics in Medicine and Biology, Vol. 16, Issue 2, 2016, p. 1650014.
[10] **Hoshi H., Shinshi T., Takatani S.** Third-generation blood pumps with mechanical noncontact magnetic bearings. Artificial Organs, Vol. 30, Issue 5, 2006, p. 324-338.
[11] **Pagani F. D.** Continuous-flow rotary left ventricular assist devices with "3rd generation" design. Seminars in Thoracic and Cardiovascular Surgery. WB Saunders, Vol. 20, Issue 3, 2008, p. 255-263.
[12] **Bogdanova Yu V., Gouskov A. M.** Left ventricular assist device (LVAD) design features: literature review. Science and Education: Scientific Publication of the Bauman Moscow State Technical University, Vol. 3, 2014, p. 162-187.
[13] **Crow S., et al.** Gastrointestinal bleeding rates in recipients of nonpulsatile and pulsatile left ventricular assist devices. The Journal of Thoracic and Cardiovascular Surgery, Vol. 137, Issue 1, 2009, p. 208-215.
[14] **John R., et al.** A decade of experience with continuous-flow left ventricular assist devices. Seminars in Thoracic and Cardiovascular Surgery. WB Saunders, Vol. 28, Issue 2, 2016, p. 363-375.
[15] **Chiba A., et al.** Magnetic Bearings and Bearingless Drives. Elsevier, 2005, p. 400.
[16] **Schweitzer G., Maslen E. H.** Magnetic Bearings: Theory, Design, and Application to Rotating Machinery. Springer-Verlag Berlin Heidelberg, 2009, p. 541.
[17] **Zhuravlev Yu N.** Active Magnetic Bearings. Polytechnic, 2002, p. 206.
[18] **Esfahani A.** Chaotic Behaviour of Active Magnetic Bearing System by Time Series Analysis. Thesis, Lappeenranta University of Technology, 2012, p. 104.
[19] **Gerami A., Allaire P., Fittro R.** Nonlinear modeling and control of a magnetic bearing with material saturation. Proceedings of the 14th International Conference on Magnetic Bearings, Linz, Austria, 2014.
[20] **Ji J. C., Hansen C. H., Zander A. C.** Nonlinear dynamics of magnetic bearing systems. Journal of Intelligent Material Systems and Structures, Vol. 19, Issue 12, 2008, p. 1471-1491.
[21] **Kang K.** Nonlinear Dynamics of a Rotor Supported by Homopolar Magnetic Bearings with Saturation. Thesis, Texas A&M University, 2010, p. 109.
[22] **Steinschaden N., Springer H.** Some nonlinear effects of magnetic bearings. Proceedings of the DETC ASME Conference, 1999.
[23] Vibration. Requirements for Balancing Rigid Rotors: Part 1. GOST ISO 1940-1-2007, 2007.

[24] Vibration. Vibration of Rotary Action Machines with Active Magnetic Bearings: Part 2. GOST R ISO 14839-2-2011, 2011.
[25] **Gomez A. D.** Control of a magnetically levitated ventricular assist device. Thesis, Rochester Institute of Technology, 2009, p. 140.
[26] **Barenblatt G. I.** Scaling, Self-Similarity, and Intermediate Asymptotics: Dimensional Analysis and Intermediate Asymptotics. Cambridge University Press, 1996, p. 388.
[27] **Sedov L. I.** Similarity and Dimension Methods in Mechanics. Elsevier, 1977, p. 376.
[28] **Gouskov A. M., et al.** Mathematical modeling of the blood flow in the flowing part of the axial pump of the artificial ventricle of the heart. Science and Education: Scientific Publication of the Bauman Moscow State Technical University, Vol. 10, 2015, p. 473-488.
[29] **Bogdanova Yu, Gouskov A., Guskov M.** Synergetic approach to control of axial left ventricular assist device rotor supported by magnetic bearings. Vibroengineering PROCEDIA, Vol. 8, 2016, p. 340-345.
[30] **Bounasla N., Hemsas K., Mellah H.** Synergetic and sliding mode controls of a PMSM: a comparative study. Journal of Electrical and Electronics Engineering, Vol. 3, 2015, p. 22-26.
[31] **Genta G.** Vibration Dynamics and Control. Springer Science, 2009, p. 812.
[32] **Kolesnikov A. A., et al.** Modern Applied Control Theory. Part II: The Synergetic Approach in Control Theory. TSET Publishing House, Moscow-Taganrog, 2000, p. 559.
[33] **Kolesnikov A. A.** Synergetic Methods of Managing Complex Systems: Mechanical and Electromechanical Systems. Librokom, Moscow, 2012, p. 300.
[34] **Kolesnikov A. A.** Synergetic Methods for Controlling Complex Systems: The Theory of System Synthesis. Energoatomizdat, Moscow, 2012, p. 340.
[35] **Lidozzi A., Solero L., Taddia P.** Synergetic control for axial-flux PM motor drives. 40th IAS Annual Meeting. Conference Record of the 2005 Industry Applications Conference, 2005.
[36] **Wang Z., Zhao Y.** The speed mode synergetic control approach for magnetic suspended reaction flywheel. Applied Mathematics and Information Sciences, Vol. 7, 2013, p. 107-111.
[37] **Rabinovich B. A.** Safety of a Person under Acceleration. Biomechanical Analysis, Moscow, 2006, p. 208.
[38] **Apel J., Neudel F., Reul H.** Computational fluid dynamics and experimental validation of a microaxial blood pump. ASAIO Journal, Vol. 47, Issue 5, 2001, p. 552-558.
[39] **Behbahani M., et al.** A review of computational fluid dynamics analysis of blood pumps. European Journal of Applied Mathematics, Vol. 20, Issue 4, 2009, p. 363-397.

Yulia Bogdanova received the Specialist degree in applied mechanics (2013) and the Candidate of Science degree in mechanical engineering (2017) from Bauman Moscow State Technical University, Russia. During her postgraduate studies at Bauman Technical University, Yulia has focused on nonlinear dynamics, control theory and rotordynamics. In parallel she works as an engineer of the Robotics Laboratory in the NRC "Kurchatov Institute".

Alexander Guskov is the Doctor of Science degree in mechanical engineering and Professor at the Department of Applied Mechanics in Bauman Moscow State Technical University and in the Vibrations Laboratory in the RAS Institute of Machine Science, Russia. His current research interests include nonlinear dynamics, stability theory, rotordynamics, control theory.

2.4. Increasing of efficiency of parts turning at spindle speed from 5,000 to 10,000 rpm by controlling the dynamics of machining

Wiliam Zaloga[1], Yurii Shapoval[2], Vitalii Kolesnyk[3]
Sumy State University, Sumy, Ukraine
E-mail: [1]*zalogav@gmail.com*, [2]*diyyura@gmail.com*, [3]*v.kolesnik@tmvi.sumdu.edu.ua*

Abstract. The article deals with the issues of increasing the productivity of turning parts at rotational speed up to 10,000 rpm. The reasons for reducing roughness of machined surface when approaching the resonant rotational speeds are analysed. The hypothesis about the dependence of the vibrational component of roughness of the machined surface on the external generating forces and natural oscillation modes and frequencies of technological system is set-up. The methods of studying the dynamic behaviour of the lathe are reviewed, as well as the way of changing system properties to improve stability in the increased cutting conditions and productivity. The authors prove the possibility of a local reduction in the oscillation amplitude of a tool by changing the machine natural oscillation modes in order to increase rotational speed during the continuous machining.

Keywords: turning at 5-10 thousand rpm, turning dynamics, stability.

1. Introduction

In the machine building, instrumentation, aircraft industry and other industries due to the reduction in machines and mechanisms, the proportion of parts representing the rotation bodies up to 20 mm is constantly increasing (bodies of measuring detectors, short axes of devices, plungers of hydraulic dispensers and power units, tips for current collectors of welding equipment, pins, etc.), manufacturing technology of which requires turning. Besides, the quality requirements for the machined surfaces of these parts are increasing, which is stipulated by the necessity to provide the relevant performance characteristics of the item, particularly strength in case of its overall dimensions reduction, durability, fatigue resistance, increase of contact stiffness, vibration stability, etc. The need to ensure a constantly changing demand for a small-diameter parts creates preconditions for increasing the process productivity of machining. Increasing the productivity of cutting off the dimensional allowance during parts turning with surface diameters of up to 20 mm, due to their relatively low rigidity, is usually possible by increasing the cutting speed.

Turning technology of machining parts made of different structural materials with relatively high cutting speeds during turning can provide the necessary quality according to requirements and in many cases eliminate the need for additional finishing. This became possible with the development of tool materials for edge cutting machining, for example, hard alloys, particularly with wear-resistant coatings which allowed to machine ferrous metal parts (steels, alloys, cast iron, etc.) at cutting speeds over 500 m/min, and for non-ferrous (aluminium, copper, etc.) metals and alloys at speeds above 1000 m/min. Thus, one can say that the potential reserves for increasing productivity during turning are the modern tool materials' ability to cut at high speed, and for parts with small dimensions (diameters up to 20 mm) with rotational speeds of 6000 rpm and more.

The analysis shows that in order to increase the cutting speed of small diameter parts by increasing rotational speed to obtain the required (given in a drawing) accuracy and roughness of the machined surfaces, it is necessary to provide a stable dynamic behaviour of machines. In this case, the influence machines' part oscillations on the cutting process should be minimal, and dynamic characteristics of movable operating elements should ensure the exact and synchronous operation of the whole technological system.

Today a sufficient number of modern machines and machining centres provide maximum spindle speed up to 5000-6000 rpm. At the same time, one of the important issues during their

application is to ensure the stable dynamic behaviour of the spindle unite, sliding carriage, auxiliary devices, etc.

Increasing of rotational speeds when machining parts with a diameter of up to 20 mm can reduce the cutting speed to the values recommended by tool manufacturers (for example, machining of steel by carbide tools require cutting speed 250-300 m/min), which can lead to the loss of dynamic stability of the spindle unite and sliding carriage decline in the corresponding quality rating. It happens due to the fact that the high rotational speed significantly increases the imbalance of "spindle – device – workpiece" system and as a result, the power of the imbalance can often significantly exceed the power of cutting and therefore significantly affect the dynamic behaviour of the entire technological system.

Thus, the development of the principles of controlling dynamics machining during turning parts with diameter up to 20 mm at high rotational speeds is an important scientific and technical task, the solution of which will improve performance of machining these parts while ensuring the drawing requirements for roughness and tolerance.

2. State of the art

In the nearest future the technical capabilities of turning lathes and machining centres will allow to machine on higher speeds compared to rotational speeds which are traditionally used in modern manufacturing. This is due to the fact that machines of other groups (for example, milling machines, grinding machines, etc.) are capable of carrying out the main motion at rotational speeds of up to 100.000 rpm. At the same time, even this is not enough to use all the capabilities of a modern cutting tool, for example, diamond or cubic boron nitride, especially for machining parts of non-ferrous metals with small diameters.

Traditionally, the scheme for small-diameter parts turning is a machining with automatic lathes and CNC machines. The worldwide manufacturing leaders of such machines are Star CNC Machine Tool Corp, Index Corporation, Haas Automation, Okuma, DMG, Mori Seiki. Serially produced machines which can provide the following maximum speeds: Haas OL-1, Haas ST-10 – 6000 rpm, Okuma MULTUS B200II – 5000 rpm, DMG Nef400 – 4500 rpm, Mori Seiki NLX 2500/750 – 3500 rpm, Yamazaki Mazak Quick turn smart 100s – 6000 rpm, Index c100 – 6000 rpm. Today only the following machine station models allow the maximum possible rotational speed for the workpiece: Star micronics AG SR20RIII - 10,000 rpm and Star micronics AG SR-10j – 15,000 rpm, Tornos SwissNano 16,000 rpm, NomuraDS NN – 10EX 15,000 rpm, HanwhaXD20V 10,000 rpm [1].

The analysis shows that during parts machining with a diameter of up to 20 mm reaching the optimum cutting speed recommended by the tool manufacturer on the mass-produced machines even at sufficiently high spindle rotational speed is very difficult due to the common use of a long bar as a workpiece in batch manufacturing. Usage of long bars generate unbalance due to its out-of-roundness and other reasons, often causing an unacceptable level of vibration (Fig. 1). For example, when turning a part with a diameter of 20 mm in order to reach the speed of 300 m/min, it is necessary to provide its rotation speed of almost 5000 rpm, which can be done on almost all modern turning lathes. However, only certain specialized models of lath machines for example, STAR machines, can provide the cutting speed of 500 m/min. But even they do not allow to reach high cutting speeds when turning parts with surfaces less than 10 mm in diameter.

Analysis of the catalogues of machine tool manufacturers showed that solutions to these problems have already been outlined. This includes, for example, length reduction of the rotating part of the bar, the use of automatic spindle balancing devices, active control of natural oscillations frequencies and modes of the machine. Thus, there are methods for automatic balancing of rotary bodies, which are described in US2331756A [2], US3953074A [3], US4043221A [4], US4075909A [5], US4755006A [6], US5460017A [7], US5605078A [8].

They have argued their efficiency in systems where a rapidly rotating body does not change the value of the speed for a long time. However, their use in machines where the rotational speed

during machining is constantly change is not directly possible.

Turning at high cutting speeds will help to increase efficiency of machining and quality of the machined surface, but only if the vibration level when during machining is not significant. The proximity of the rotational speed to the natural oscillation modes of the technological system causes concerns of increasing vibrations and deterioration of quality of the machined surface. That is why there is a necessity of the development of method of controlling dynamic behavior of technological system in order to establish it stability under the oscillation when machining.

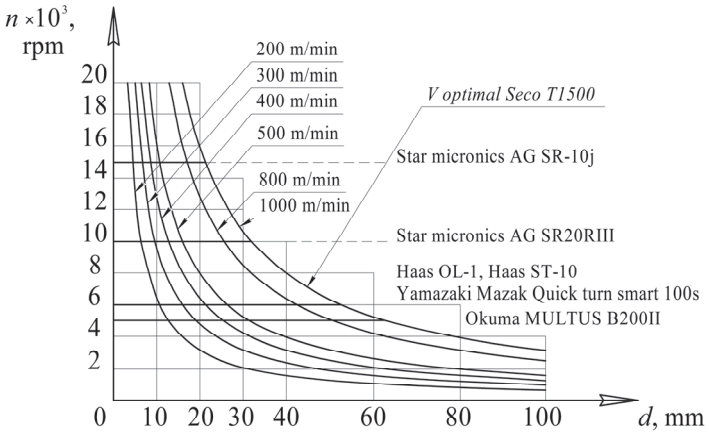

Fig. 1. Effect of rough workpiece diameter on the spindle rotation speed, providing different cutting speeds [1]

The methods of dynamics control of machine processing were studied in the works by Yu. M. Vnukov [9, 10], I. H. Zharkov [11], M. F. Kashirin [12], S. S. Kedrov [13], V. O. Kudinov [14], Yu. M. Kuznietsov [15], I. V. Lutsiv [16], P. P. Melnychuk [17], V. M. Poduraiev [18], V. M. Svinin [19], V. B. Strutynskyi [17], N. I. Tashlitskiy [20], Otto O. [21], J. S. Park [22] and others. The researches of these scientists have proved that increasing rotational speed tends to result in insufficient vibrational stability of cutting, which results in poor roughness of the machined surface, and, therefore, a decrease in the productivity of the machining. It was experimentally found that the roughness of the machined surface is most sensitive to vibrations in technological system than other quality parameters, since the relative oscillation of the tool and spindle along with the workpiece is precisely reflected on microgeometry of machined surface. For example, it is known that with a size tolerance for the 6th quality grade, the roundness oscillation within 2-3 μm is not critical, while an increase in roughness of 2-3 μm is inadmissible.

Along with the analytical and experimental methods of modelling the dynamical behaviour of technological systems, numerical methods for modelling dynamic processes in technical systems, in particular during machining at lathe modelling, have now become widely used. The most significant achievements in this direction were made by such Ukrainian researchers as N. E. Veselovska, Yu. M. Kuznietsov, I. V. Lutsiv, P. P. Melnychuk, V. B. Strutynskyi, V. M. Chupryna and others. Most works are dedicated to the development of mathematical models of the lathe elastic system that consider spatial rigidity of the individual subsystems of the lathe. In mathematical modelling of separate subsystems at a cyclic load it is suggested to perform an influence analysis of the correlation of rigidity of the technological system elements on the deformation of the subsystem "tool-workpiece", which allowed to determine the trajectories of mutual movement of the tool and the part and determine the degree of influence of the system dynamic behaviour on the accuracy and roughness of the machined surface. Prof. V. M. Svinin proved that reducing vibrations in the technical system is possible by varying the frequency and depth of modulation (change) of cutting speed.

In experimental and numerical studies, the existence of a displacements plane attached to the

tool edge point was revealed. This plane proves to be inclined compared to the machines tool axes, which contains an ellipse that is the place of the points of the tool tip displacements. It was established that the tool tip point describes an ellipse. This ellipse is very small and can be considered as a small straight-line segment for the stable cutting process (without vibrations). The ellipse of displacement became more visible in unstable mode (with vibrations). A difference in phase occurred between the tool tip displacements on the radial direction and in the cutting direction which was almost in phase to feed motion direction. The ratio of small and long ellipse axes increases proportionally to feed rate. A weak growth (6 %) of the long and small axes ratio is obtained when the feed rate value decreases. The axis that goes through the stiffness center and the tool tip represents the maximum stiffness direction. The maximum (resp. minimum) stiffness axis of the tool is perpendicular to the large (resp. small) ellipse displacements axis. The self-excited vibrations appearance is strongly influenced by the system stiffness values, their ration and their direction. FFT analysis of the accelerometers signals allows to reach several important parameters and establish coherent correlations between tool tip displacements and the static – elastic characteristics of the machine tool components was tested [23].

M. Siddhpura and R. Paurobally summarized that chatter vibrations are present in almost all cutting operations and they are major obstacles in achieving desired productivity. Vibration between the tool and the workpiece forced regenerative chatter, resulting in a poor surface finish, high-pitch noise and accelerated tool wear which in turn reduces machine tool life, reliability and safety of the machining operation. [24].

G. Urbikain, F. J. Campa, et al. proposed two numerical methods which are combined with multimode analysis to predict chatter in big horizontal lathes. First, a traditional single frequency model (SFM) is used. Secondly, the modern collocation method based on the Chebyshev polynomials (CCM) is alternatively studied. This model can be used to identify the machine design features limiting lathe productivity, as well as the threshold values for choosing good cutting parameters [25].

H. Liu, S. Tang, et al. developed indirect measurement method: the vibration of the tool tip is obtained from the vibration of the measurement point on the turret. The relationship between the tool tip vibration and the turret measurement point vibration is obtained through impact tests. The vibration of the measurement point on the turret is measured via an accelerometer. The measurement point is so far away from the cutting area and chip evacuation zone that the accelerometer and its measurement results will not be affected by the chips and cutting fluid. The accuracy of the measurement method in study was checked by comparing the calculated tool tip vibration calculated from the vibration of the turret measurement point to the directly measured results, which was measured via an accelerometer installed below the tool tip. The comparison results show that the calculated tool tip vibration at main frequencies as well as low frequencies has a high accuracy. Moreover, the effectiveness of the measurement method is verified through machined surface profile [26].

However, not all the important issues are reflected in modern literature. Therefore, the implemented analysis allowed to formulate the purpose and main objectives of the study.

3. Aim and objectives of study

The aim of reported study was to increase efficiency of parts machining on turning lathes by controlling the dynamic behaviour of the technological system to ensure roughness of the surface finish in according to drawing requirements.

To reach this purpose the following objectives were set and realized:

– Analyse the possibility to increase machining efficiency of parts with a diameter of 5-20 mm and to establish the source of influence on roughness of the surface finish during turning at high rotational speed.

– Methodology of oscillations study of turning lathe during cutting process with high rotational speed was developed and implemented at experimental set-up.

– Finite element model of the bench and experimentally verify the effect of natural oscillation frequencies and modes of machine elements on roughness of the surface finish was developed.

– Ways of oscillation amplitudes reduction of the turning lathe working parts during machining at high rotation speed was identified.

– Develop practical recommendations for research results implementation in order to increase productivity of processing by turning parts with relatively small diameters, while complying with drawing requirements used for processed surfaces roughness.

Object of study – dynamics of turning process.

Subject of study – dynamic behaviour of a turning lathe during turning surfaces of the parts with a small diameter at high rotational speed and with set roughness of the surface finish.

4. Methodology of experimental study

Experimental studies were carried out on an experimental set-up (Fig. 2) consisting of: an upgraded high-accuracy turning lathe with computer numerical control (CNC) 1700ВФ30 with increased power of main motion actuator up to 1500 W which allowed to increase rotational speed in the range from 300 to 10.000 rpm; vibration diagnostic equipment which made it possible to measure and digitize signals of oscillation amplitudes of the parts and the cutting tool, and also to perform a modal analysis of the experimental set up, determine its frequency response, and signal modulator of the task (Fig. 2). The modulator allowed to control rotational speed according to the sinusoidal law during the workpiece turning by a left bent straight turning tool with main angle in the plane of 93° equipped with a rhombic throwaway indexable carbide cutting insert CT35M with coating.

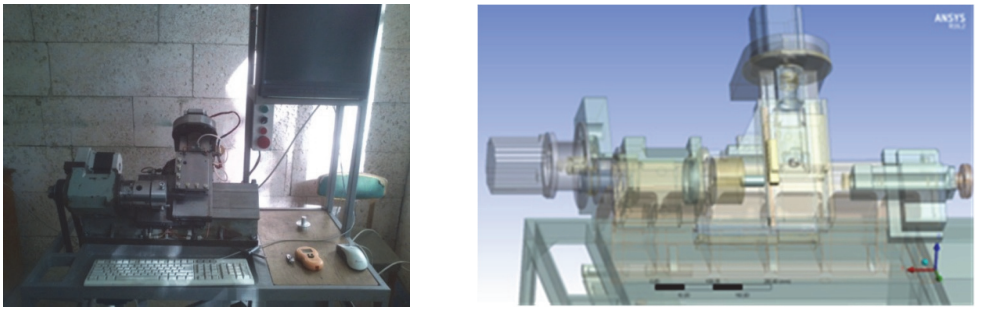

a) b)

Fig. 2. General view of the bench

The signal modulator is designed to change rotational speed according to the harmonic law. The device changes signal of the task that comes from CNC system to power converter of the main motion actuator (Fig. 3). For rotation of a spindle with a given frequency, CNC system produces a signal of U_3 DC task which is proportional to the required spindle rotational speed. The modulator consists of two main components - generator and adder.

The generator produces sinusoidal signal the amplitude of which is proportional to the depth of spindle rotation modulation, while signal frequency is proportional to modulation frequency. With the help of the adder, these two signals are combined and sent to power converter of the main motion actuator. Thus, using a modulator, it is possible to change spindle rotational frequency with set values of modulation depth and frequency, which provides the ability to control the disruption of regeneration of self-oscillations due to the reconstruction of the “trace” cutting.

The vibrational acceleration of the frame was measured by standard Analog Device accelerometer ADXL 321, mounted on a spindle assembly next to spindle bearing and serves as a basis for measuring vibrational acceleration of the tool using the ADXL326 sensor. The vibratory displacement values are determined by further double integration with trapezoidal methods.

Spindle displacement relative to the head stock is measured with the help of the contactless inductive displacement sensor XS1 M18AB120.

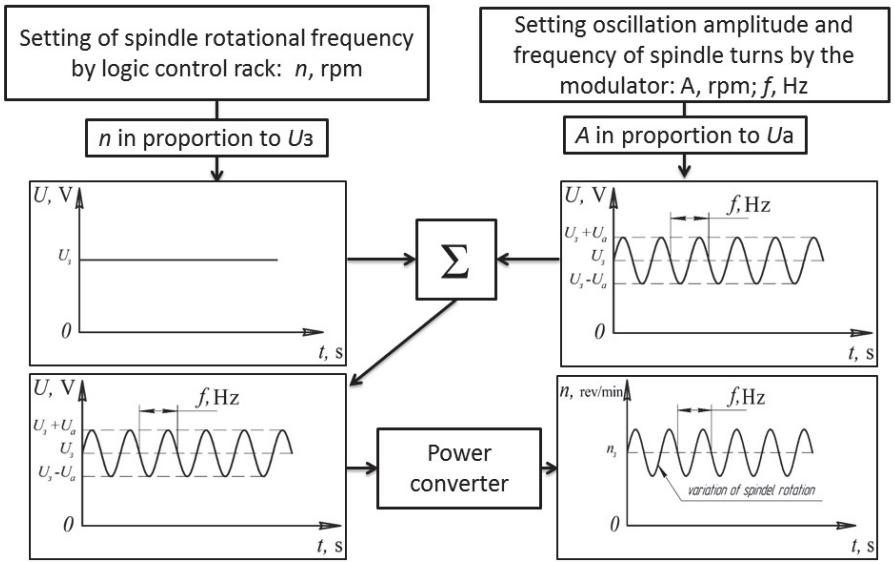

Fig. 3. The basic diagram of the modulator work

The coordination of the operation of all sensors in time occurs on the front edge of a zero-tag of spindle rotation sensor. The signals of all sensors are digitized and transferred to a personal computer (PC) with the help of a four-channel analog-to-digital converter (ADC) with independent inputs for LT-22 model L-CARD vibroacoustic researches (Fig. 4) [27].

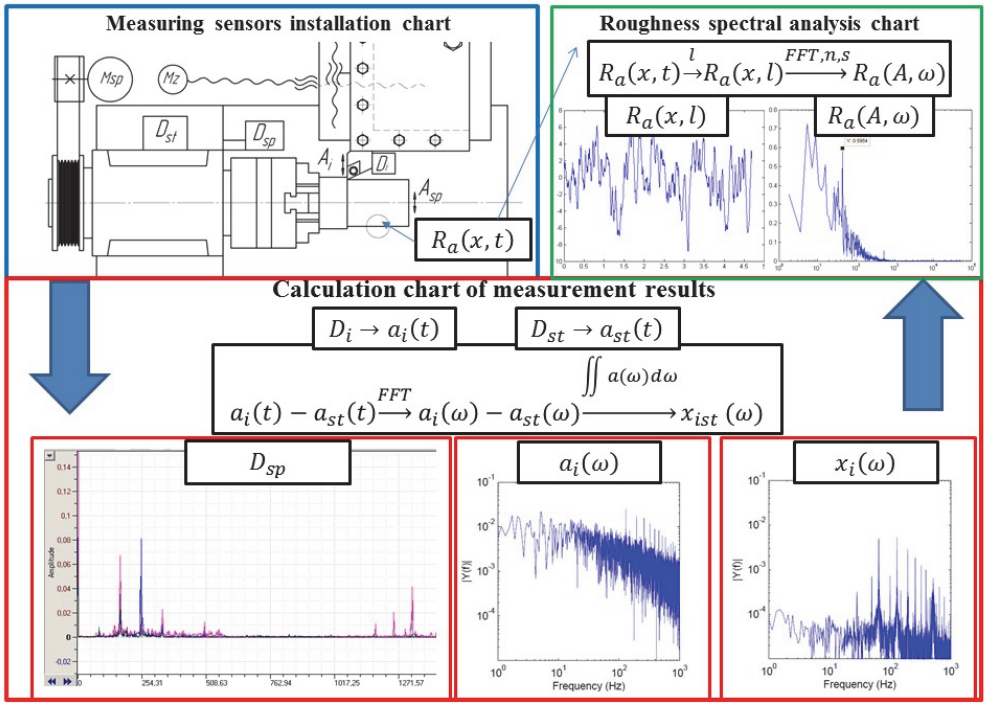

Fig. 4. Methodology of dynamic behaviour study

The quality assessment of the surface finish was carried out according to the roughness parameter Ra using a modernized profilograph-profilometer П-283 to a precision of 12 % in accordance with GOST 27964-88 and ISO/R-468 methods. The modernization of the П-283 profile recorder (Fig. 5) was meant to equip it with a sensor to measure the real length of the surface of the part 4, which allowed tracing the cutter tip displacement in relation to the part at set spindle rotational frequency and feed when turning the test samples of different machined materials (steel, aluminum alloy, etc.). The modernization with a description of hardware being subjected to modernization procedure was implemented by connecting RPM sensor of the drive engine 5, which moves the probe head 2 via reducer 3. The digital signal received was transmitted through the ADC LTR-22 7 to PC 9, which allowed performing a spectral roughness analysis of processed surface 1. The actual roughness value is recorded from the instrument scale 6 (Fig. 4) [28].

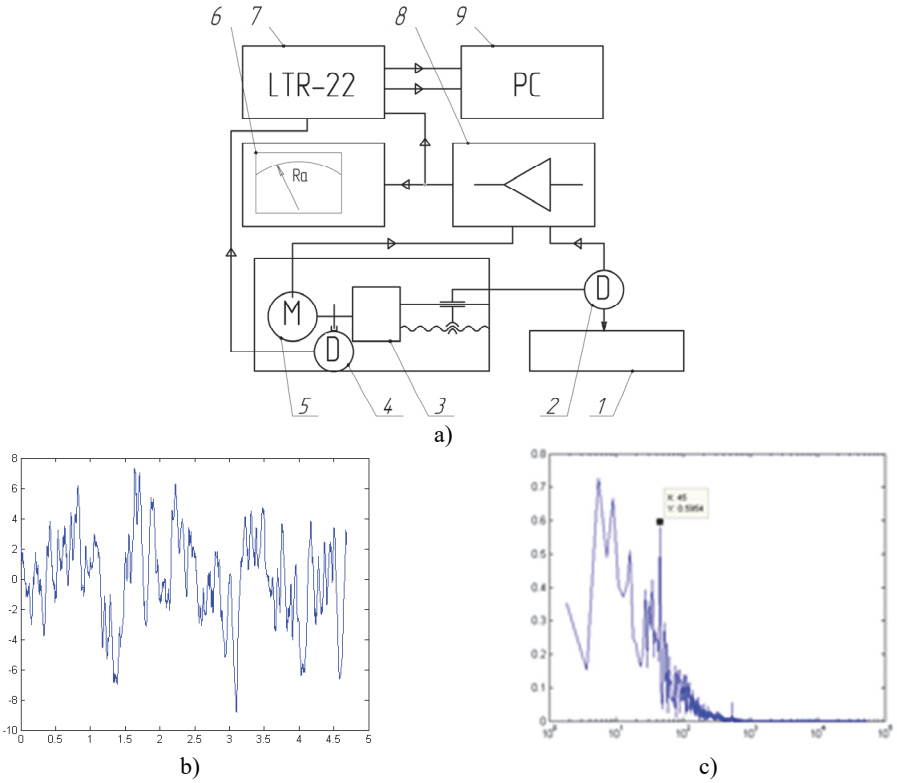

Fig. 5. a) Profilograph-profilometer П-283, b) profile record, c) spectral analysis

5. Results

During the turning with dynamic variation of rotational speed, it had been experimentally proven that the maximum achievable depth of modulation depending on the mass of rotating parts of the main actuator of the lathe and engine power essentially depends on the average rotational speed and the required modulation frequency. Thus, the lathe 16K20T1 at the rotational speed of 800 rpm and the modulation frequency of 4 Hz can maximally change its rotational speed by 180 rpm, and the lathe 1700ВФ30 at rotational speed of 1900-7000 rpm at a frequency of modulation of 5 Hz maximally changes the frequency by 50 rpm, and for the modulation frequency of 3 Hz by 150 rpm.

While researching the failure of regeneration of secondary self-oscillations due to the reconstruction of the “trace” cutting on the lathe 16K20T1 during the processing of the 60 mm

diameter rough workpiece from 40X steel, with a hardness of 58 HRC at cutting speed of 40 m/min, depth of 0.5 mm and a feed of 0.2 mm for normal turning, the roughness value was Ra 1.7 μm with visible traces of self-oscillations. When machining with modulation frequency of 1 Hz at a modulation depth of 60 rpm with same cutting parameters surface finish decreased to Ra 0.8 μm without the traces of self-oscillations on the surface.

Conducting the same research on the 1700ВФ30 lathe when machining D16T aluminum alloy workpiece at rotational speed of 4500-6000 rpm did not give a clear result. During parts machining with a modulation frequency of 1-5 Hz and a maximum modulation depth of 50-150 rpm at frequencies of 4500-6800 rpm, the roughness values of the surface finish were within the same class and there was a tendency toward its small oscillation (within the measurement error of profilometer П-283) (Fig. 6) [29].

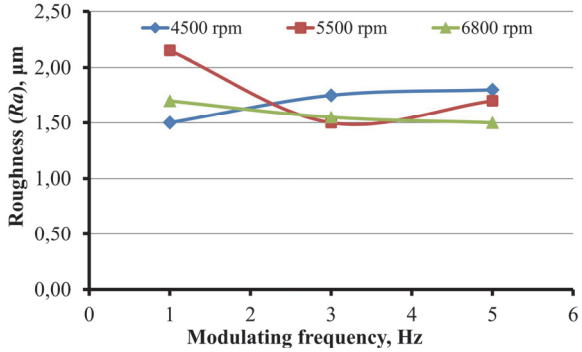

Fig. 6. Impact of modulation depth at rotational speeds of 4500, 5500, 6800 rpm on roughness of the processed surface

During the machining the qualitative dependence of surface finish on the amplitude of the spindle mutual oscillations with the workpiece and the point of cutting insert depending on rotational speed was experimentally determined, and the oscillation amplitude of spindle and the tool was determined depending on rotational speed at idle (Fig. 7) [30].

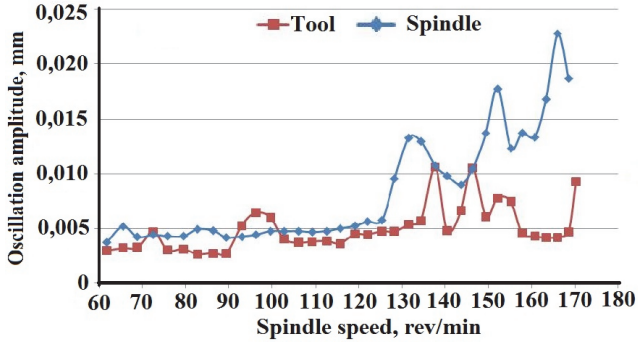

Fig. 7. Oscillation amplitude of a spindle and a tool tip depending on spindle rotational speed at idle

It has been established that the oscillations amplitude significantly increases at the resonance frequencies of the technological system: 135, 152 and 166 Hz, amplitude is 0.013, 0.017, and 0.022 mm respectively. At intermediate values between the resonance rotational speed (143 and 160 Hz), the oscillations amplitude decreases to 0.009 and 0.012 mm respectively. Similarly, the oscillation amplitude of the tool under 138 and 146 Hz is about 0.01 mm, and for other modulation frequencies, including large ones, is about 0.005 mm.

By mean of finite element modelling, the amplitude of the mutual oscillation of spindle with the workpiece and blade tip of the tool was determined by analysing the Frequency Response of

the Ansys Software (Fig. 8) and compared with the experimental studies of the effect of rotational speed during steady cutting parameters ($V = 500$ m/min, $S = 0.05$ mm/rev, $t = 0.5$ mm) on the roughness of the surface finish.

Comparing the charts, one can see that the mutual oscillations amplitudes of the tool and spindle, as well as roughness depending on rotational speed used during the machining are similar. Thus, it can be argued that the amplitude of the relative oscillations of spindle with the workpiece and the blade tip of the tool is displayed on the machines surface of the part as a vibration component of roughness [29].

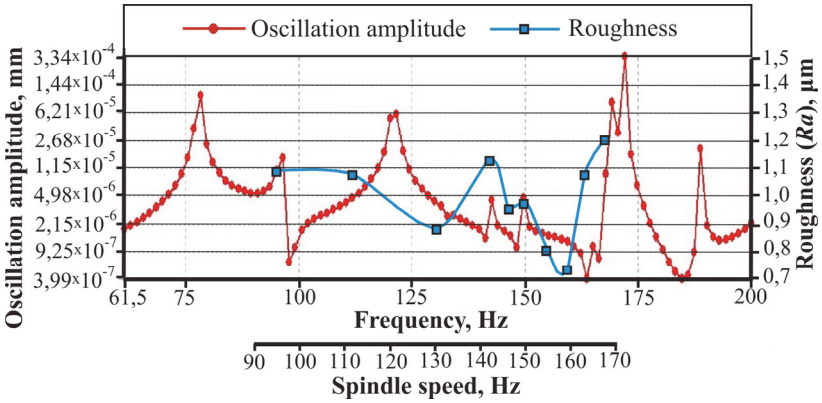

Fig. 8. The effect of mutual oscillations amplitude of spindle with the workpiece and blade tip of the tool on the roughness of the processed surface under various spindle rotational speeds

Experiment has been carried out to confirm the effect of natural oscillations modes of technological system on the mutual oscillations of a tool point and a workpiece. The oscillations amplitudes of the tool at the sliding carriage positions at a distance of 20 mm and 200 mm from the spindle front face, as well as at a distance of 20 mm from the spindle front face, are determined with a foot block mounted on the base, weighing 8 kg or without it. The oscillation amplitudes of the tool under different rotational speeds and tool positions are shown in Fig. 9. It has been proved that the additional mass leads to a change in the amplitude-frequency characteristic of cutter oscillation in relation to spindle. In this case, the maxima of the oscillations amplitudes are shifted. During turning without mass (without dead head), the minimum oscillations amplitude in the fixed position of the cutter occurs at frequencies of 6800 and 8800 rpm, and with mass – at frequencies of 4800 and 7800 rpm. Thus, by changing the position of the tool relative to the frame, and also by setting the additional controlled mass to the stand, it is possible to change the tool oscillation amplitude (for this lathe in the range from 0.2 to 0.45 μm), which will be reflected on processed surface roughness [29].

One of the effective methods for improving dynamic control of the lathe support oscillations is the method of implementation of additional actions that allows tracking oscillations amplitude of the sliding carriage by increasing the inertial properties of lathe and reducing logarithmic oscillation decrement of the cutter, which improves accuracy of machining and roughness of the surface finish at higher spindle rotation speeds. Oscillation control sensor (cutter displacement) at coordinate X located on a cutter connects to the control unit. During machining at first the minimum oscillation amplitude of the cutter is determined, then the signal from oscillation control sensor of the cutter is sent to the additional mass actuator, with which it moves along the frame at a distance proportional to the minimum amplitude of cutter oscillation. This method of dynamic control of oscillations in the cutting could be realised and experimental set-up which consists of: 1 – cutter; 2 – vibratory acceleration sensor; 3 – sliding carriage; 4 – communication channel between sensor and control unit; 5 – control unit; 6 – additional mass actuator communication channel; 7, 8 – tool oscillation vectors; 9 – additional mass (Fig. 10) [29].

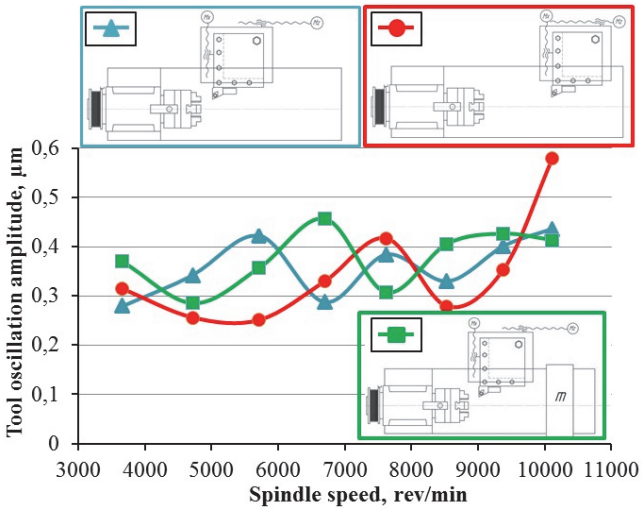

Fig. 9. Tool oscillation amplitudes at different spindle rotation speeds and tool positions

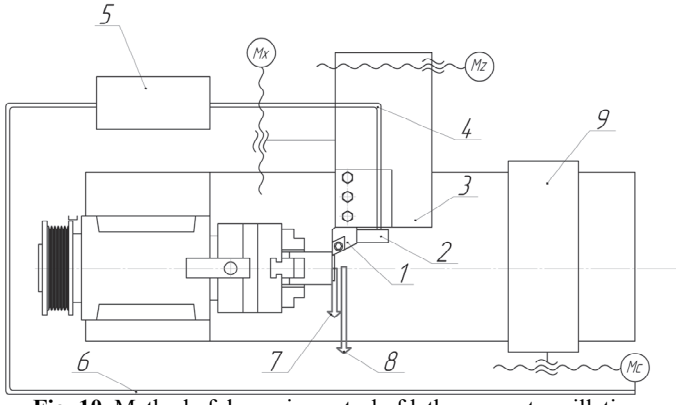

Fig. 10. Method of dynamic control of lathe support oscillations

An equally effective method of controlling the dynamic state of the technological system is the method of loading the metal cutting machine by a bar, when a long bar stock is cut into shorter bars using a special device located on the side of spindle opposite the operating area. In this case, the bar part (1) of the required length is clamped in spindle (2) and the rest of the bar is cut off next to the back side (3) of the spindle assembly (4). In addition, the rest of the bar is connected to the loading device (6) till the rod (7) and used as an elongated size rod. After the last cutting, the end of the bar remainder is disconnected with the loading device rod and sent to spindle as rod for machining fixed by clamping device (8). Feature machining is realised be combination of main rotational motion of the spindle and axillary motion of cutoff carriage (9) tool support bar (10) and cutter (11) (Fig. 11).

The suggested method of loading a metal-cutting lathe with a bar is aimed at solve a technical task of reducing dynamic loads at higher rotation speeds when lengthy bars are present in the loading mechanism by using the bar itself as an elongated rod for loading bars of reduced length and address the need for equipment for preparing (slicing) bars of the required length [32].

6. Scientific novelty of the results obtained

– For the first time, for the turning process at high rotation speeds, functional dependence of vibration component of roughness of the surface finish on the external driving forces and natural

oscillation modes and frequencies of the TL (turning lathe) was established, which made it possible to effectively manage the machining.

– For the first time it has been established that the combination of the oscillation node of the system by moving the additional mass with the processing area during turning at high spindle rotational speed leads to a decrease in roughness of working surface by means of reducing the oscillation amplitude of the tool, due to changes in natural oscillation modes of the TL.

– Further development of the definition of application limits of inhibition effect of regenerative oscillations using the method of dynamic variation of rotational speed in connection with the change in ratio between the oscillation wave length of cutting edge and the distance covered by it during this time along the surface of part.

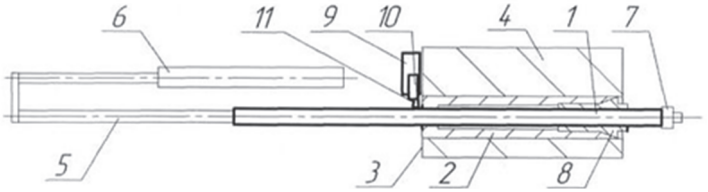

Fig. 11. Metal-cutting lathe loading method with a bar

7. Conclusions

In this work the scientific and practical task of increasing efficiency of machining parts on turning lathes is solved by controlling the process dynamics at higher rotational speeds to ensure the cutting speed recommended by tool material manufacturer and drawing requirements for accuracy and roughness of surfaces finish.

1. The reasoned assumption is made stating that increasing the efficiency of machining parts on turning lathes is possible by controlling the process dynamics through improving productivity at increased rotation speeds to meet the drawing requirements for roughness of the machined processed surface of parts with a diameter of 5-20 mm using cutting speeds recommended by tools manufacturers.

2. The method and testing bench developed on the basis of the turning lathe model 1700ВФ30 allow: a) to provide a rotational speed of up to 10,000 rpm; b) measure the immediate value of vibratory displacement and vibration acceleration of tool spindle and tool point in real time; c) perform spectral analysis of the profile record of the processed surface; d) establish the relationship between the profile of the machined surface and oscillations of spindle and tool.

3. In experimental study it has been established that the main sources of tool oscillations are self-oscillation and oscillations from excitatory force in the system “spindle-device-workpiece”, which limit the maximum rotation speed with the workpiece by increasing roughness of the surface finish. It is proved that the minimum roughness of the surfaces finish is achieved by reducing the system response to the force in the cutting area by:

– Modulation of rotational speed with frequency from 1 to 5 Hz, which allowed to control failure of self-oscillations regeneration due to the reconstruction of the “trace” cutting.

– The combination of node of natural oscillation modes and the cutting area, due to dynamic control of oscillation of turning lathe sliding carriage by increasing inertial properties of lathe and reducing the oscillation amplitude of the cutter, which allows to improve the processing accuracy and reduce roughness of the surface finish at higher rotation speeds.

It has been proven that for small rotational speeds, in particular the coercive force frequency, the possibility of reducing vibrations in technological system at the expense of mass redistribution is difficult to implement, at the same time, at relatively high spindle rotational speeds (more than 6,000 rpm) it is possible to substantially affect the dynamic behaviour of the technological system, because even small masses lead to changes in modes and frequencies of its natural oscillations, which are close to oscillation frequencies of coercive force.

References

[1] **Zaloga W. A., Zinchenko R. N., Shapoval Y. V.** Machining of part with small diameter when turning with high rotational speed. Problems and development perspective. Modern Technologies in Manufacturing Engineering, Vol. 9, 2014, p. 50-63.

[2] **Zobel R.** Automatic Balancing Device. US2331756A, United States Patent Office Claims, 1942.

[3] **Wilson Cox W.** Automatic and Substantially Permanent Wheel Balancing Device. US3953074A, United States Patent Office Claims, 1975.

[4] **Peschel D., Funke D.** Mass-Imbalance Oscillation Generator. US4043221A, United States Patent and Trademark Office, 1974.

[5] **Deakin J. E.** Automatic Shaft Balancer. US4075909A, United States Patent and Trademark Office, 1976.

[6] **Clay S. C., Clay R. A.** Dynamic Wheel Balancing Device. US4755006A, United States Patent and Trademark Office, 1986.

[7] **Taylor G. R.** Weight Compensating Apparatus. US5460017A, United States Patent and Trademark Office, 1992.

[8] **Taylor G. R., Wierzba P., Hannah R. C.** Weight Compensating Method and Apparatus. US5605078A, United States Patent and Trademark Office, 1992.

[9] **Kuchuhurov M. V., Vnukov Yu N., Diadia S. Y.** Method and device for studying regenerative self-oscillations during turning. Cutting and Tools in Technological Systems, ONPU, Odesa, Vol. 83, 2013, p. 42-54, (in Russian).

[10] **Vnukov Yu. N. Germashev A. I. Komorkin P. A. Kozlova E. B.** Estimation of efficiency and quality of processing of thin-walled parts at end milling. Information Technologies in Education, Science and Production, Vol. 7, Issue 2, 2014, p. 97-108, (in Russian).

[11] **Zharkov I. G.** Vibrations During Processing with a Blade Tool. Mashinostroyeniye, 1986, p. 184, (in Russian).

[12] **Kashirin M. F.** Investigation of Vibrations during Cutting. Nauka Publishing, USSR, 1944, p. 262, (in Russian).

[13] **Kedrov S. S.** Oscillations of Metal-Cutting Machines. Mashinostroyeniye, Moscow, 1978, p. 198 (in Russian).

[14] **Kudinov V. A.** Dynamics of Machines. Mashinostroyeniye, Moscow, 1967, p. 367, (in Russian)

[15] **Podolskyi M. I., Kuznietsov Yu M., Dmytriiev D. O., Sidorov V. A.** Experimental studies of dynamic parameters of a rod support system of a multipurpose lathe during cutting technological complexes. Mizhnarodnyi naukovyi zhurnal, Vol. 10, Issue 2, 2014, p. 175-181, (in Ukrainian).

[16] **Anelchyk Ie D., Shvets S. V., Lutsiv I. V., Dubetskyi I. D.** Cutting System: Physical Basics of Optimization. TDTU, Odesa-Ternopyl, 2000, p. 145, (in Ukrainian).

[17] **Strutynskyi V. B.** Mathematical Modeling of Metal-Cutting Machines. ZhITI, Zhytomyr, 2002, p. 570, (in Ukrainian).

[18] **Podurayev V. N.** Processing by Cutting with Vibration. Mashinostroyeniye, Moscow, 1970, p. 350, (in Russian).

[19] **Svinin V. M.** Milling with a Modulated Cutting Speed. IrSTU Publishing, Irkutsk, 2007, p. 304, (in Russian).

[20] **Tashlitskiy N. I.** The primary source of excitation energy of self-oscillations during metal cutting. Vestnik Mashinostroyeniya, Vol. 2, 1960, p. 10-20.

[21] **Otto A., Radons G.** Application of spindle speed variation for chatter suppression in turning. CIRP Journal of Manufacturing Science and Technology, Vol. 6, Issue 2, 2013, p. 102-109.

[22] **Park J. S.** The prediction of chatter stability in hard turning. Ph.D. Thesis in Mechanical Engineering, Atlanta, 2004.

[23] **Bisu C. F., Darnis P., G´erard A., et al.** Displacements analysis of self-excited vibrations in turning. The International Journal of Advanced Manufacturing Technology, Vol. 44, Issues 1-2, 2009, p. 1-16.

[24] **Siddhpura M., Paurobally R.** A review of chatter vibration research in turning. International Journal of Machine Tools and Manufacture, Vol. 61, 2012, p. 27-47.

[25] **Urbikaina G., Campaa F.-J., Zulaikab J.-J.** Preventing chatter vibrations in heavy-duty turning operations in large horizontal lathes. Journal of Sound and Vibration. Vol. 340, 2015, p. 317-330.

[26] **Liu H., Tang S., He S.** A method of measuring tool tip vibration in turning operations. The International Journal of Advanced Manufacturing Technology, Vol. 85, Issues 5-8, 2016, p. 1325-1337.

[27] **Zaloga W. A., Zinchenko R. N., Shapoval Y. V.** Increasing stability of cutting process by varying cutting speed when machining. 23rd International Technical Science Seminar, 2015, (in Ukrainian).

[28] **Zaloga W. A., Shapoval Y. V.** Methodology of evaluation of dynamic behavior of cutting system by determining geometric parameters of surface finish quality. Cutting and Tool in Technological System, Vol. 87, 2017, p. 63-81, (in Ukrainian).

[29] **Zaloga W. A., Shapoval Y. V.** Increasing efficiency of machining parts by controlling dynamics of turning with high rotational speed. Herald of Zhitomyr State Technical University, Vol. 80, Issue 2, 2017, p. 175-184, (in Ukrainian).

[30] **Zaloga W. A., Kryvoruchko D. V., Shapoval Y. V., Drofa K.** Dynamic control of oscillation when turning. Mechanics and Advanced Technologies, Vol. 79, 2017, p. 100-107, (in Ukrainian).

[31] **Korotun N. N., Kryvoruchko D. V., Shapoval Y. V.** Dynamic Control of Sliding Carrier Oscillation**.** Patent No. UA107301U, 2016, (in Ukrainian).

[32] **Kryvoruchko D. V., Shapoval Y. V., Korotun N. N.** Method of Loading of Machine Tools Rod. Patent No. UA103688U, 2015, (in Ukrainian).

Zaloha William Oleksandrovych born 29 August, 1936, in Kyiv, Ukrainian. Started working in 1954 at Kuianivska sugar plant in Sumy oblast. In 1954 graduated from Kharkiv Polytechnic Institute (KhPI) where he studied machine building. In 1965-1969 worked by the assignment at a plant (military base 44528, Bataysk, Rostov Oblast) as a master workman, manufacturing technician, and deputy shop foreman. Has been working in Sumy State University since 1969 as an Assistant, senior teacher, Docent, Professor, and head of a department. In 1970-1973 pursued postgraduate studies in KhPI under the supervision of professor M.F. Semko, Doctor of Engineering Science, and docent A.I. Hrabchenko, Candidate of Engineering Science. He became Candidate of Engineering Science himself in 1974. In 1977 was awarded with the title of Assistant Professor. From 1978 to 1990 was a head of the Metal-cutting machines and tools (MRV) department and starting from 1993 has been working as a professor. In 1995 was given a title of Professor in MRV department. In 2000 he passed his Doctor of Engineering Science. Defence in the speciality 05.03.01 - Machining Processes, Lathes and Tools. Since 2002 worked as a head of MRV department again in Sumy State University, and since 2007, after the unification of the departments Manufacturing Engineering and Metal-cutting machines and systems, works as the head of the department Manufacturing Engineering, Machines and Tools.

Shapoval Yurii Volodymyrovych born 28 of April, 1982, in Sumy. In 1999, he graduated from the Physics and Mathematics class of Sumy Educational Complex No. 7 with a silver medal. In 2004 graduated with honour from Sumy State University, receiving a Master's degree in metal-cutting machines and systems. Started to work in Sumy Scientific and Production Association named after Frunze as designing engineer at the Industrial Electronics Administration where he was engaged in repairing and modernization of CNC machines. In 2008, he worked as the Chief Mechanic of the Kiev Drilling Equipment Plant. In 2012-2015 pursued postgraduate studies at Sumy State University, where he has been working since 2015 as an Assistant of the department Technology of Machine-Building, Machines and Tools.

Kolesnyk Vitalii Oleksandrovych born 31 of May, 1988, in Sumy. In 2010 graduated from Sumy State University, receiving a Master's degree in manufacturing engineering. Started to work in Sumy Plant "Nasosenegomash" as Manufacturing Engineer at the Chief Manufacturing Engineer office where he was engaged in manufacturing preparation of production. In 2011-2014 pursued postgraduate studies at Sumy State University, where he has been working since 2015 as an senior teacher of the Department Manufacturing Engineering, Machines and Tools. In 2016 defended a Ph.D. thesis in manufacturing engineering. His research interests include machining of CFRP/Ti alloy stacks, insurance of accuracy and quality of machining.